

UNIVERSITY OF OKLAHOMA

GRADUATE COLLEGE

SHAKE TABLE TESTING OF SCALED RAMMED EARTH MODELS

A THESIS

SUBMITTED TO THE GRADUATE FACULTY

in partial fulfillment of the requirements for the

Degree of

MASTER OF SCIENCE

By

CARMEN MARLENE DIAZ

Norman, Oklahoma


2008


UNIVERSITY OF OKLAHOMA
LIBRARIES


BU
THESIS
DIA
cop.2

SHAKE TABLE TESTING OF SCALED RAMMED EARTH MODELS

A THESIS APPROVED FOR THE
SCHOOL OF CIVIL ENGINEERING AND ENVIRONMENTAL
SCIENCE

BY 

Dr. Kyran Mish, Chair


Dr. Chris Ramseyer


Dr. Amy Cerato

ACKNOWLEDGEMENTS

This thesis is dedicated to the memory of my grandfather, Milton Perez, who fervently reminded me to pursue this journey by saying, “Be faithful to your boyfriend, ‘Mr. Master’s Degree’.” He was a constant source of wisdom, piercing encouragement and amazingly difficult games of Connect Four.

I have to thank my committee Dr. Kyran Mish, Dr. Chris Ramseyer, and Dr. Amy Cerato. Thank you for contributing your knowledge and creativity into this project. I have to point out that this started with Dr. Ramseyer’s idea of using rammed earth. Having never heard of rammed earth before, I was surprised at how I grew to be passionate about the subject. Thank you for your vision. Dr. Mish, thank you for your ability to notice each person’s gifts and encourage them to grow. Dr. Cerato, your perseverance and path of success encourage me to do the same with my own life.

In getting me across the threshold, I thank the several undergraduate and graduate students who were incredible at sweating and building four rammed earth models less than two months. It would have been clearly impossible to finish the research without you. Shelby Pankop, you were the best assistant anyone could want. Roozebeh Kiaminish, thank you for all the programming, wiring, calibration and even food preparation. Mike Schmitz, the unsung hero of Fears Lab, thank you for your patience and depth of knowledge when it comes to building anything or using any of the equipment at the lab.

Acknowledgements.....	iv
List of Tables.....	viii
List of Figures.....	ix
Abstract.....	xiv
Chapter 1: Introduction.....	1
1.1 Earth and Earthquakes.....	1
1.2 Literature Review.....	4
1.2.1 Rammed Earth Research.....	5
1.2.2 Seismic Adobe Research.....	9
1.3 Objectives and Scope.....	13
Chapter 2: Experimentation.....	15
2.1 Introduction.....	15
2.2 Soil Mix Design.....	15
2.3 Model Design.....	20
2.3.1 Model Geometry.....	20
2.3.2 Reinforcement.....	22
2.3.3 Formwork Design.....	25
2.4 Mixing and Compaction of Models.....	30
2.5 Test Setup.....	36
2.6 Loading Protocol.....	41

2.7 Data Processing.....	44
Chapter 3: Test Results.....	45
3.1 Introduction.....	45
3.2 Test 1: Unreinforced Model at Scaled Frequency.....	46
3.2.1 Preparation Observations.....	46
3.2.2 Test and Video Observations.....	46
3.2.3 Picture and Demolition Observations.....	47
3.2.4 Data Observations.....	49
3.3 Test 2: Unreinforced Model at Fundamental Frequency.....	59
3.3.1 Preparation Observations.....	59
3.3.2 Test and Video Observations.....	59
3.3.3 Picture and Demolition Observations.....	59
3.3.4 Data Observations.....	60
3.4 Test 3: Wooden Ring Beam Reinforcement.....	69
3.4.1 Test and Video Observations.....	69
3.4.2 Picture and Demolition Observations.....	69
3.4.3 Data Observations.....	71
3.5 Test 4: Plastic Mesh Reinforcement.....	83
3.5.1 Test and Video Observations.....	83
3.5.2 Picture and Demolition Observations.....	83
3.5.3 Data Observations.....	84
3.6 Discussion.....	92

	3.6.1 Calculation of Forces.....	92
Table 2.1	3.6.2 Similarities Between Tests.....	95
Table 2.2	3.6.3 Effects of Reinforcement.....	98
Table 2.3	3.6.4 Effects of Workmanship.....	100
	3.6.5 Loading Protocol.....	100
 Chapter 4: Conclusions and Recommendations.....		102
	4.1 Summary.....	102
	4.2 Conclusions.....	102
	4.3 Recommendations.....	103

LIST OF TABLES

Table 2.1	Summary of soil mix design.....	19
Table 2.2	Summary of model variables and loading protocol.....	43
Table 3.1	Summary of Shaketable Test Results.....	45

LIST OF FIGURES

Figure 1.1	Earthquake damage to rammed earth in Peru.....	2
Figure 2.1	Sieve analysis of sand.....	17
Figure 2.2	Typical failures of test cylinders.....	20
Figure 2.3	Typical geometry used for rammed earth models.....	21
Figure 2.4	Plan view sketch of ring beam.....	23
Figure 2.5	View of Ring beam on Test 3 model with accelerometers.....	23
Figure 2.6	Cross-section of shaketable platform with plywood base.....	25
Figure 2.7	Plan view sketch of base with outer walls (shaketable not shown).....	26
Figure 2.8	Elevation sketch of shorter outer wall formwork.....	27
Figure 2.9	Picture of shorter outer wall formwork.....	27
Figure 2.10	Elevation sketch of longer outer wall formwork.....	28
Figure 2.11	Picture of longer outer wall formwork.....	28
Figure 2.12	Elevation sketch of inner wall formwork.....	29
Figure 2.13	Plan view picture of all inner wall formwork (Test 1).....	29
Figure 2.14	Picture of 1/4in wire mesh used to sieve the clay.....	31
Figure 2.15	Typical layout of soil batch (equivalent to one compacted layer).....	32
Figure 2.16	Vertical drum mixer, wheelbarrow and scoops for mixing and transporting.....	32
Figure 2.17	Pouring of soil into mixer.....	33
Figure 2.18	Placement of soil into formwork.....	35
Figure 2.19	View of soil inside formwork prior to compaction.....	35

Figure 2.20	Compaction of soil with steel tampers.....	36
Figure 2.21	Elevation view sketch of test setup.....	38
Figure 2.22	Photograph of test setup.....	39
Figure 2.23	Plan view sketch of test setup on tests 2, 3 and 4.....	40
Figure 3.1	Test 1 view of east wall before test.....	50
Figure 3.2	Test 1 cracks above lintel in east wall.....	50
Figure 3.3	Test 1 interior view of crack above lintel in NE corner.....	51
Figure 3.4	Test 1 closeup view of exterior crack near lintel.....	51
Figure 3.5	Test 1 view of two balls of silt along cracked surface in SE corner.....	52
Figure 3.6	Test 1 view of north wall, with roof, before test.....	53
Figure 3.7	Test 1 elevation view of cracked northwest corner after test.....	54
Figure 3.8	Test 1 plan view above cracked northwest corner.....	54
Figure 3.9	Test 1 diagonal crack on exterior north wall.....	55
Figure 3.10	Test 1 close up of diagonal crack in lower half of north wall.....	55
Figure 3.11	Test 1 interior view of crack along north wall.....	56
Figure 3.12	Test 1 post-test fragments with large clumps of red clay.....	56
Figure 3.13	Test 1 accelerations at beginning of Test 1-B.....	57
Figure 3.14	Test 1 relative torsion between northeast and northwest corners at end of Test 1-C.....	58
Figure 3.15	Test 2 east wall before test (initial crack above lintel outlined in red).....	61
Figure 3.16	Test 2 Interior view of east wall with cracks above lintel and delamination.....	61

Figure 3.17	Test 2 close up view of crack in NE corner above lintel after test, note less compacted soil adjacent to edge of lintel.....	62
Figure 3.18	Test 2 view of north and west walls before test.....	63
Figure 3.19	Test 2 delamination along north and west walls after test.....	63
Figure 3.20	Test 2 view of south and east walls before test.....	64
Figure 3.21	Test 2 delamination along south and east walls after test.....	64
Figure 3.22	Test 2 view of west and south walls before test.....	65
Figure 3.23	Test 2 delamination along west and south walls after test.....	65
Figure 3.24	Test 2 vertical crack at NW corner below delaminated layer.....	66
Figure 3.25	Test 2 vertical crack at SW corner below delaminated layer.....	67
Figure 3.26	Test 2 relative accelerations between NE, NW, and SW corners towards end of test.....	68
Figure 3.27	Test 3 view of east wall before test, note crack above door opening.....	71
Figure 3.28	Test 3 cracks above lintel near SE corner of east wall.....	72
Figure 3.29	Test 3 cracks above lintel near NE corner of east wall.....	72
Figure 3.30	Test 3 view of interior southeast corner after test, note cracks outlined in red.....	73
Figure 3.31	Test 3 view of west wall before test.....	74
Figure 3.32	Test 3 view of west wall after test.....	74
Figure 3.33	Test 3 view of crack near base of west wall at SW corner.....	75
Figure 3.34	Test 3 width of fractured section at SW corner along base of west wall.....	76
Figure 3.35	Test 3 view of cracks across SW corner.....	77

Figure 3.36	Test 3 view of south wall before test.....	78
Figure 3.37	Test 3 view of south wall after test. Arrows point to fractures.....	78
Figure 3.38	Test 3 close-up of previous photograph.....	79
Figure 3.39	Test 3 measurement of diagonal crack at interior of SW corner.....	80
Figure 3.40	Test 3 model after demolition (arrows point to cracks from testing).....	81
Figure 3.41	Test 3 view of suspended rammed earth at ring beam.....	81
Figure 3.42	Test 3-B relative accelerations between corners from 8 Hz to 10 Hz, note increase in accelerations at approximately 270 seconds.....	82
Figure 3.43	Test 3-B relative accelerations, note uniform accelerations between corners.....	82
Figure 3.44	Test 4 view of east wall before testing.....	85
Figure 3.45	Test 4 view of east wall after test with the mesh removed.....	85
Figure 3.46	Test 4 interior of east wall before testing.....	86
Figure 3.47	Test 4 view of cracks with nails above lintel in east wall after test.....	86
Figure 3.48	Test 4 view of diagonal crack along north wall with mesh after test.....	87
Figure 3.49	Test 4 view of diagonal crack along north wall after test.....	87
Figure 3.50	Test 4 interior view of NW corner after test.....	88
Figure 3.51	Test 4 view of diagonal crack at northwest corner of west wall after test.....	89
Figure 3.52	Test 4 view of exposed failure planes at north and west walls during demolition.....	90
Figure 3.53	Test 4 view of wall that fractured upon impact with the floor.....	91
Figure 3.54	Test 4 relative accelerations between corners at failure.....	91

Figure 3.55 Sketch of location of base shear and eccentricity.....93

Figure 3.56 Sketch of resultant forces on model.....94

Figure 3.57 Summary of cracks on exterior walls of all models.....96

CHAPTER ABSTRACT SECTION

The ancient method of rammed earth construction has been used in various parts of the globe, including Central and South America, which experience high seismic activity. Although some studies have been done on rammed earth, relatively little is known about the extent of its shear and tensile capacities or practical methods for improving the seismic survivability of these structures.

This research explored not only the effects of dynamic testing on scaled models of a simplified rammed earth house but also two types of reinforcement: a wooden ring beam, and a plastic mesh. The objective was to observe gross failure, catalogue different failure modes and determine which type of reinforcement best preserved the structure. Each model was loaded by a sine wave starting at the fundamental frequency of the model, then increasing both the amplitude and the frequency until failure. Each model was designed at one-third scale with one door opening, 6 inch wall thickness, 3 foot wall height, and a 4 foot by 4 foot plan. All models were tested on a shaketable at the Fears Structural Engineering Laboratory.

Results showed that sine wave base motion, starting at the fundamental frequency, can be an effective dynamic test method. Results also showed that the wooden ring beam was the more effective type of reinforcement. Although the plastic mesh did not serve as structural reinforcement, it still prevented collapse of the rammed earth model.

CHAPTER 1 INTRODUCTION

1.1 Earth and Earthquakes

Of all forces of nature with the potential to destroy homes, earthquakes seem to strike the most fear because of their inherent element of surprise. Earthquakes are relatively few and far in between but their effects can range from generating a queasy feeling in the stomach to structural collapse for several miles. Industrialized nations like the United States, Europe and Australia have building codes to provide guidelines for construction of housing, with architects and engineers to ensure the safety of the design. In some developing nations however, like Peru or Nicaragua, residential structures can still be constructed by the homeowner without any engineering or building code. Earthen construction is popular in these areas because of the availability of the main material: earth. The homeowner can use soil that is abundantly available on site. Unfortunately earthen construction does not perform well in seismic areas. Of the different types of earthen construction, rammed earth was chosen for this particular study because it is still used in some developing nations where earthquakes can be severe, yet its structural behavior as a whole during an earthquake is not widely understood (**Figure 1.1**).



Figure 1.1: Earthquake damage to rammed earth in Peru (www.lamasperu.com)

“Rammed earth” is exactly as it sounds: earth that is rammed. Moist soil is placed into wooden formwork and compacted into layers or blocks. It is an ancient form of construction that can be found across the world including portions of the Great Wall of China, 1000 year old Buddhist monasteries in India, and Muslim fortresses from the 8th century throughout Spain and North Africa (Augarde, et al., 2006). The advantage to rammed earth, in addition to the availability of its main component, is that the homeowner can be the builder. The formwork is relatively simple and the method of compaction can be done manually.

Developing nations with high seismic activity face the added challenge of building sustainable rammed earth structures that are both earthquake resistant as well as inexpensive to construct. Because earthquakes produce lateral forces, which can provoke bending and shear in a structure, high shear and tensile strengths are essential for

withstanding seismic activity. Unfortunately, rammed earth has low shear and tensile strengths relative to its compressive strength, which lead to brittle failures and sudden collapse of a rammed earth structure (Maniatidis and Walker, 2003). One way to combat the brittle failure is to reinforce the rammed earth with materials that have higher tensile and shear strengths, similar to the methodology used in reinforced concrete design. Like rammed earth, concrete has a higher compressive strength than tensile strength, therefore it is commonly reinforced with steel that has a higher tensile strength than the concrete. The two materials complement each other, therefore the concrete resists loads in compression and should the concrete crack then the steel is designed to carry the load in tension. To maintain compatibility between the two materials, the size and shape of the steel is controlled by the capacity of the concrete to contain the steel, which leads to constraints typically known in engineering design such as minimum cover and spacing of thin bars of steel inside concrete.

Such an approach is needed in rammed earth design for developing nations, yet the designers are the homeowners who are less familiar with engineering and typically cannot afford transporting large loads of materials to the site. Therefore, in the seismic areas of developing nations, the rammed earth needs to be reinforced with compatible, local and inexpensive materials. Based upon experimental results from seismic adobe research (Blondet et al., 2006), potential reinforcement for rammed earth include wood or left-over materials from construction sites such as plastic construction fencing. For the purposes of this study, the term “reinforcement” is simplified to refer to the addition of materials to prevent collapse of a structure. The better definition of reinforcement, in the

engineering sense, is related to the addition of materials to enhance the effectiveness of a structural member or system.

Focusing on methods to reinforce rammed earth in developing nations that experience earthquakes is not simply a charitable measure. The solutions used in a developing nation can be applied anywhere, including more industrialized nations that suffered a major tragedy such as the Northridge Earthquake in the United States. In the aftermath of a disaster, properly reinforced rammed earth structures can be thought of as an emergency housing alternative where materials and transportation costs are limited. This study will evaluate the effectiveness of two types of reinforcement for rammed earth—a wooden ring beam and plastic mesh—by constructing four scaled rammed earth models and testing each of them on a shaketable.

1.2 Literature Review

In recent past, rammed earth has become a research interest in areas such as England, Australia and Peru for the sake of rehabilitating historic structures, re-introducing it as a form of green architecture, or to enhance the safety of low income dwellings. In addition to rammed earth, there has been research in the seismic properties of adobe, another form of earthen construction that has been used in historic structures as well as low income dwellings. Adobe is similar to rammed earth in that it is weaker in tension than compression, but is constructed differently. Rammed earth is compacted soil while adobe is created from sun-dried blocks of soil and is built using mud mortar joints. Adobe has a weaker compressive strength than rammed earth but the seismic studies on

adobe are valuable as points of comparison. Research in both rammed earth and adobe are presented here.

1.2.1 Rammed Earth Research

By the early 1990s, rammed earth construction was more widely used in Peru than adobe construction, yet the majority of the research and building codes were aimed at the seismic resistance of adobe. Rammed earth construction techniques in Peru emigrated from Europe, mainly France and Spain where seismic activity was less severe. In effort to build knowledge on rammed earth properties and modify existing rammed earth construction techniques to better survive earthquakes, the Catholic University of Peru conducted a large study involving a variety of different tests to better understand the capabilities of rammed earth under seismic loads. The broad study consisted of diagonal compression tests on 87 small (60x60x15 cm) rammed earth walls, horizontal quasi-static tests on full scale walls (200x200x20 cm), compression tests on 10cm square cubes for dry strength, as well as granulometric and Atterburg Limit tests for studying the physical properties of the rammed earth (Vargas, 1992). Their areas of focus were soil granulometry, moisture content, compaction level, use of natural additives (straw, coarse sand), and joint treatment. Their conclusions were as follows:

- Earthquake resistant rammed earth must be made with as much clay and water as possible.
- Increasing clay increases shear strength.
- Increasing moisture content increases shear strength.
- Moisture content is more effective than compactive effort.

- Add water after compaction and immediately before placing next layer (every 10-12 cm).
- Moisture content greater than 17% makes rammed earth unworkable.
- Dry strength decreases strongly with increase of sand.
- No natural additives tested increased dry strength of soil.
- Recommended compaction of 60-70 hits with a 10 kg piston of 1000 cm² area.
- Mix 0.25-0.50% of straw (5 cm length) with soil to help control micro cracking of walls.
- Compatible reinforcement is cane or wood used as an inner mesh in wall, anchored to foundation and attached to a collar beam at top of wall.

PUCP contributed their results to the International Association for Earthquake Engineering (IAEE) manual titled, "Guidelines for Earthquake-Resistant Non-Engineered Construction," section 7.4.3 (IAEE, 2004), which include guidelines for rammed earth construction.

Hamilton, et al. (2006) tested the effects of using post-tensioning steel reinforcement, similar to that used in masonry, in rammed earth. Eight walls were constructed using a screened engineered soil and type 1 Portland cement which were then compacted with a pneumatic tamper typically used for installing fence posts. Density of a compacted wall was approximately 125 pcf. Four of the walls were tested for in plane shear and the other four for out of plane flexure. Dimensions of the test walls for flexure were approximately 16 inches thick, 4 feet wide and 9.75 feet tall. Dimensions for the

test walls for shear were approximately 16 inches in thickness, 6 feet wide and 7.3 feet tall. Two out of the four shear walls were constructed with welded wire mesh as internal horizontal reinforcement every third layer, while one shear wall used carbon fiber grid as internal horizontal reinforcement at every layer. All walls contained a reinforced concrete cap and base of 3.5 inches each. Post tensioning consisted of 1 1/16 inch diameter bars with a yield strength of 100 ksi, which were incased in 1.5 inch diameter PVC pipes. Intermediate couplings were required to allow the bars to reach from the base anchors to the cap anchors. Bars were post-tensioned to approximately 28 kips. One post-tensioned bar was used in each flexure test wall, and two post-tensioned bars were used in each shear wall.

Test cylinders were created for each wall using 4x8 inch molds to calculate compressive strength. Average compressive strength of the rammed earth cylinders was approximately 1,100 psi, but with a high coefficient of variation that ranged from 24% to 79% likely due to inconsistencies in the testing and/or in the material. All walls were subjected to cyclic loading based upon displacement, with a maximum displacement of 2.5 inches. Hysteresis loops were developed to study the energy dissipation of each wall. Results of the tests showed that both shear and flexure walls exhibited a bilinear elastic behavior, similar to the behavior of unbonded post-tensioned concrete members, and very little energy dissipation. Maximum loads sustained by the flexural walls ranged between 1.0 kips to 3.0 kips, with maximum drifts ranging from 1.5 inches to 2.5 inches. Severe spalling and crushing occurred near the base, in the high-moment regions of the flexural walls, during later cycling. Maximum loads sustained by the shear walls ranged from 16.5 kips to 23.9 kips, with maximum drifts ranging from 0.8 inches to 1.4 inches. The

general failure mode was by overturning of the wall. Some crushing and spalling was observed at the base of the wall, but no shear (diagonal) cracking or sliding was observed, and the horizontal reinforcement had no notable effect of the capacity or behavior. Of the eight walls tested, post-tensioning couplings rods failed in two of the tests for reasons that were unclear.

In addition to the experimental research, shear and flexure capacity calculations were made based upon the 2002 Masonry Building Code to compare to the experimental results. Compressive strength used in the calculations was 1000 psi, while tensile strength was assumed to be zero. Results of the calculations showed that using the masonry code provisions alone underestimated the compressive strength of the rammed earth walls. The post tensioned rods were believed to have played a role during overturning of the walls that increased the compressive strength of the walls during testing. Shear calculations based upon the code were inconclusive since the rammed earth walls did not fail in shear during testing.

For a comprehensive view of rammed earth building codes, Maniatidis and Walker (2003) from Bath University, England compiled information on various building codes from around the world into one document, titled the DTi Partners in Innovation Project, to provide recommendations for rammed earth construction in England. The various codes included countries such as Australia, Germany, New Zealand, Spain, and the United States (New Mexico state code). Information is divided into chapters ranging from design to quality control and maintenance of rammed earth structures. Their Chapters 4 and 5 discuss design and detailing of rammed earth.

Chapter 4 includes a range of formulas for the values of compressive strength, shear strength and the Modulus of Elasticity. For example, compressive strength (f_c) = $\Phi * f_{uc}$, where f_{uc} is unconfined compressive strength, and Φ is a capacity reduction factor of 0.4, 0.45 or 0.60 depending upon the country's building code. Shear strength can be calculated as either the compressive strength multiplied by a capacity reduction factor, 7%, or is related to the height of the rammed earth wall when test data is available. If the rammed earth is stabilized, the shear strength could be calculated as the square root of the compressive strength. For design purposes in Australia, without test data the shear is assumed to be zero.

Chapter 5 discusses architectural detailing, including lintels and ring beams. Tables are provided for typical spans and depths for timber lintels, which range from approximately 4 to 10 feet in span and 4 to 10 inches in depth. According to the authors, ring beams are a common practice in rammed earth construction. The majority of codes have specifications for either timber or reinforced concrete ring beams. Timber ring beams typically include large or small sections embedded into a mortar bed on top of the wall, and are secured with "holding down" bolts. Reinforced concrete ring beams can be constructed in-situ or pre-cast, and are typically used in areas expecting high lateral loads.

1.2.2 Seismic Adobe Research

As part of an awareness to preserve cultural ties, the Getty Conservation Institute in California investigated how to rehabilitate historic adobe structures that lie in seismic

areas (Tolles et al., 2000). In their study, eleven scaled models were constructed and tested on a shaketable at various percentages of the maximum estimated peak ground acceleration of the N21E component of the 1952 Taft Earthquake. The intent was to consider the effects of building geometry, gravity loading, and different retrofit measures on the seismic capacity of the adobe models. Retrofit measures included fiberglass center core rods, nylon straps, collar (bond) beams and combinations thereof. General assessments of the different retrofit measures were that vertical straps were the most effective in preventing out-of-plane wall collapse, and vertical center core rods were surprisingly effective in “delaying and limiting the damage to both in-plane and out-of-plane walls,” (Tolles et al., 2000).

The Catholic University of Peru (PUCP) provided a summary of previous research investigating various materials for reinforcement of adobe and critiqued of some of the current requirements in the Peruvian Adobe Code (Vargas et al., 2004). The summary began with discussing the effects of earthquakes on adobe. Because adobe has lower tensile strength than compressive strength, cracking in the adobe originates in regions of the structure subjected to tension. Walls perpendicular to the lateral seismic forces experience out of plane bending, where cracking originates at the lateral corners of the walls due to higher tensile stresses at the corners. Out of plane walls subjected to the seismic loads tend to fail first. In plane walls, parallel to the seismic forces, develop diagonal cracks, usually along the mortar joints, due to shear forces. Windows and door openings develop diagonal cracks at the corners of the openings due to stress concentrations at the corners.

Because of the exhibited behaviors of adobe during earthquakes, PUCP investigated the use of different materials for reinforcement of adobe. They started with horizontal placement of crushed cane within every fourth layer of adobe brick. Results showed the use of cane was successful at preventing sudden collapse of adobe during an earthquake, but disadvantages of the cane reinforcement included lack of availability in some regions, and if available, large quantities of cane were required for proper reinforcement. In 1996 PUCP turned to alternate materials. Instead of cane, wooden boards, rope, chicken wire mesh and welded wire mesh were used. Of those four materials, the most successful was the use of welded wire mesh nailed with metal bottle caps against adobe walls, which were then covered with cement-sand mortar. In 2001 a moderate earthquake occurred in the southern region of Peru where some of the adobe houses were reinforced with the welded wire mesh. Most of the adobe houses in the affected region collapsed, yet the reinforced houses did not suffer damage and in fact, were used as shelters. Despite the field success, the welded wire mesh was too expensive for most Peruvian adobe users, and the post-elastic behavior of the wire mesh with the cement mortar showed stiffness and strength degradation, which could result in a sudden collapse during a severe earthquake.

Based upon research experiences, PUCP critiqued some of the recommendations provided by the 2000 Peruvian Adobe Code. Their critiques included:

- Slenderness ratios of wall height to wall thickness between 8 and 9 is unsafe in high seismic areas.
- Slenderness ratios between 6 and 8 should require continuous reinforcement along entire walls instead of only wall joints.

- Continuous reinforcement should be required regardless of slenderness.
- Maximum slenderness ratios should depend on seismicity of building site.

Parts of the code not contested by PUCP included the geometry of wall openings and strength formulas. Wall openings must be centered, and width of the openings must be less than or equal to one-third of the length of the wall. Length of wall to the corner should be at least 3 times the wall thickness and no greater than 5 times the wall thickness. All walls should be adequately braced, either by transverse walls, buttresses or reinforced concrete columns. Strength formulas for adobe design included an average compressive strength for adobe masonry as approximately 29 psi and an average shear strength of approximately 4 psi.

Finally, the authors stressed the importance of making the information available to people who were not normally aware of the building code. Since most inhabitants of adobe dwellings made the houses themselves, code provisions needed to be translated in such a way that they would be easily understood and implemented.

After the success of incorporating wire mesh or cane as reinforcement in adobe houses, in the past few years the Catholic University of Peru (PUCP) investigated the use of externally applied polymer mesh as a form of seismic reinforcement of adobe houses (Blondet et al., 2006). They investigated two types of polymer meshes: an industrial geogrid, and a plastic mesh used in construction site fences. Five full-scale adobe houses were built, three reinforced with the geogrid, one reinforced with the construction fence, and one unreinforced. All models were built using traditional techniques. All had a reinforced concrete ringbeam as a foundation, and a wooden crown beam was used on 4

of the 5 models. The single-slope roof consisted of wood joists with cement tiles. Central window openings were in both shear walls (parallel to shaking), one door opening was in the front transverse wall while the back wall had no openings. All models were tested on a unidirectional shaketable to 30 seconds of the 1970 Huaraz earthquake at increasing amplitudes. The 3 models using the geogrid had different percentages of wall-cover: 100%, 75%, and 50% to determine if there is an optimum amount of mesh necessary to stabilize the structure. The model with the plastic mesh had 80% of the walls covered. The mesh was applied via plastic strings that were laid between the adobe brick courses. Mud plaster was applied on half of each model after the mesh was snug and in place. After testing, none of the mesh-reinforced models collapsed—although they suffered significant damage. Less mesh reinforcement increased the non-linear response of the structure, while addition of mud plaster appeared to increase the initial shear strength and stiffness of the walls. PUCP concluded that more research is required to find the optimum amount of mesh required, but so far using a polymer mesh such as the plastic mesh could be sufficient to avoid structural collapse.

1.3 Objectives and Scope

The general goals of this study are to better understand the dynamic behavior of rammed earth as a complete structure, and to incorporate methods of reinforcement that have been tested in seismic adobe. Rammed earth is susceptible to brittle failure since it is typically weak in shear and tension. Since earthquakes can cause shear stresses in a structure, reinforcement is needed in rammed earth to prevent sudden collapse during an earthquake.

It is hypothesized that conducting dynamic tests with a shake table on a complete model structure will provide a more realistic view into the behavior of rammed earth during an earthquake. Instead of using a scaled time history of a previous earthquake, the loading onto each model will be a sine wave starting at the fundamental frequency of the model. As the test progresses, both frequency and displacement will be increased until failure of the model is achieved. The two types of reinforcement used in the study are a wooden ring beam and plastic mesh. Previous research results in adobe indicated that wood is a more compatible material for earthen construction. The plastic mesh was chosen to compare its effectiveness in rammed earth construction versus adobe. Plastic mesh is not a typical material in all areas, but where available, it can be a useful method of recycling materials left behind in construction sites. There are two objectives to this study: catalog the different failure modes, and assess the effectiveness of the ring beam and plastic mesh as reinforcement.

2.2 Soil Mix Design

In the spirit of a developing nation scenario, soils and stabilizers were based upon what was locally available, and what might be feasible in a developing nation. According to McHenry (1984), the typical rammed earth mixture would include some percentage of small gravel aggregate, sand, silt, and clay with stabilizing agents such as Portland

CHAPTER 2: EXPERIMENTATION

2.1 Introduction

Preparation of the rammed earth models involved several phases: soil mix design, model design, mixing and compaction of models, and data collection. This chapter is divided into four sections to describe each phase. The first section, Soil Mix Design, explains the reasons for the soils and stabilizer used for the rammed earth, as well as the process used in preparing the unconfined compression tests. The second section, Model Design, highlights the decisions behind the chosen geometry of the model, reinforcement and design of the formwork. The third section, Mixing and Compaction of Models, leads the reader through the iterative process in preparing each model for a test. Finally, the Data Collection section describes the various tools used to collect data on each of the rammed earth models before, during, and after testing, as well as the loading protocol used for the shaketable testing. As a general note, the majority of the mixing and preparation methods were not done to ASTM standards but instead with the mindset of being reproducible in a developing nation where laboratory tools are not available and manual labor is more common.

2.2 Soil Mix Design

In the spirit of a developing nation scenario, soils and stabilizers were based upon what was locally available, and what might be feasible in a developing nation. According to McHenry (1984), the typical rammed earth mixture would include some percentage of small gravel aggregate, sand, silt, and clay with stabilizing agents such as Portland

cement or lime. Since some developing nations, such as Nicaragua, use reinforced concrete or confined masonry for their newer structures, cement was chosen as a possible stabilizer for the mix design. No definition of "small" was provided for the aggregate, therefore the mix used in this study consisted of sand, silt, clay, type II Portland cement and water. There were several key factors to consider: compressive strength, shear strength, and moisture content. The challenge was to look for a balance between compressive strength (provided by the sand and cement) and shear strength (provided by the clay). Too much sand reduces the shear strength while too much clay reduces the compressive strength and introduces shrinkage cracks in the structure (Vargas, 1992). Because the rammed earth models were to be tested on a shaketable, shear strength was crucial to resist the lateral forces. For testing purposes, local red Oklahoma clay was chosen and classified as lean clay (CL) with a liquid limit of 30% and a plasticity index of 13%. The silt (ML) had a liquid limit of 28% and a plasticity index of 8%. The sand used was Dover concrete sand, and is poorly graded (**Figure 2.1**). Atterburg limit tests were done according to ASTM D4318, and soil classification was done according to ASTM D2487.

Sieve Analysis

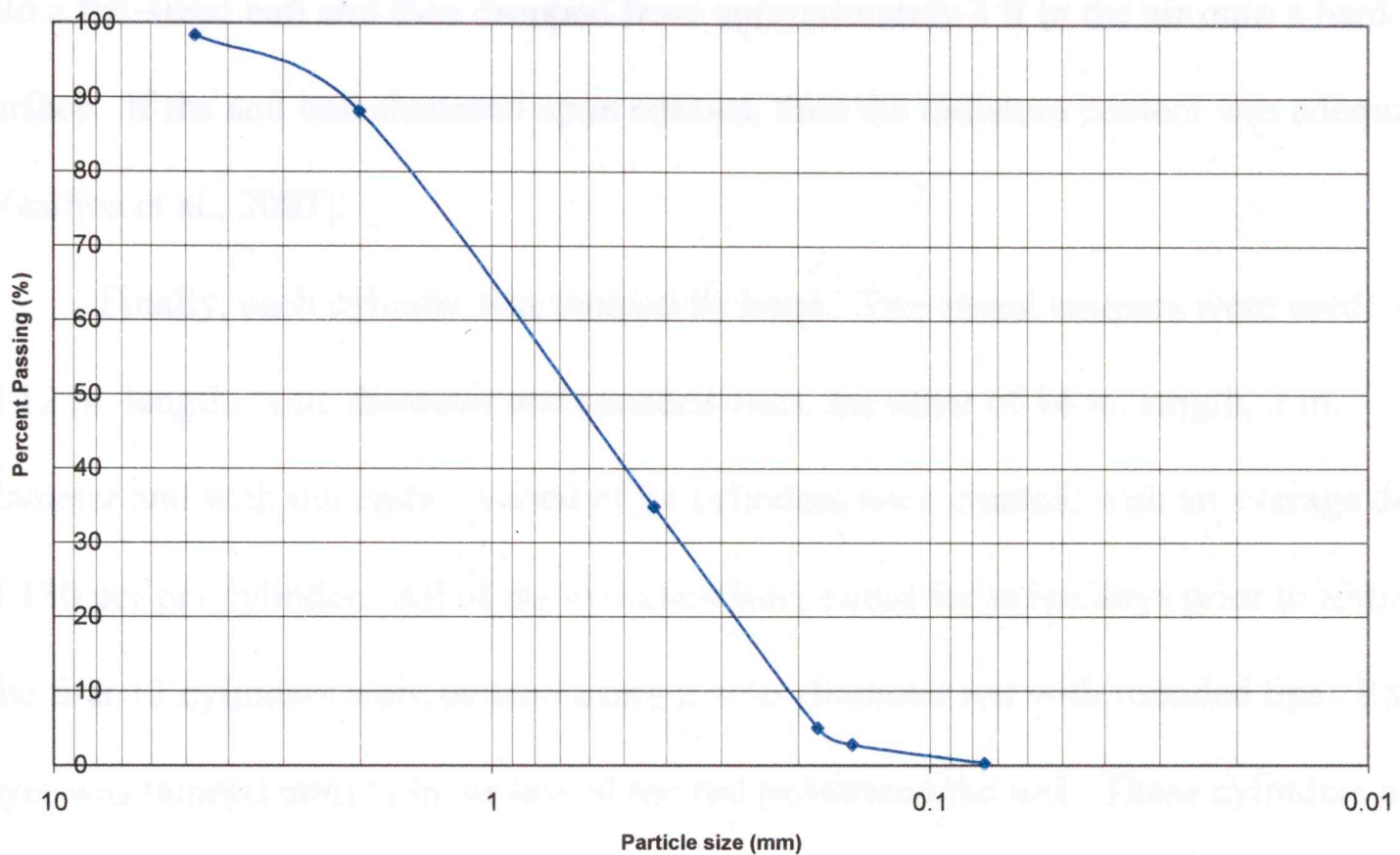


Figure 2.1: Sieve analysis of sand

Determination of the appropriate mixture for the rammed earth models was achieved through an iterative process of experimenting with different proportions of soil, compacting them into cylinders and then testing unconfined compressive strengths. The mix was deemed appropriate when it achieved a minimum unconfined compressive strength of 400 psi as well as optimum moisture content.

When preparing the cylinders for the unconfined compression tests, the different soils were mixed into batches. Each batch represented a different combination of soil proportions and was small enough to produce three 8 in. x 4 in. diameter cylinders used for the unconfined compression tests, or approximately 25 lbs of soil. In each batch the different soils were mixed together dry with the desired amount of water added at the end. Within the manual process of mixing, the optimum moisture content was

determined by using a field test. In the field test the soil mixture was hand-compacted into a fist-sized ball and then dropped from approximately 3 ft in the air onto a hard flat surface. If the soil ball shattered upon contact, then the moisture content was adequate (Vasilios et al., 2003).

Finally, each cylinder was tamped by hand. Two metal tampers were used: one of 12 in. length, $\frac{1}{2}$ in. diameter and rounded ends, the other of 14 in. length, 2 in. diameter and with flat ends. A total of 24 cylinders were created, with an average density of 130 pcf per cylinder. All of the cylinders were cured for seven days prior to testing. The first 12 cylinders were tamped using a $\frac{1}{2}$ in. diameter rod with rounded tips. Each layer was tamped until $\frac{1}{2}$ in. or less of the rod penetrated the soil. These cylinders had about 3-5 layers each. The remaining 12 cylinders were tamped with a flat-end 14in x 2in diameter aluminum rod, with about 8 layers of soil per cylinder. Each layer was tamped until the rod penetrated the soil $\frac{1}{8}$ in or less. Cure time was constant—7 days—for all cylinders while the curing locations varied. Cylinders #1-18 were cured in a humidity chamber, while cylinders 19-24 were cured outside where outdoor temperatures were on average 90°F during the day and 70°F at night.

After seven days of curing, each batch of cylinders was tested for unconfined compressive strength at 15,000 lb/min – 18,000 lb/min until failure. After testing of the 24 cylinders, the final proportions of each soil by total weight were: 50% sand, 25% silt, 9% cement, 8% clay and 8% water (**Table 2.1**). Average unconfined compressive strength of cylinders with these proportions was 528 psi, although compressive strengths increased as workmanship improved. Cylinders containing 15% cement reflected higher compressive strengths, however, for the purpose of the study the 9% cement proportion

was selected for the sake of a more economical design. Proportion values were based upon the field-tested optimum moisture contents, compressive strength and what might be more economically feasible for a homeowner in a developing nation. Although proportions were based upon total weight instead of dry weight, the moisture content in each soil was low upon visual inspection because each soil was stored outside in the summer heat. The test cylinders failed either by splitting or by shear near the corner. Failure by shear at a corner was most common. Typical failures in cylinders are shown in **Figure 2.2**.

Avg	Test No.	Stress	Sand (%)	Silt (%)	Clay (%)	Water (%)	Cement (%)
145 psi	1	103 psi	29	28.8	17.3	14.4	10.8
	2	140 psi	29	28.8	17.3	14.4	10.8
	3	191 psi	29	28.8	17.3	14.4	10.8
145 psi	4	154 psi	29	28.8	17.3	14.4	10.8
	5	169 psi	29	28.8	17.3	14.4	10.8
	6	113 psi	29	28.8	17.3	14.4	10.8
216 psi	7	248 psi	40	30	10	10	10
	8	231 psi	40	30	10	10	10
	9	169 psi	40	30	10	10	10
439 psi	10	423 psi	50	25	8	8	9
	11	425 psi	50	25	8	8	9
	12	468 psi	50	25	8	8	9
483 psi	13	474 psi	50	25	8	8	9
	14	449 psi	50	25	8	8	9
	15	525 psi	50	25	8	8	9
1,290 psi	16	1,146 psi	50	17	8	10	15
	17	1,357 psi	50	17	8	10	15
	18	1,367 psi	50	17	8	10	15
663 psi	19**	706 psi	50	25	8	8	9
	20**	503 psi	50	25	8	8	9
	21**	780 psi	50	25	8	8	9
1,452 psi	22**	1,588 psi	50	17	8	10	15
	23**	1,321 psi	50	17	8	10	15
	24**	1,448 psi	50	17	8	10	15

Table 2.1: Summary of soil mix design



Figure 2.2: Typical failures of test cylinders

2.3 Model Design

2.3.1 Model Geometry

Geometry of the model was based upon current rammed earth building dimensions, recommendations based upon the Peruvian building code for seismic adobe, and the size of the shaketable platform. According to McHenry (1984) rammed earth buildings typically were no more than 2 stories in height, had wall thicknesses between 10 in. and 24 in., and needed to maintain a height-to-thickness slenderness ratio of 15 or less. Based upon the Peruvian code (Vargas et al., 2004) door openings were recommended to be no more than one third of the width of the wall, and must be centered in the wall. Finally, the size of the shaketable platform was 4 ft in width and 6 ft in length. Based upon all the above criteria, the model geometry design was 4 ft x 4 ft x 3 ft

x 0.5 ft in length, width, height, and thickness, respectively. One door opening was centered in one of the shear walls. The door opening measured 1 ft in width and 2.33 ft (28 in.) in height. The doorway included a wooden lintel beam of 18 in. in length, providing a 3 in. bearing length on either side of the door opening. Current standards in the United States required a minimum of 8 in. bearing length (McHenry, 1984). Since the model was designed as 1/3 scale, the 3 in. bearing length on the model would equate to a 9 in. bearing length on the full scale prototype. The intent was to create a simplified house at 1/3 scale, although realistically the full-size version of the model would have been only a room: 12 ft x 12 ft footprint with walls 9 ft in height and 1.5 ft (18 in.) in thickness. A sketch of the model is provided in **Figure 2.3**.

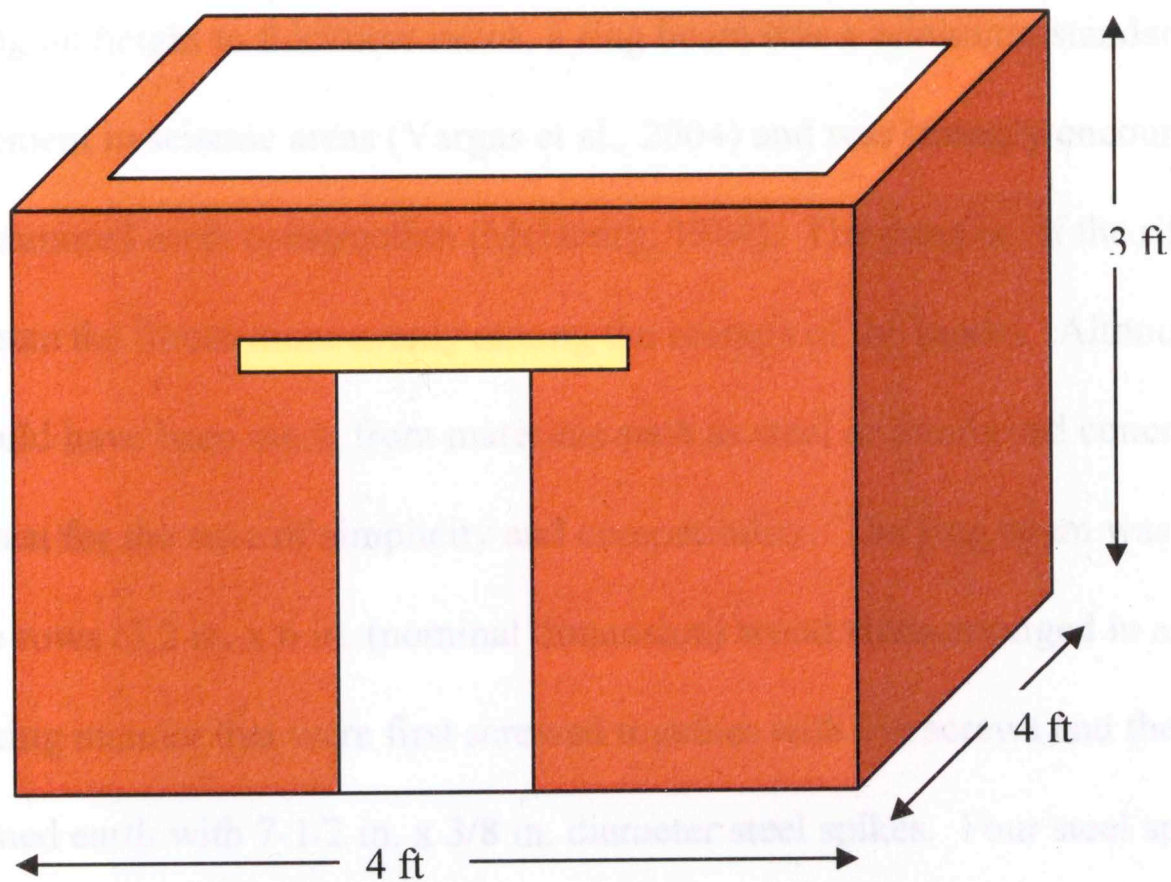


Figure 2.3: Typical geometry used for rammed earth models

2.3.2 Reinforcement

One of the objectives of the research was to determine the effectiveness of reinforced rammed earth during an earthquake. To do this, two of the four models were designed without reinforcement (as controls), while the third model was designed with a wooden ring beam and the fourth model was wrapped with a plastic mesh. The reasons for using two unreinforced models instead of only one were that the first model was expected to be a trial run. If the results were good, they were kept, but otherwise the first model was expected to serve as a tool for learning how to build the other models more effectively. The second model was built without reinforcement to experiment with a different loading protocol—as discussed later in the Data Collection Section.

A ring beam was chosen as the type of reinforcement for the third model because depending on height to thickness ratios, a ring beam was a minimum standard of reinforcement in seismic areas (Vargas et al., 2004) and was strongly encouraged in modern rammed earth construction (McHenry, 1984). The purpose of the ring beam was to distribute the forces more evenly among the corners of the model. Although the ring beam could have been made from materials such as steel or reinforced concrete, wood was chosen for the sake of simplicity and compatibility. The ring beam was designed with two rows of 2 in. x 6 in. (nominal dimension) wood studs arranged in an interlocking manner that were first screwed together with 3in screws and then secured to the rammed earth with 7-1/2 in. x 3/8 in. diameter steel spikes. Four steel spikes were placed per wall, through pre-drilled holes in the wood, at a spacing of 9 in. from each end and 10 in. spacing in the center (**Figures 2.4 and 2.5**).

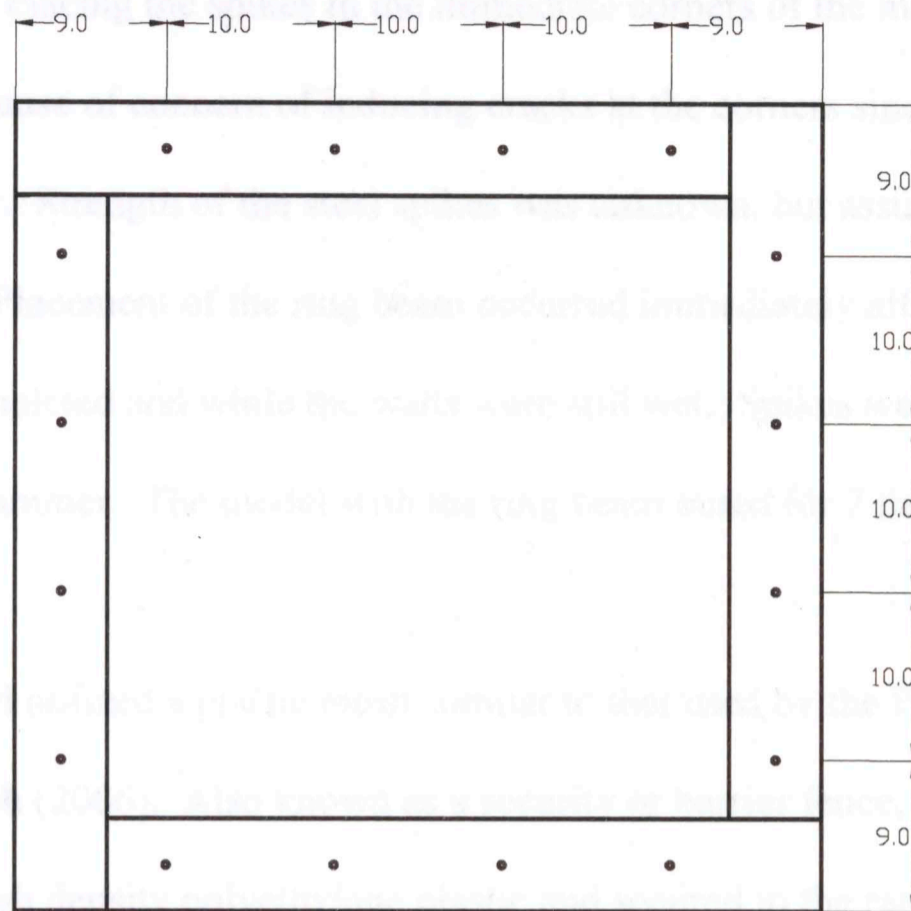


Figure 2.4: Plan view sketch of ring beam

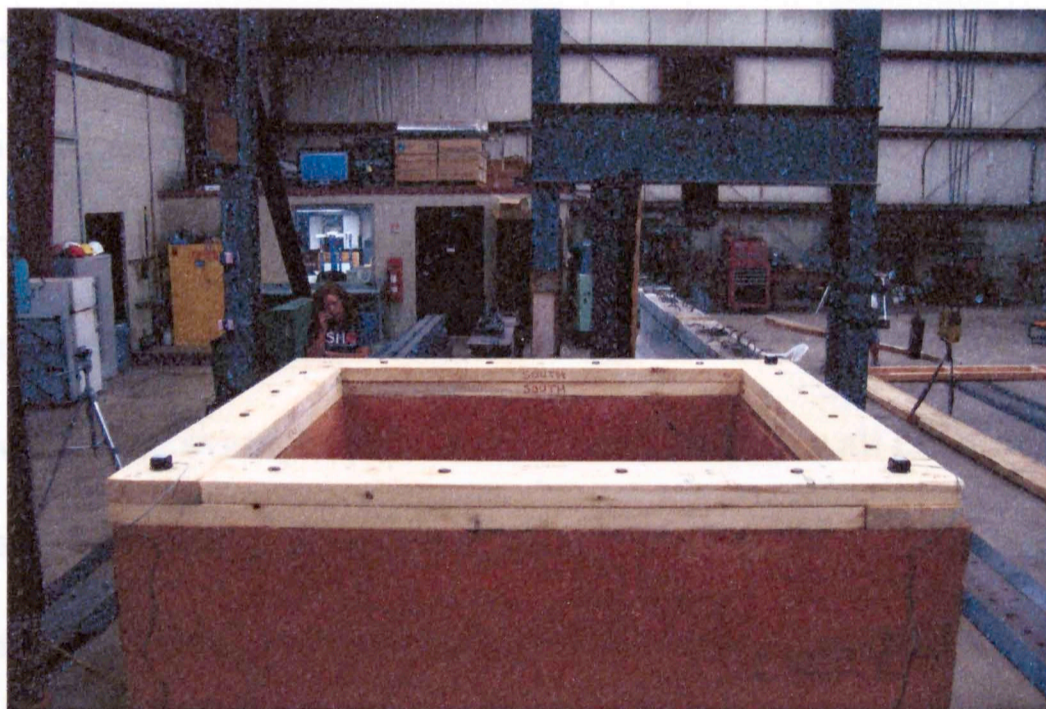


Figure 2.5: View of Ring beam on Test 3 model with accelerometers

Spacing of the spikes was intended to be as even as possible and greater than the wall thickness itself. Placing the spikes in the immediate corners of the model was avoided however because of concern of inducing cracks at the corners since rammed earth is weak in shear. Strength of the steel spikes was unknown, but assumed to be a minimum of 36 ksi. Placement of the ring beam occurred immediately after compaction of the model was completed and while the walls were still wet. Spikes were secured into place with a sledge hammer. The model with the ring beam cured for 7 days prior to testing.

The last model utilized a plastic mesh, similar to that used by the PUCP study of external polymer mesh (2006). Also known as a security or barrier fence, the orange mesh was made of high density polyethylene plastic and secured to the rammed earth model using 1 in galvanized "Grip-Rite" nails with round plastic caps to avoid punching of the nail through the wall surface. Nail spacing on the wall was originally intended to be no less than the wall thickness (6 in.), but the nail pattern resulted to be more random than systematic. Realistically, in a developing nation where someone is building his/her own home, a random nail pattern is more probable than an evenly spaced nail pattern. The random nail pattern was therefore considered a worst-case scenario. A total of 131 nails were used. On the average there were 25 nails on each wall exterior, 4 nails at each wall interior, and 4 more nails at the top of each wall. Care was taken, however, to ensure the mesh was as snug as possible around the corners and the door opening without yielding and that the wider bands of the mesh were horizontal. The intent behind using the mesh was to prevent collapse of the structure, instead of providing structural reinforcement.

2.3.3 Formwork Design

To construct the models, wooden formwork was used similar to that used for concrete. Wall panels were made of $\frac{3}{4}$ in. plywood and 2 in. x 4 in. studs. The base consisted of plywood bolted directly to the table with $\frac{3}{8}$ in. diameter bolts (A325) and $\frac{3}{8}$ in. washers. Screwed to the base was a “lip” built from 2 in. x 4 in. (nominal dimension) wood studs. The “lip” was created to secure the rammed earth to the shaketable and transfer the base shear into the model (**Figure 2.6 and Figure 2.7**).

Formwork walls were designed to be reused. The outer walls were bolted together with $\frac{3}{4}$ in. diameter bolts, while the inner walls were attached by 3 in. lag screws and $\frac{1}{4}$ in. bolts and washers. Sketches of the walls with the corresponding pictures are provided in **Figures 2.8 through 2.13**.

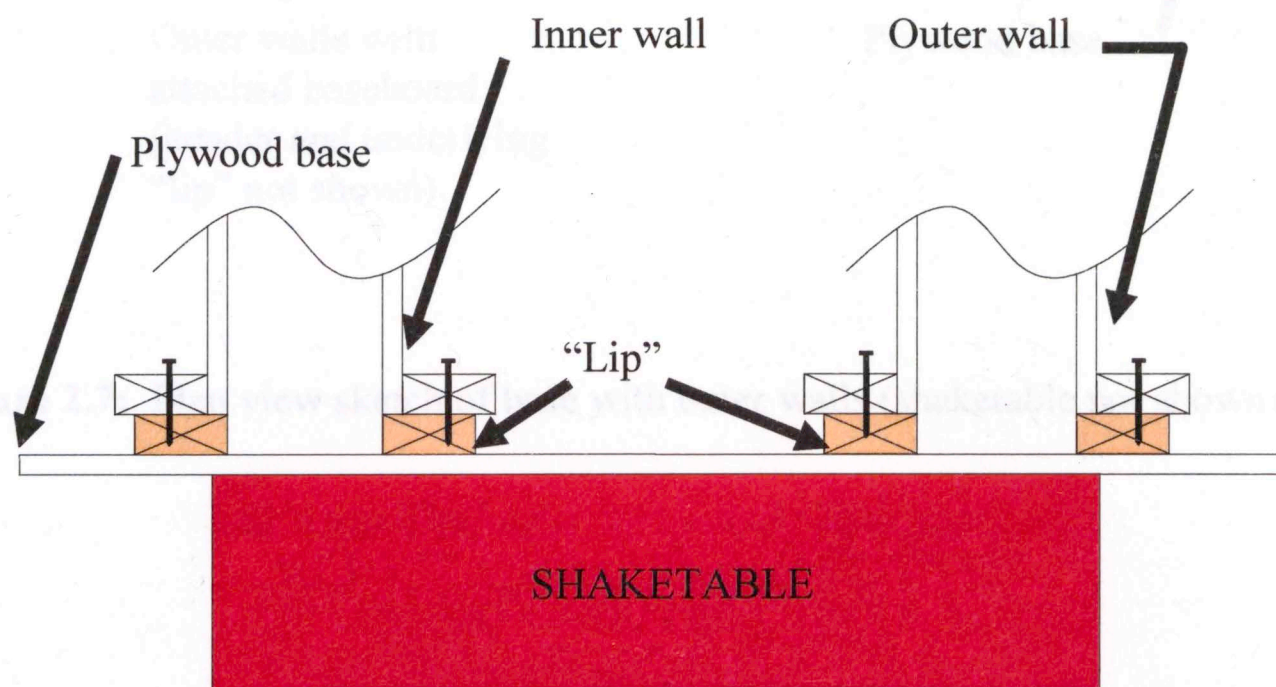


Figure 2.6: Cross-section of shaketable platform with plywood base

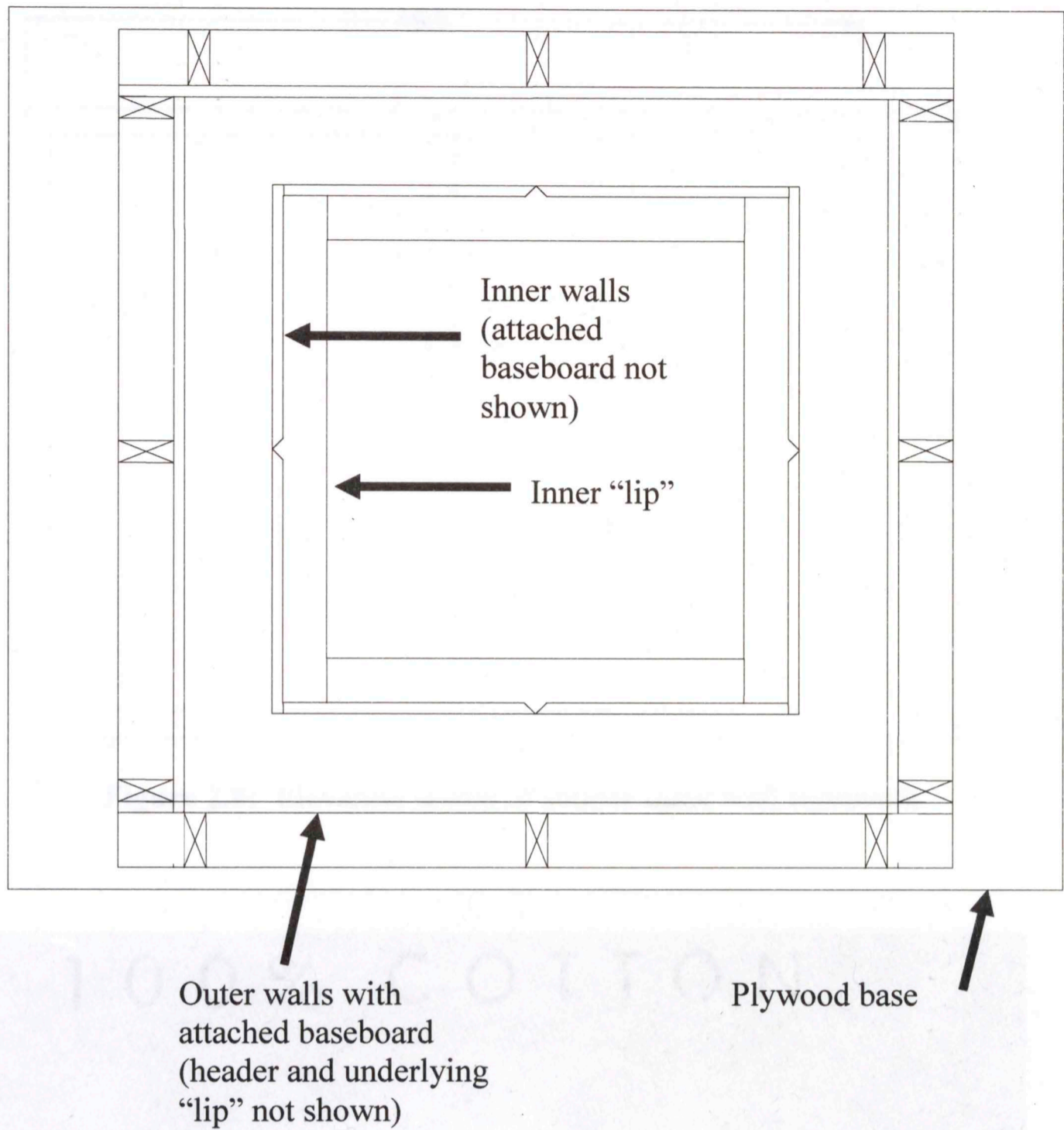


Figure 2.7: Plan view sketch of base with outer walls (shaketable not shown)

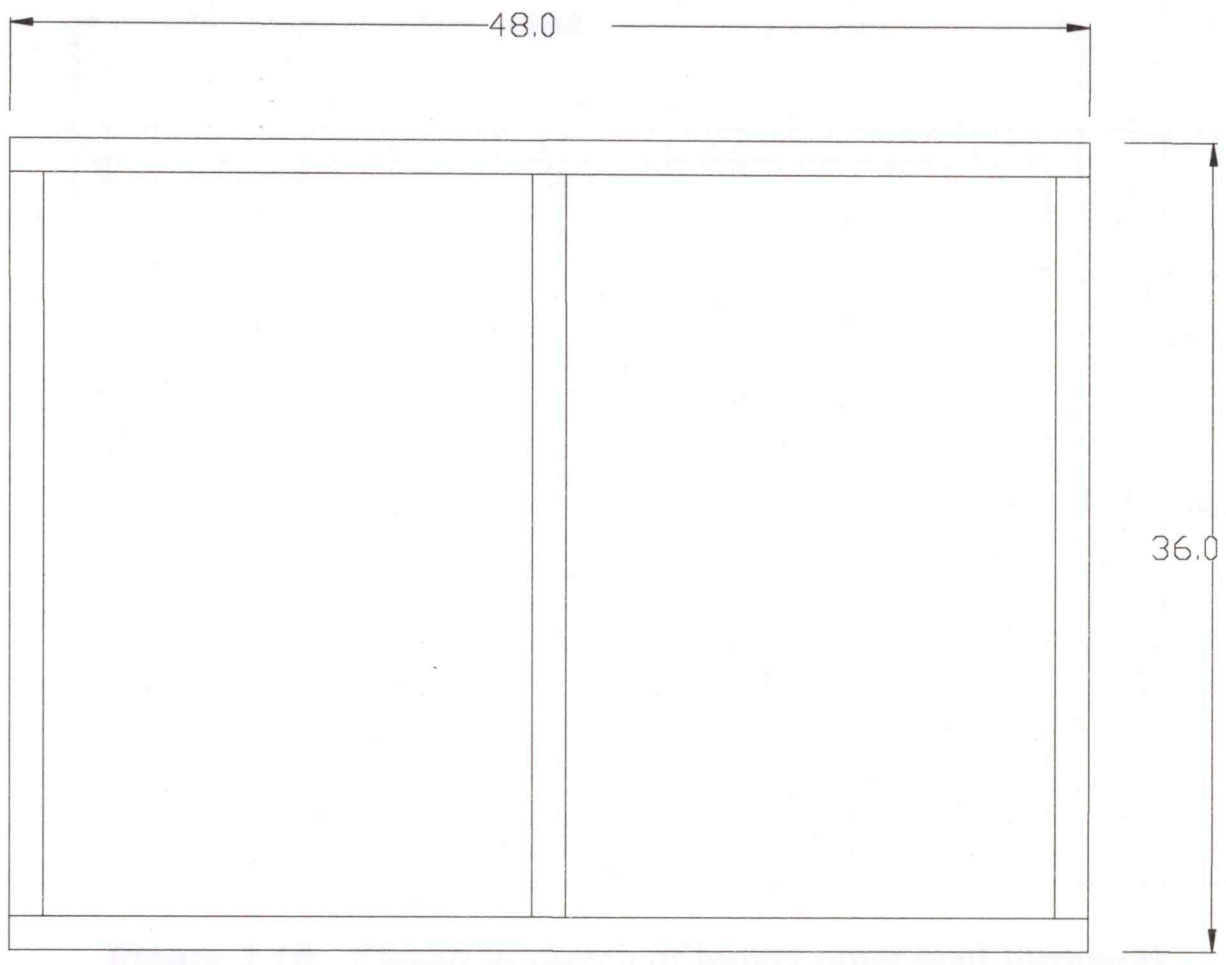


Figure 2.8: Elevation sketch of shorter outer wall formwork



Figure 2.9: Picture of shorter outer wall formwork

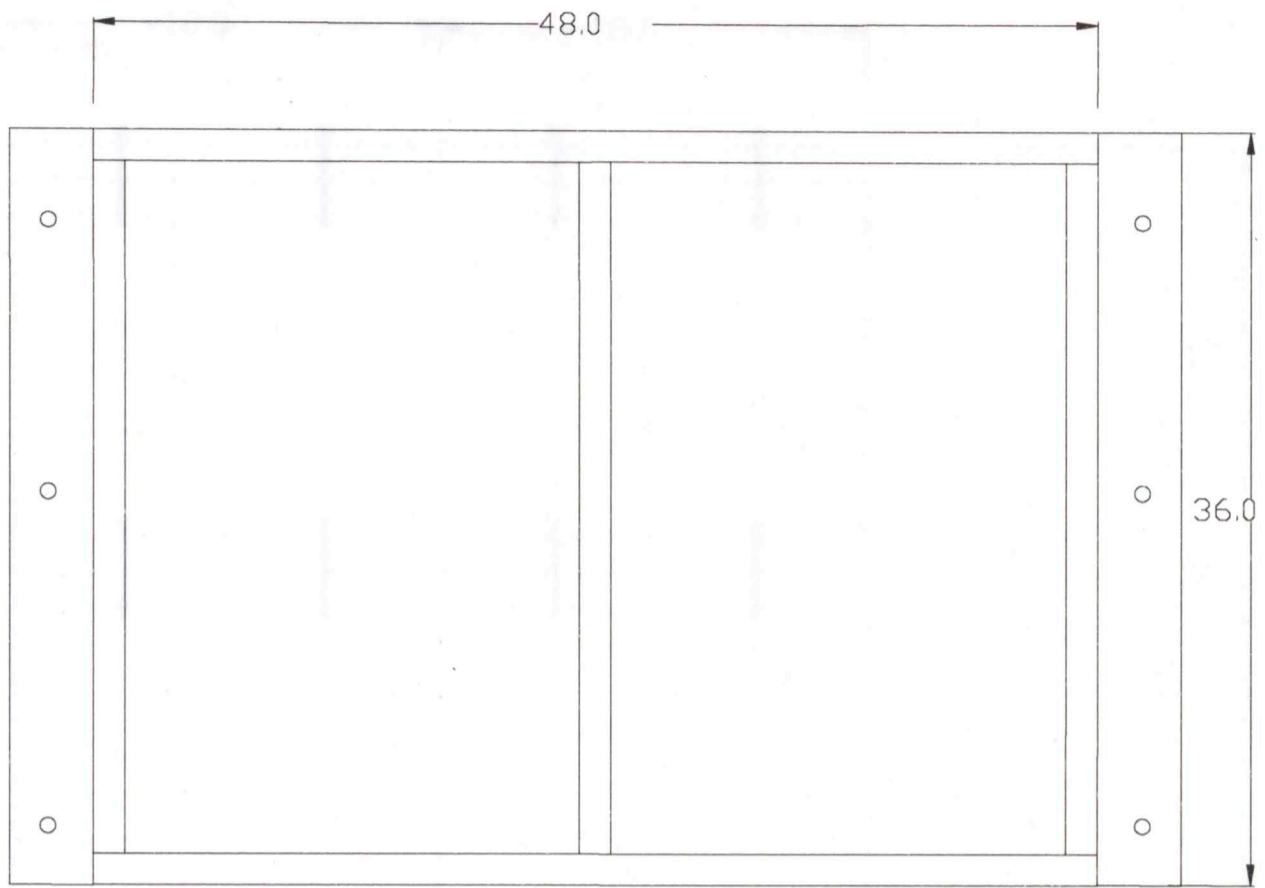


Figure 2.10: Elevation sketch of longer outer wall formwork

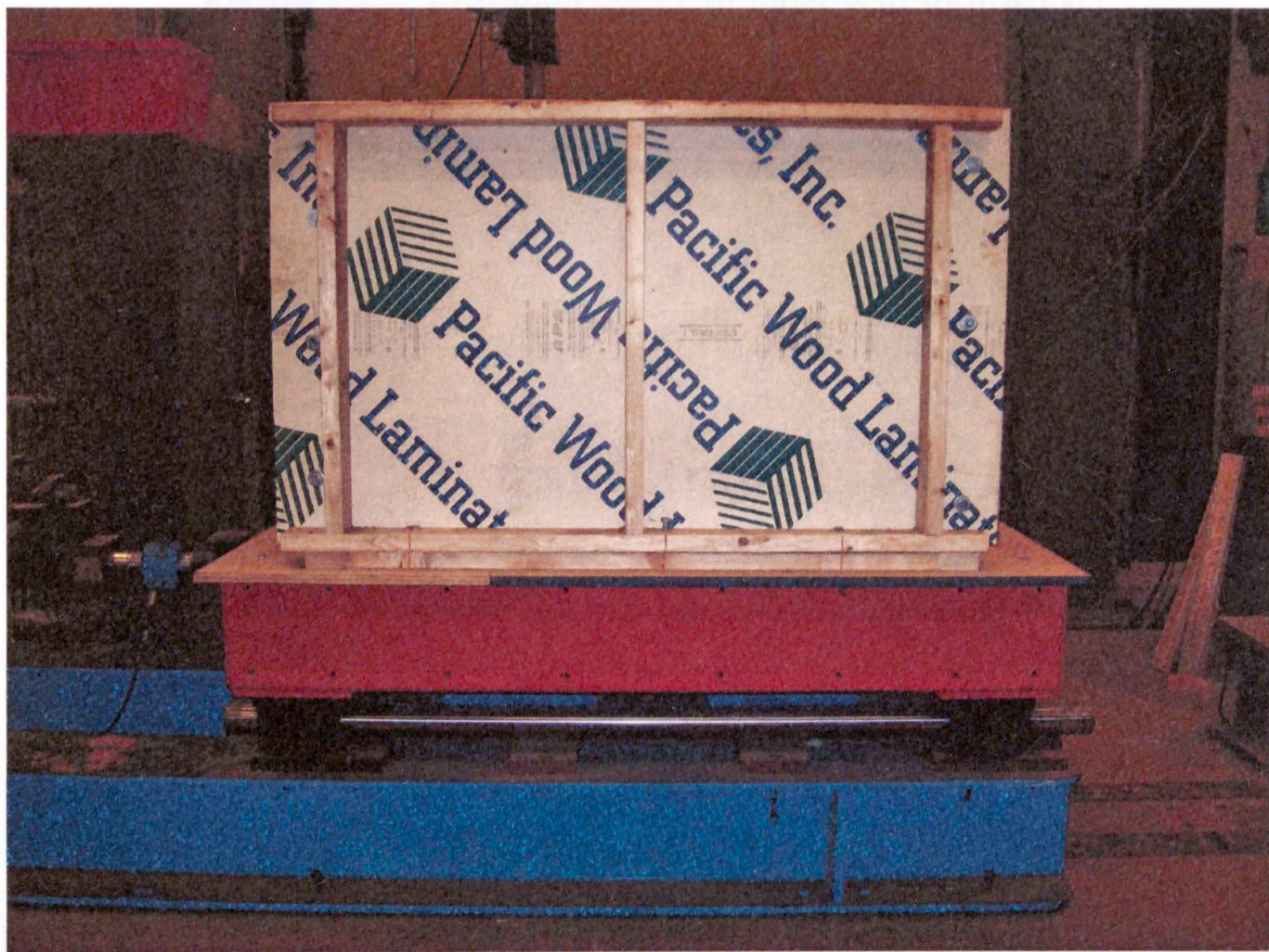


Figure 2.11: Picture of longer outer wall formwork

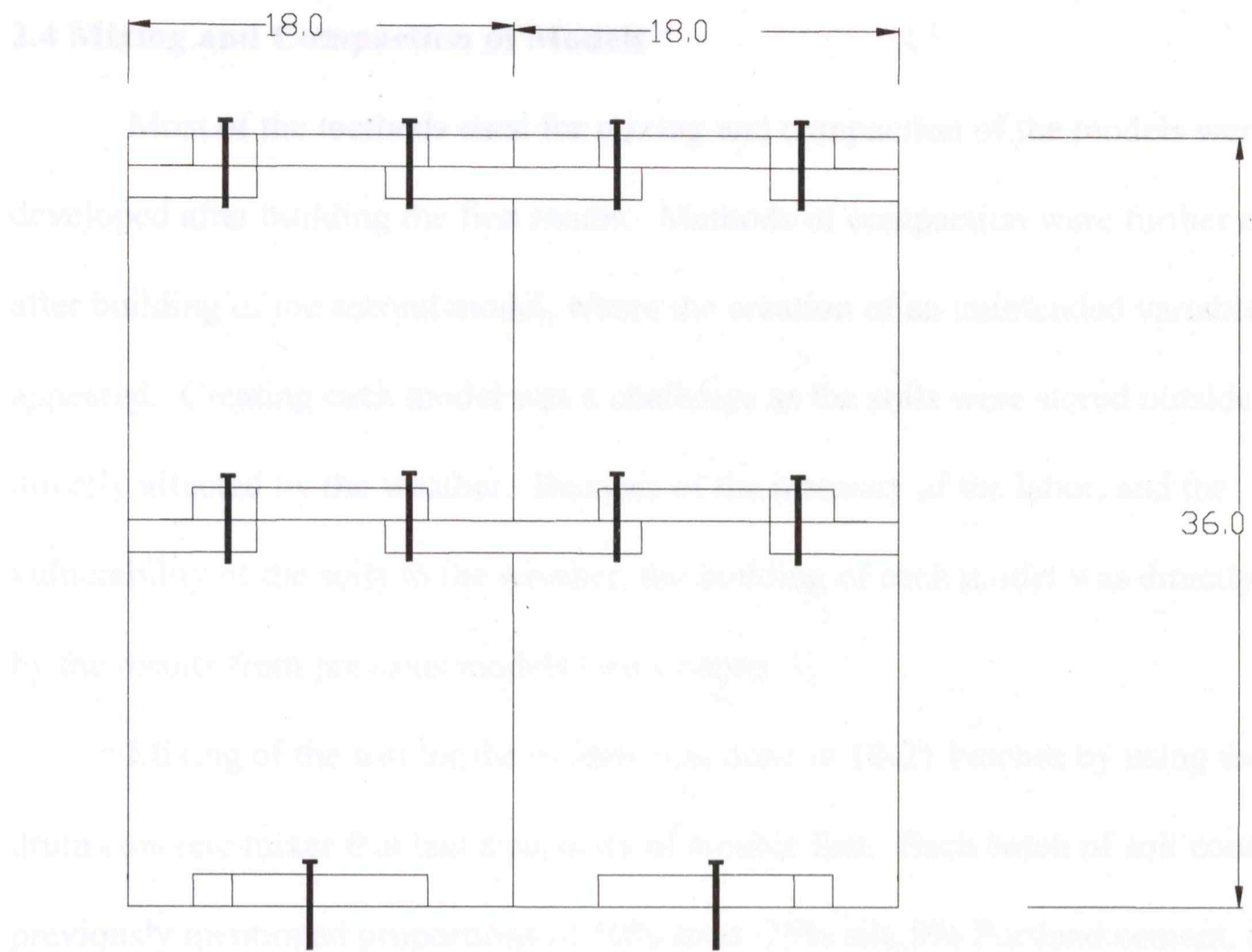


Figure 2.12: Elevation sketch of inner wall formwork

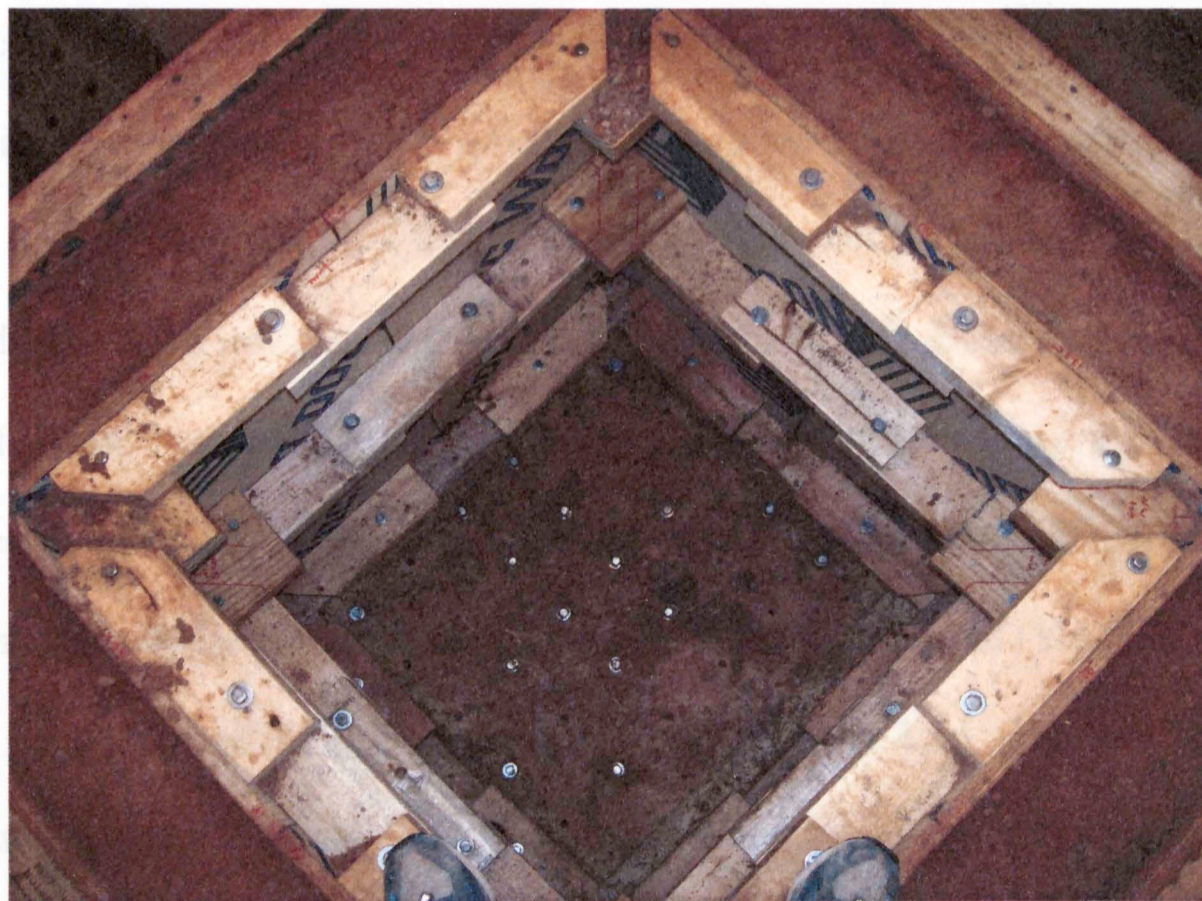


Figure 2.13: Plan view picture of all inner wall formwork (Test 1)

2.4 Mixing and Compaction of Models

Most of the methods used for mixing and compaction of the models were developed after building the first model. Methods of compaction were further modified after building of the second model, where the creation of an unintended variable appeared. Creating each model was a challenge as the soils were stored outside and directly affected by the weather. Because of the intensity of the labor, and the vulnerability of the soils to the weather, the building of each model was directly affected by the results from previous models (see Chapter 3).

Mixing of the soil for the models was done in 18-21 batches by using the vertical drum concrete mixer that had a capacity of 4 cubic feet. Each batch of soil contained the previously mentioned proportions of 50% sand, 25% silt, 9% Portland cement, 8% clay and 8% water by total weight. Based upon a 130 pcf density, estimated from the test cylinders, the percentages equated to: 96.6 lbs of sand, 48.2 lbs of silt, 17.3 lbs of type II Portland cement, 15.4 lbs of clay and 15.4 lbs of water. The sand was stored in an outdoor pile, open to the changes in weather. The silt was stored in aluminum garbage cans with lids, although stormy winds occasionally removed the lids and wet the silt. Because the silt had a low plasticity, wet silt was tolerable and easier to mix than dry silt. The clay for Test 1 was not processed and had a moisture content above the plastic limit, but for Test 2, 3 and 4 the clay was dried and pulverized to pass through a ¼ in. wire mesh (similar to a # 4 sieve) until more than 80% of the clay passed (Vasilios et al., 2003). A photograph of the wire mesh is provided in **Figure 2.14**. The amount of water was adjusted during mixing depending on visible moisture content of the silt and field optimum moisture content tests of the rammed earth mixture. Weights of soil were total

weight as opposed to dry weight. Photographs of a typical batch layout and the vertical drum mixer are provided in **Figures 2.15** through **2.17**.



Figure 2.14: Picture of 1/4 in. wire mesh used to sieve the clay



Figure 2.15: Vertical drum mixer, wheelbarrow and scoops for mixing and transporting



Figure 2.15: Typical layout of soil batch (equivalent to one compacted layer)



Figure 2.16: Vertical drum mixer, wheelbarrow and scoops for mixing and transporting



Figure 2.17: Pouring of soil into mixer

After mixing, the soil was transported with a wheelbarrow and gradually scooped, distributed and compacted into layers (**Figures 2.17** through **2.20**). Compaction was done manually by using 2 customized steel tampers weighing approximately 15 lbs each. One tamper had a rectangular footprint of 5inx6in while the other had a similar area but with a rounded-edge rectangular footprint. The rounded-edge tampers were cut from circular tampers in order to fit inside the formwork. Tampers were dropped at 6-12 inches above the soil layer 20 times per 36 square inches of soil area (Vargas, 1992). Each layer was approximately 2 in. thick after compaction. Projected density of the rammed earth was 130 pcf. The process of mixing and compaction was continuous and ranged from 6 to 12 hours of work, depending on the number people assisting. Because of the heavy materials and constant manual labor, it was impossible to maintain a

constantly running operation. Labor was rotated between mixing, transporting, and compacting, but a break was still needed. Stopping for a one hour lunch created the unintended variable of a cold joint, or a lack of bond between two layers, in the second rammed earth model. Location of the cold joint along the height of the wall was modified for tests 3 and 4. In test 2 the cold joint was located approximately one foot from the base of the model. In tests 3 and 4 the cold joint was located approximately 2 to 2.5 ft from the base of the model—or the upper third of the height of the model. After compaction each model was cured for 7 days and then tested on the shaketable. The formwork remained on the model through the first day of curing to prevent any accidents that would damage the model until the soil had hardened.

After testing of each model, random fragments were measured for density and moisture content. The moisture content was measured by weighing a sample of the rammed earth, placing it in an oven at 110°C for at least 24 hours, and then measuring the sample again. Difference in the weights between the wet and dry samples was the weight in water in the rammed earth. Density was measured by weighing the sample and then submerging it into a beaker full of water. The displaced volume before and after the rammed earth was submerged into the beaker was recorded. Results of the moisture content and density tests for each sample are presented in Chapter 3.

Figure 2.19: View of soil inside formwork prior to compaction



Figure 2.18: Placement of soil into formwork



Figure 2.19: View of soil inside formwork prior to compaction



Figure 2.20: Compaction of soil with steel tampers

2.5 Test Setup

Several instruments were involved in the testing of each rammed earth model: a shaketable to deliver a base motion, a function generator to deliver the type of load, accelerometers to record the dynamic motion of the model, LabView software to record the accelerations from the accelerometers, digital cameras to record the motion of each model, and pictures before and after testing.

The shaketable consisted of a 1,400 lb (635kg) welded steel motion platform, with a 6 ft x 4 ft horizontal footprint. Motion of the platform was on a single axis (north-south direction), facilitated by four Thompson extra rigid precision linear bearings of 3 in. (75°mm) in diameter. Each bearing had a dynamic load capacity of 10,000 lbs providing a maximum load rating of 40,000 lbs. Each rammed earth model weighed approximately

2,800 lbs. Actuating the platform was a fatigue-rated 11,240 lbf (50 kN) hydraulic cylinder with an effective piston area of 3.875 in.² (2.5×10^3 mm²), and a ± 2.95 in. (± 75 mm) dynamic stroke. The steel platform was supported by W12x65 beams bolted to the concrete strong floor, which had a depth of 4 ft with W36x150 embedded beams (Kuehn, 2000).

The type of load was controlled by a function generator which could deliver sine waves, square waves, or saw-tooth waves. The function generator also controlled the frequency up to several hundred hertz, but physical aspects of the shake table including mass of the table and speed of the hydraulic pump limited the maximum deliverable frequency to approximately 100 Hz. For the purposes of the research only up to 20 Hz was needed. The amplitude of the wave was controlled by the displacement range of the shaketable.

To record the relative acceleration of the structure with respect to the shaketable, a total of four ADXL150 EM-1 single axis accelerometers were used. Three accelerometers in Test 1 were used: one on the shaketable, the second on top of the northeast corner of the model, and the third on top of the northwest corner of the model. For Tests 2, 3 and 4 an additional accelerometer was placed on top of the southwest corner of the model. The intent was to record accelerations between each corner of the model, and compare changes in the data against video observations. Data from the accelerometers was recorded using LabView software.

Digital cameras were used to record the visible response of each model during testing. One camera was used for Test 1, which faced only the east wall. After the results of Test 1, two cameras were used for the remaining tests in order to view all sides

of the model at the same time. For Tests 2, 3 and 4, one camera was located near the southeast corner to view both the south and the east walls, while the second camera was located near the northwest corner in order to view the north and west walls. The videos allowed the opportunity to view the shaking of the models in slow motion, providing more detailed information on the occurrence of different cracks or other observations and elapsed time between events.

Before each shaketable test, pictures were taken of each wall of the model. Any pre-existing cracks were outlined with a marker, and each wall was labeled as North, South, East or West. After each test, more pictures were taken of each wall of each model to record locations of all visible cracks. Sketches and photographs of the test setup are provided in **Figures 2.21** through **2.23**.

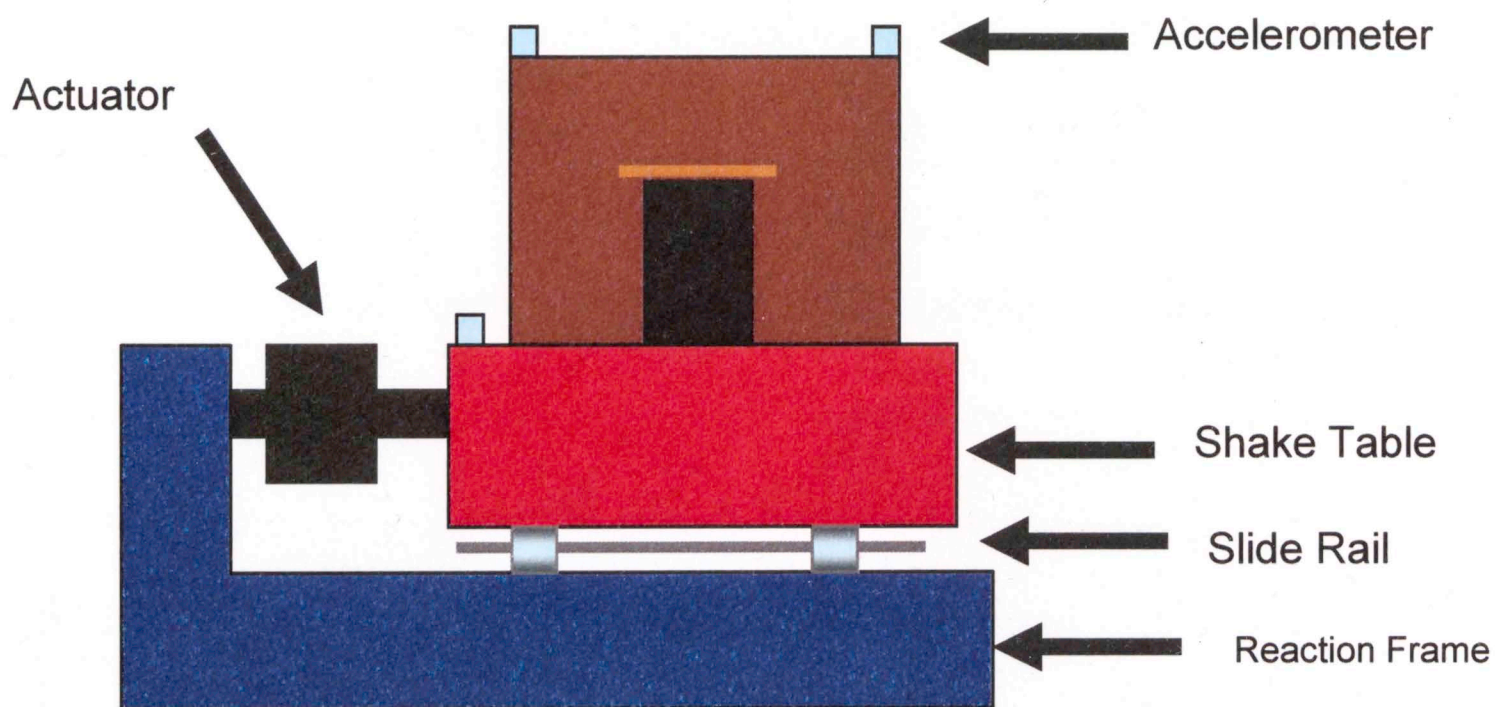


Figure 2.21: Elevation view sketch of test setup

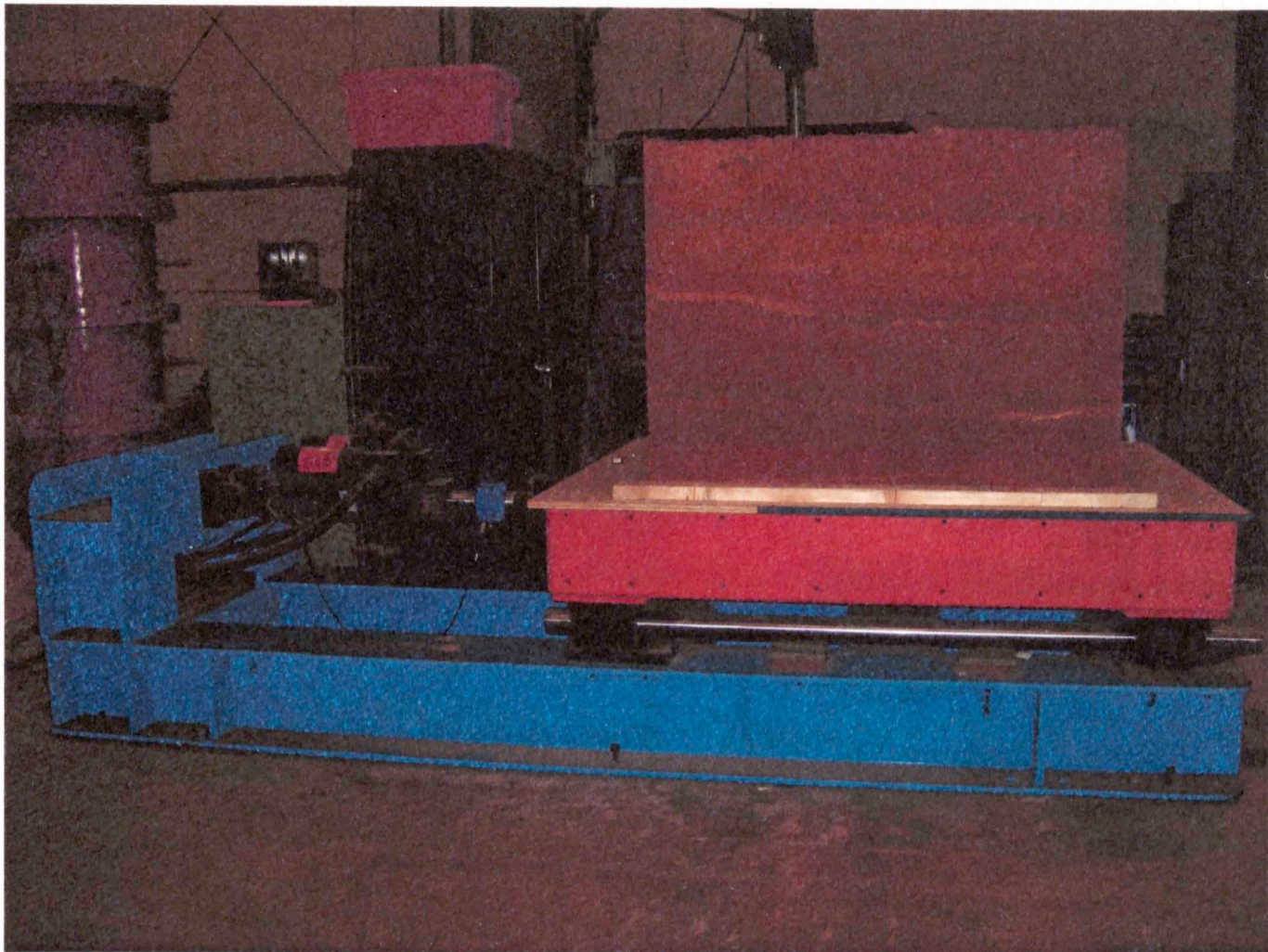


Figure 2.22: Photograph of test setup

- 1 = Accelerometer at shaker table
- 2 = NE = accelerometer at top of wall of model at the northeast corner
- 3 = NW = accelerometer at top of wall of model at the northwest corner
- 4 = SW = accelerometer at top of wall of model at the southwest corner
- 5 = Camera at northeast corner
- 6 = Camera at northwest corner

Figure 2.23: Plan view sketch of test setup (in tests 2, 3 and 4)

2.6 Leading Protocol

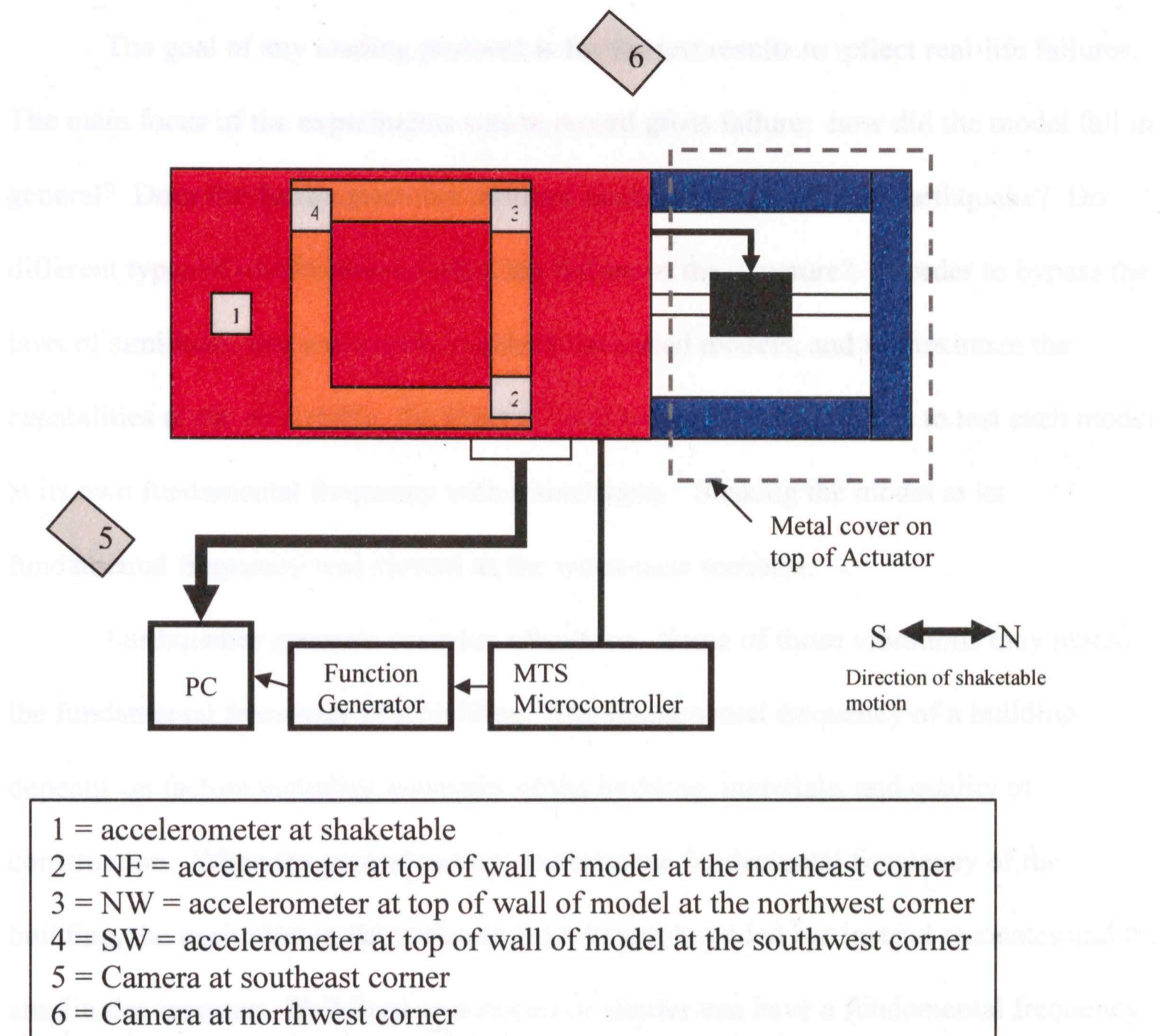


Figure 2.23: Plan view sketch of test setup on tests 2, 3 and 4

2.6 Loading Protocol

The goal of any loading protocol is for the test results to reflect real-life failures. The main focus of the experiments was to record gross failure: how did the model fail in general? Does the failure resemble rammed earth structures after an earthquake? Do different types of reinforcement affect the failure of the structure? In order to bypass the laws of similitude that are usually required for scaled models, and to maximize the capabilities of the shaketable, the strategy used to load the models was to test each model at its own fundamental frequency with a sine wave. Shaking the model at its fundamental frequency was viewed as the worst-case scenario.

Earthquakes generate complex vibrations. Some of those vibrations may match the fundamental frequency of a building. The fundamental frequency of a building depends on factors including geometry of the building, materials, and quality of construction. When the ground motion matches the fundamental frequency of the building, the excitation in the structure is no longer bounded but instead resonates and the amplitudes increase. Buildings two stories or shorter can have a fundamental frequency of approximately 5 Hz. Fundamental frequencies tend to decrease with the building height, so taller buildings may have frequencies of approximately 2 Hz or less.

Fundamental frequencies are unique to each structure, so it is not necessary to scale the fundamental frequency for a 12 ft width x 9 ft height prototype onto a 4 ft wide x 3 ft high model. The model is made of the same materials and density as the prototype, but is obviously shorter and would resonate at a higher frequency. Shaking each model at its own fundamental frequency is theorized as a simpler method of dynamic testing because the purpose is to create the undamped resonance in the structure, which is

considered the worst-case scenario. Therefore, instead of comparing model frequencies to prototype frequencies, the method of relating model results to prototype results is to project the final gross failure. The prototype should fail in a similar manner to the model if each experience resonance at their own fundamental frequencies.

The model was designed with one door opening to create an imbalance of stiffness between the shear walls parallel to the motion of the shaketable. A door opening reduces the shear capacity along the east wall by reducing the amount of area possible to resist shear forces. Diagonal cracks propagating from door (or window) openings are typical in structures damaged from earthquakes because of the stress concentrations at the reentrant corners. Research on adobe models under seismic loads showed out-of-plane bending on walls perpendicular to the shaketable motion as a common failure mode. Both adobe and rammed earth are made primarily of soil, but the rammed earth models in this study are built as monolithic structures with continuous joints, so out-of-plane bending may occur differently than in adobe models.

To locate the fundamental frequencies, each model was first tested with a resonance test. The resonance test was a small amplitude ($\frac{1}{4}$ in.) shaking of the model. Fundamental frequency was estimated by LabView and displayed through a graph on a screen. On some of the models the graph fluctuated between two peaks of frequencies, and the fundamental frequency was recorded as an average between the peak frequencies.

In Test 1, the method of loading was to shake the model at three times the recorded fundamental frequency. This was due to an initial misunderstanding of the similitude laws where it was thought that the fundamental frequency needed to be scaled three times since the model was a one-third scale. At the beginning of the test, the model

included a roof weighing approximately 850 lbs as an attempt to use a scaled roof weight based upon a 2 psf roof weight (wood framing with metal panel) on a full-scale structure. This was also an initial misunderstanding of the similitude laws, and the roof was omitted in later tests. Test 2 was created to experiment with a simpler method of initiating the experiment with the fundamental frequency of the model and increase the displacement of the shaketable until a failure occurred. If no failure occurred, then the displacement of the shaketable was held constant (at maximum displacement) while the frequency was gradually increased until failure of the model occurred. After the results from Test 2, the protocol was modified to start at the fundamental frequency of the model while displacement of the shake table was gradually increased until full displacement of the shake table was reached (± 3 in.). Then while the shake table was at maximum displacement, the frequency was gradually increased at increments of 2 Hz every 30 seconds until failure of the model was achieved. During testing, a model was considered as failed when cracks were fully propagated across the height or width of a wall, or the area above the door opening. See **Table 2.2** for a summary of model variables and loading protocol.

Test	Reinforcement	Load	Load increase
1	none	3ff	to max d
2	none	ff	to max d, then f @ 2 Hz increments
3	ring beam	ff	to max d, then f @ 2 Hz increments
4	plastic mesh	ff	to max d, then f @ 2 Hz increments
Notes: ff = fundamental frequency f = frequency d = shaketable displacement			

Table 2.2: Summary of model variables and loading protocol

2.7 Data Processing

The fundamental frequency was recorded initially through LabView, and later with MatLab. Processing of the data was through Matlab to view the recorded fundamental frequencies, different increments of frequencies and the relative accelerations of each corner during testing. Frequencies in Matlab were calculated using a spectral plot, where the frequency is calculated using the squared value of the Fast Fourier Transform (FFT). Time history graphs of the acceleration (in units of gravity) versus time (in seconds) were plotted of each corner with respect to the shaketable. Relative accelerations were calculated using simple algebraic manipulations: acceleration data from one corner was subtracted from another corner, or acceleration from one corner was subtracted from the shaketable acceleration. Time history graphs of the relative acceleration between corners of each model were developed in order to observe which corners of the model moved in the same direction. For example, if the northeast and the northwest corners of the model moved in the same direction during testing, the difference between their accelerations would be zero. If the northwest corner moved in a different direction than the northeast corner, however, the difference in accelerations would reflect a value; the larger the difference in value, the larger the disparity in direction between the two corners. Reasons for disparities between the corners of the model will be discussed in Chapter 3.

CHAPTER 3: TEST RESULTS

3.1 Introduction:

This chapter summarizes the observations and results made per shaketable test of each model, with a discussion of the results at the end of the chapter. Information was gained from pictures, video and accelerometer data. Observations were recorded during preparation, testing, demolition, viewing of the videos, and data processed through MatLab. Pictures of the models before and after failure are provided, as well as the graphs of the relative accelerations.

The primary focus was to record the gross failure of each model and determine if the reinforcements were effective in preventing collapse. Secondary goals were to observe whether each model provided any signs of weakening prior to collapse, and if there was a pattern of failure among the models. A summary of the shaketable test results is provided in **Table 3.1**.

Table 3.1: Summary of Shaketable Test Results

Test No.	Failure Freq. (Hz)	measured	calculated	Density (pcf)	Moisture Content (%)
		Natural Freq. (Hz)			
1	15	4-6	5.3	154	5.4
2	12	4-6	4.8	128	(not recorded)
3	10-12	4-6	5.0	126	7.9
4	10	4-6	5.0	145	7.5

In Table 3.1, the measured fundamental frequency refers to the frequency calculated using LabView at the time of the test. The calculated fundamental frequency refers the accelerometer data processed through Matlab. All failure frequencies were

calculated from the accelerometer data, through Matlab. There is no value of the moisture content for the model in Test 2 because the rammed earth fragments were misplaced.

3.2 Test 1: Unreinforced Model at Scaled Frequency

3.2.1 Preparation Observations

During preparation of the model there was a 30 minute delay between compaction of the first and second layer, and another delay of one to two hours at the midheight of the model. Layers in the upper half of the model were more wet than optimum moisture content because the soil was stored outside and received the rains of an afternoon thunderstorm on the day of compaction. Despite attempts to reduce the amount of water added due to the increased moisture of the silt and sand, tamping was noticeably more difficult as the soil mixture kept shifting inside the formwork. Visible differences in moisture content were reflected in the pictures as more distinct layers appeared on the lower half of the model than the upper half. During the quick pace of preparing the mixture, the red clay was omitted from the third layer of the model (measured from the base). In the pictures the third layer was noticeably greyer than the other layers. White hydro-stone plaster was placed on the top of the model to provide a flat surface for the roof on the model.

3.2.2 Test and Video Observations

Prior to testing, the door opening was bowed and exhibited a few shrinkage cracks (**Figure 3.1**). The fundamental frequency was measured between 5Hz and 6Hz. Test 1

evolved into three sub-tests on the same model. The first test, Test 1-A was to record the fundamental frequency. The second test, Test 1-B utilized the roof made of steel and wood. Frequency of shaking was held at three times the fundamental frequency, 15 Hz, with gradually increasing amplitude of 0 inches to ± 0.5 inches of the shaketable displacement. During testing, the roof started to vibrate off the model so the test was stopped and the roof was removed. In Test 1-C, the model was again shaken at 15 Hz with increasing amplitude from 0 to ± 1.2 inches of the shaketable displacement. The shrinkage crack above the door was the first to develop through the east wall. Approximately one minute later, diagonal cracks from the corners of the door opening were visible. At ± 0.94 inches of the shaketable displacement the diagonal cracks above the lintel had fully developed. After the diagonal cracks developed in the east wall, the lintel began to vibrate out of the model. Eighteen seconds later, the lintel fell onto the floor. Five seconds after the lintel fell, fragments from the north wall were observed falling. Three seconds later, or a total of eight seconds after the lintel fell, the northwest corner of the model fell with a sudden "pop," taking the accelerometer with it. The video camera was placed only in front of the east wall, therefore although the northwest corner was seen falling, there was no video record of when that corner started cracking. The test continued for another 21 seconds until the unsupported sections of the rammed earth above the door finally collapsed. **Figure 3.2** through **Figure 3.11** show walls of the model before and after testing.

3.2.3 Picture and Demolition Observations

Figures 3.2 through 3.5 show the failures observed on the east wall. The diagonal crack north of the lintel continued until it reached the reentrant corner at the

northeast end of the model. A close-up view was taken at the exterior wall on the southeast corner, near the lintel, where the cracks eroded during testing (**Figure 3.4**). Also found along the cracked surfaces were isolated “balls” of silt as seen in **Figure 3.5**. The silt was originally recorded to have a low plasticity, and the balls of silt were easily crushed between the fingers. **Figure 3.13**. The collapse of the lintel was apparent at

Failure at the northwest corner of the model was localized, as seen in **Figures 3.7 and 3.8**. Vertical cracks were contained above the midheight of the model, as seen in **Figure 3.9**. A diagonal crack occurred at the lower half of the north wall. On the outside of the north wall, the diagonal crack was approximately at a 45 degree angle (**Figure 3.10**). Upon inspection of the interior of the north wall, the crack was horizontal along the grey third layer, or the layer in which the clay was omitted (**Figure 3.11**). The transition from a diagonal crack on the north wall to a vertical crack at the reentrant corner occurred approximately at midheight of the northwest corner. Rammed earth layers were visibly less defined above midheight of the model (**Figure 3.8**).

During demolition, the model separated along two horizontal layers. The first separation was at midheight of the model—the location where the model was left to air-dry for 1-2 hours, and the second separation occurred between the first and second layers where there was an elapsed time of 30 minutes between compaction of layers. The bottom of the second layer was not well compacted and predominantly consisted of $\frac{1}{2}$ in. diameter balls of silt. Portions of rammed earth were collected and observed to contain large balls of the red clay and silt (**Figure 3.12**). Both the balls of clay and silt were soft and easily crushed between the fingers.

3.2.4 Data Observations

In viewing the plotted data from the beginning of Test 1-B, the northeast corner reflected a higher acceleration during most of the test. When plotting the relative accelerations between the northeast and northwest corners, a disparity was visible starting at approximately 90 seconds (**Figures 3.13**). The collapse of the lintel was apparent at approximately 300 seconds where the accelerations at the northeast corner increased sharply from 2 g to 4 g. After the lintel fell at 300 seconds, the disparity between the northeast and the northwest corner increased even further. Because the accelerometer fell with the northwest corner, the signals to all accelerometers were lost. Correlating the video with the accelerometer data, the loss of signal was apparent at 305 seconds (**Figure 3.14**).

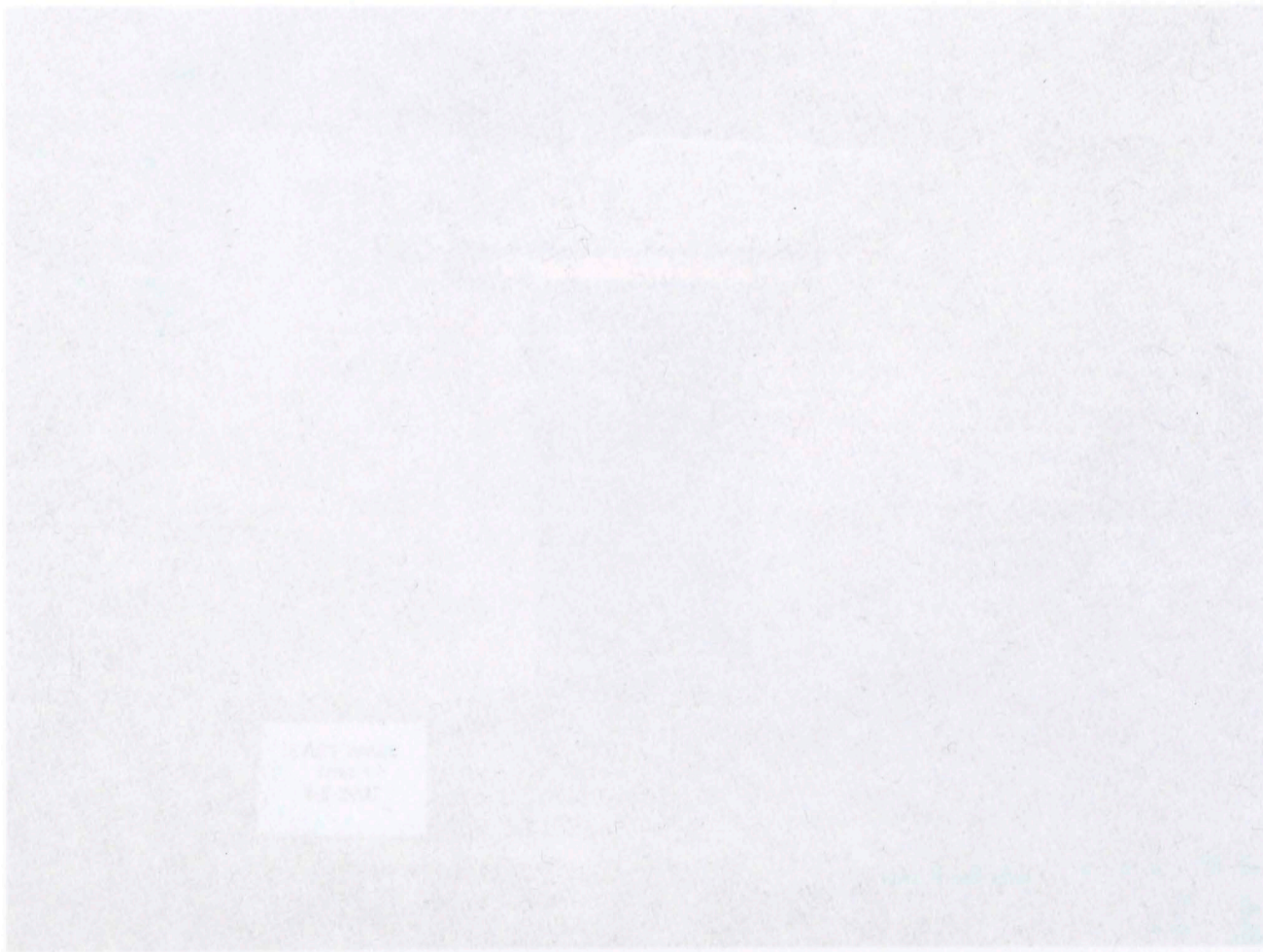


Figure 3.2: Test 1 cracks above lintel in east wall after test

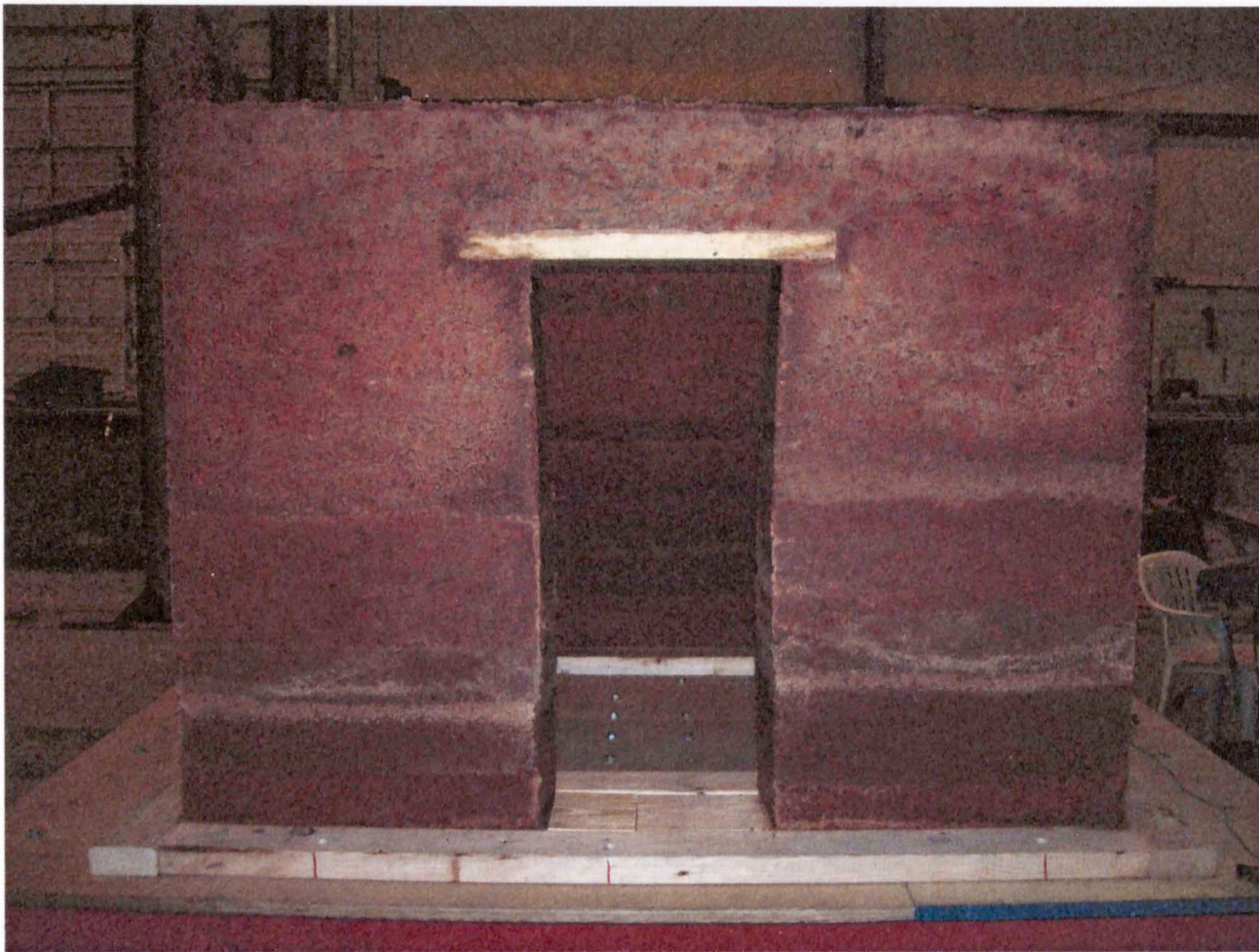


Figure 3.1: Test 1 view of east wall before test



Figure 3.2: Test 1 cracks above lintel in east wall after test



Figure 3.3: Test 1 interior view of crack above lintel in NE corner



Figure 3.4: Test 1 closeup view of exterior crack near lintel

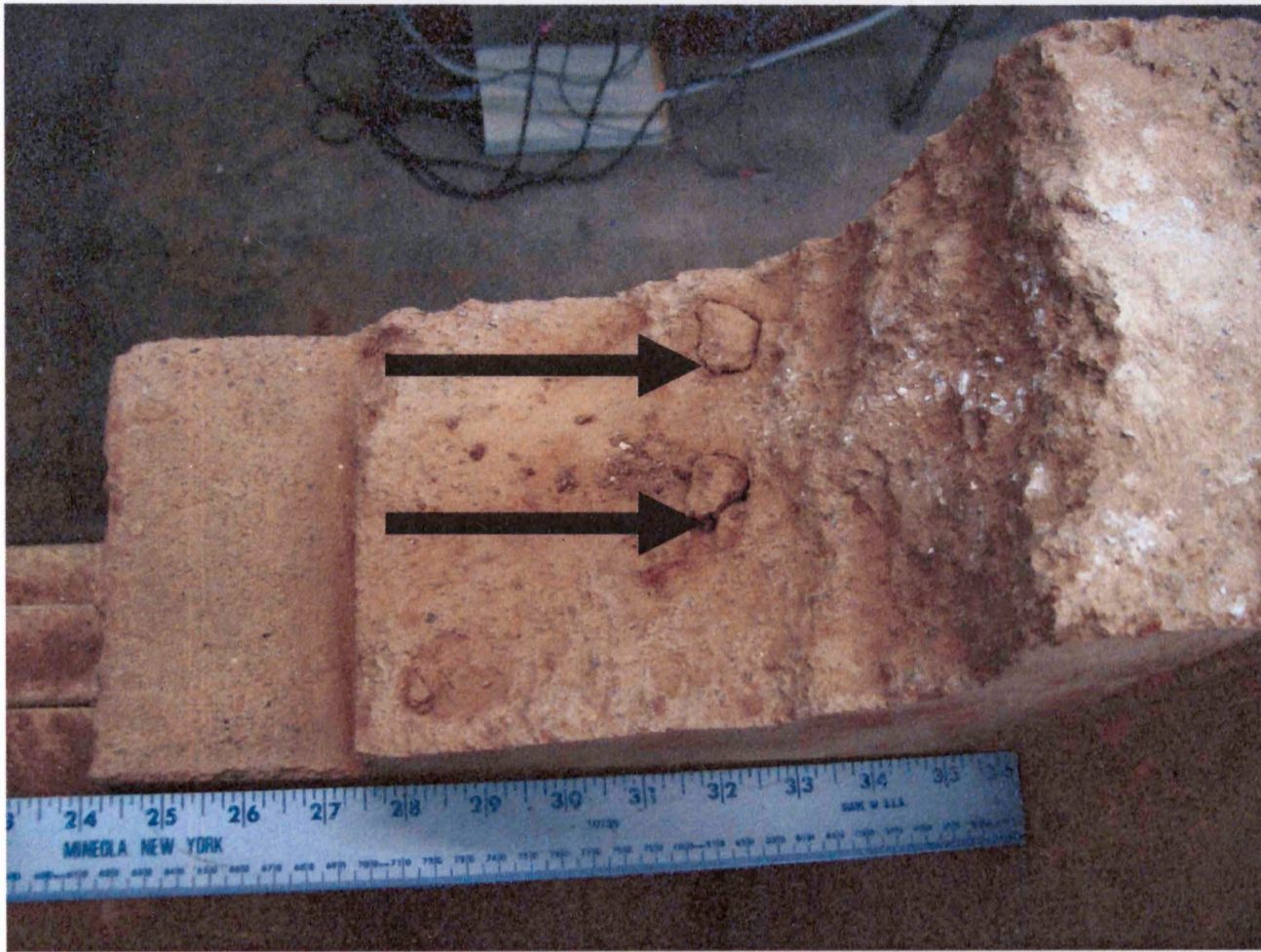


Figure 3.5: Test 1 view of two balls of silt along cracked surface in SE corner

Figure 3.6: Test 1 view of north wall, with roof, before test

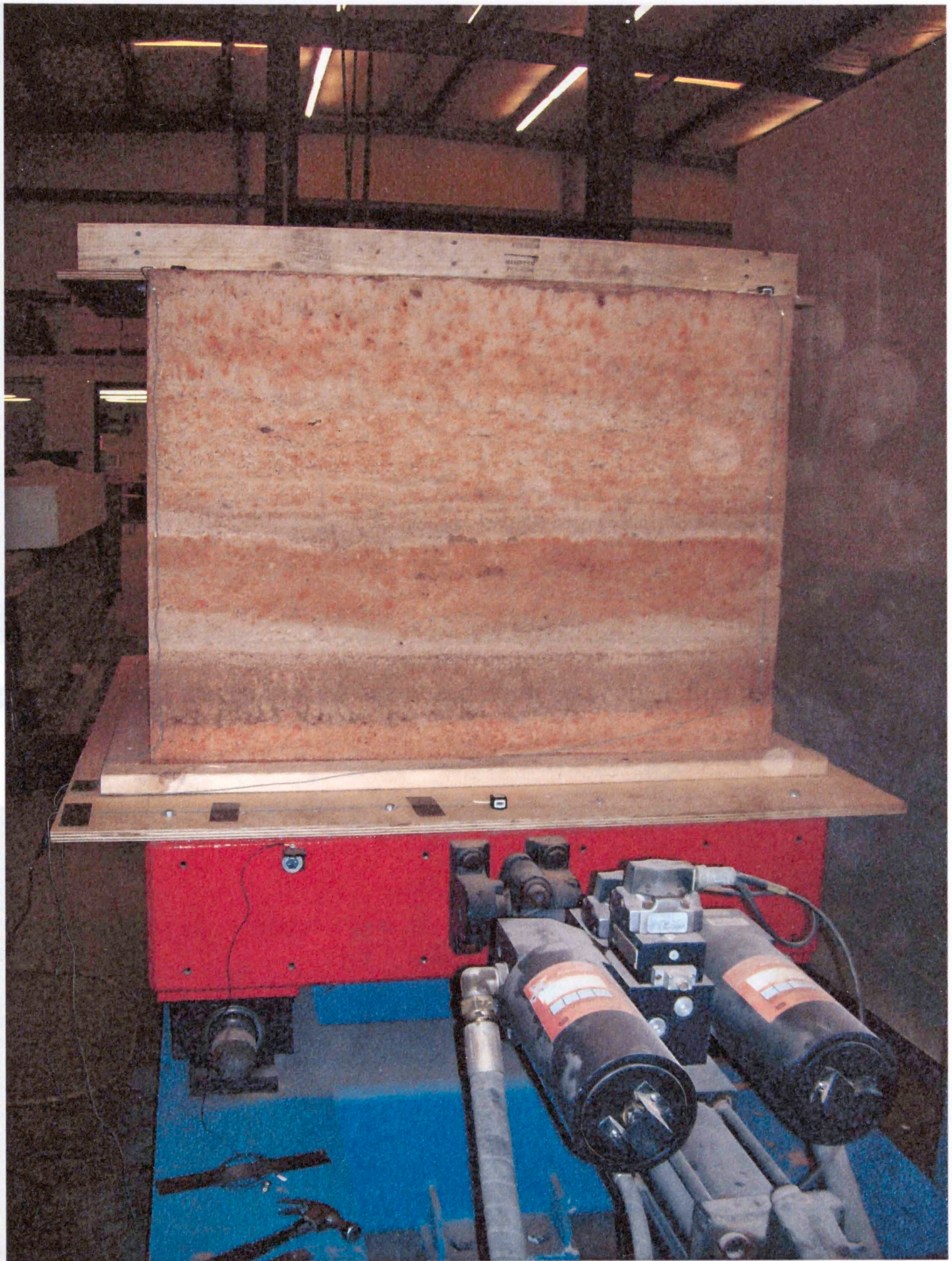


Figure 3.6: Test 1 view of north wall, with roof, before test

Figure 3.8: Test 1 plan view above cracked northwest corner



Figure 3.7: Test 1 elevation view of cracked northwest corner after test



Figure 3.8: Test 1 plan view above cracked northwest corner of north wall



Figure 3.9: Test 1 diagonal crack on exterior north wall



Figure 3.10: Test 1 close up of diagonal crack in lower half of north wall



Figure 3.11: Test 1 interior of crack along north wall

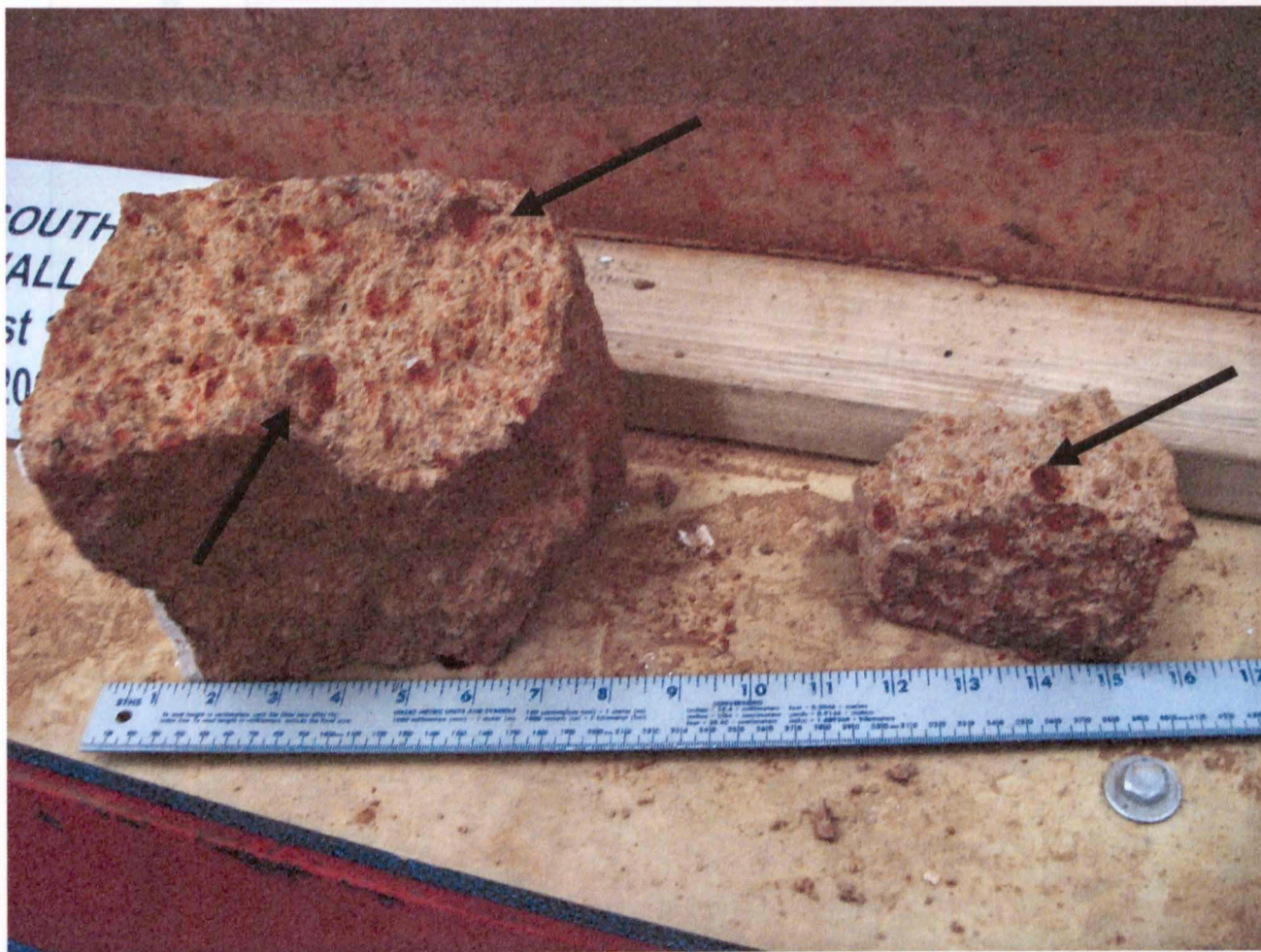


Figure 3.12: Test 1 post-test fragments with large clumps of red clay

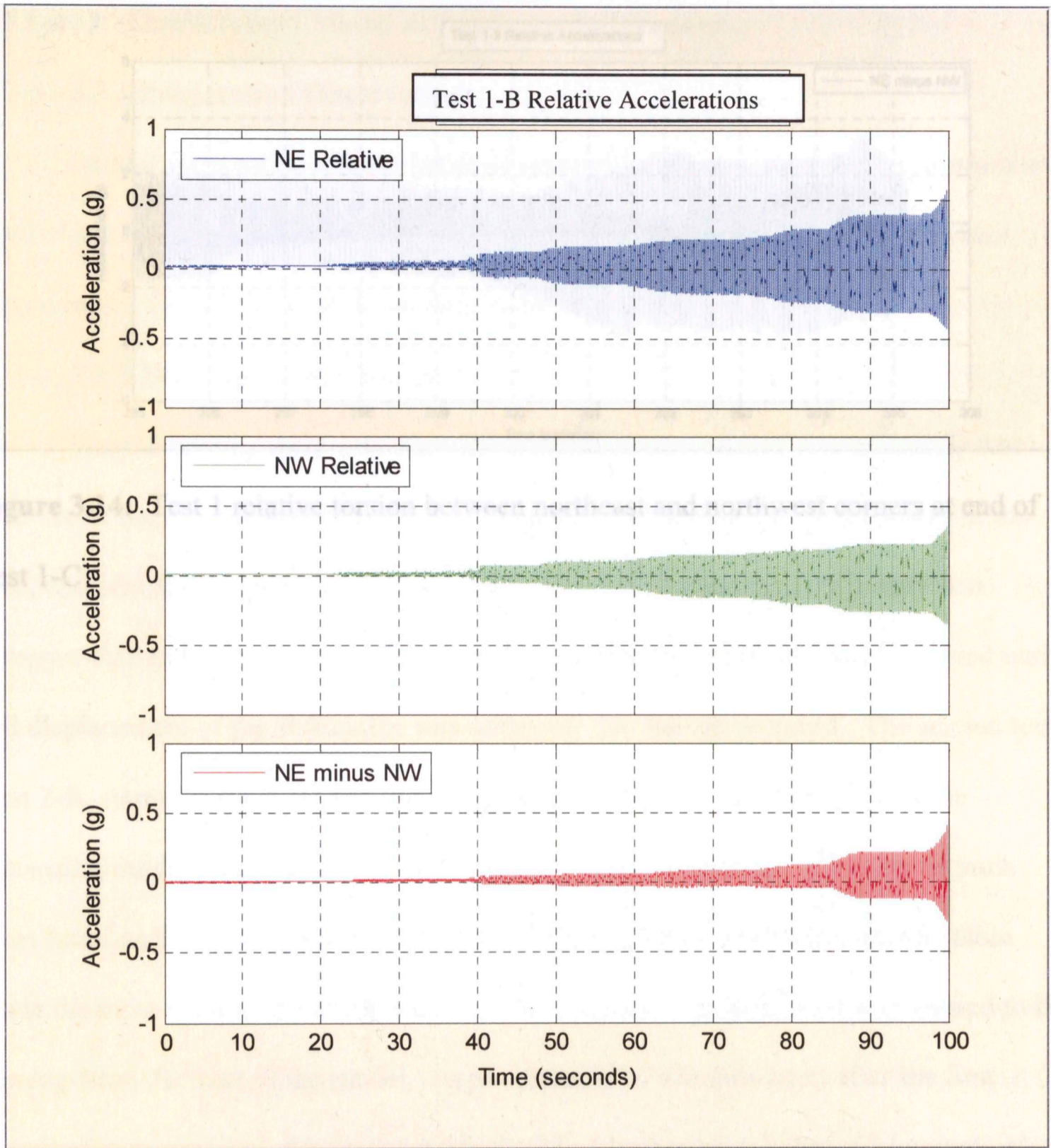


Figure 3.13: Test 1 accelerations at beginning of Test 1-B

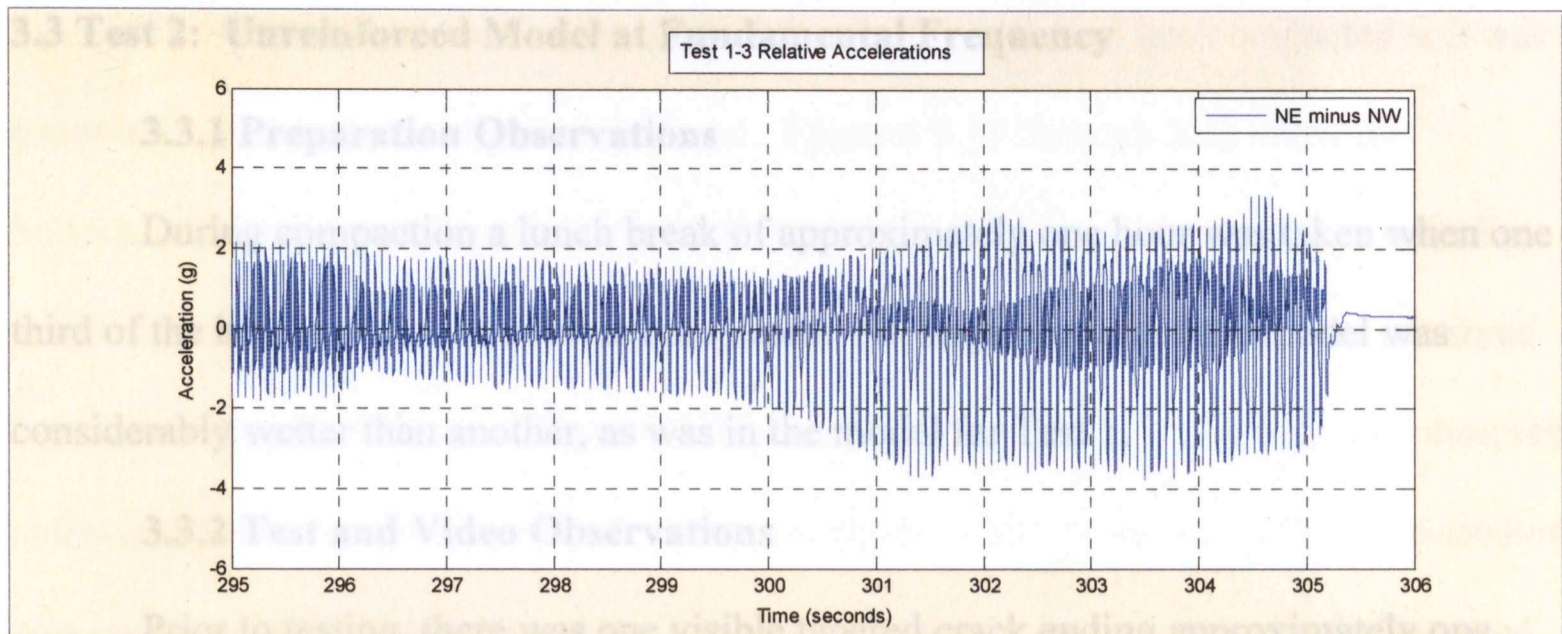


Figure 3.14: Test 1 relative torsion between northeast and northwest corners at end of Test 1-C

was slightly wider at the top. The measured fundamental frequency was between 4 Hz and 6 Hz. Test 2-A began at 4 Hz, while the amplitude was increased until full displacement of the shaketable was achieved. No failure occurred. The second test, Test 2-B, started at the 4 Hz and maximum displacement of the shaketable while increasing the frequency by 2 Hz approximately every 30 seconds. Changes in pitch were heard as the shaking transitioned from 8 Hz to 10 Hz. The model and the table made the most noise at the transition to 12 Hz. Ten seconds later, dust was viewed to be coming from the base of the model. Approximately 17 seconds later, after the first clouds of dust appeared, the model suddenly failed by horizontal shear (delamination) at all of the walls towards the lower third of the height of the model (at the cold joint). Figure 3.15 through Figure 3.25 show walls of the model before and after testing.

3.3.3 Picture and Demolition Observations

The tapered crack above the lintel prior to testing had fully propagated to the top of the lintel (Figure 3.16). In addition, a diagonal crack formed at the corner of the door opening towards the northeast corner of the model as seen in Figures 3.17. Unlike the

3.3 Test 2: Unreinforced Model at Fundamental Frequency

3.3.1 Preparation Observations

During compaction a lunch break of approximately one hour was taken when one third of the height of the model was completed. No large portion of the model was considerably wetter than another, as was in the model for Test 1.

3.3.2 Test and Video Observations

Prior to testing, there was one visible tapered crack ending approximately one inch above the lintel (**Figure 3.15**). The crack penetrated through the thickness of the wall, and was slightly wider at the top. The measured fundamental frequency was between 4Hz and 6Hz. Test 2-A began at 4 Hz, while the amplitude was increased until full displacement of the shaketable was achieved. No failure occurred. The second test, Test 2-B, started at the 4 Hz and maximum displacement of the shaketable while increasing the frequency by 2 Hz approximately every 30 seconds. Changes in pitch were heard as the shaking transitioned from 8 Hz to 10 Hz. The model and the table made the most noise at the transition to 12 Hz. Ten seconds later, dust was viewed to be coming from the base of the model. Approximately 17 seconds later, after the first clouds of dust appeared, the model suddenly failed by horizontal shear (delamination) at all of the walls towards the lower third of the height of the model (at the cold joint).

Figure 3.15 through **Figure 3.25** show walls of the model before and after testing.

3.3.3 Picture and Demolition Observations

The tapered crack above the lintel prior to testing had fully propagated to the top of the lintel (**Figure 3.16**). In addition, a diagonal crack formed at the corner of the door opening towards the northeast corner of the model as seen in **Figures 3.17**. Unlike the

model for Test 1, cracks were more vertical than horizontal, and less compacted soil was observed adjacent to the edges of the lintel. **Figures 3.19 through 3.23** show the horizontal delaminated layer at the same elevation on all sides of the model. Vertical cracks approximately 3 inches from each exterior corner of the west wall were observed below the delaminated layer (**Figures 3.24 and 3.25**). A vertical crack was also observed at the northwest reentrant corner. With the exception of the delaminated layer, no erosion was observed in the cracks above the lintel or along the base of the west wall. Rammed earth near the delaminated layer spalled near the outer surface of the wall. No other cracks were observed. During demolition, the rammed earth above the delaminated layer remained fully intact and was difficult to break. Later in the demolition process, the upper 12 inches separated from the southeast corner.

3.3.4 Data Observations

At approximately 640 seconds, the northeast corner exhibited an increase in relative acceleration at 10 Hz. Delamination of the model occurred at approximately 656 seconds while the model was at 12 Hz. In plotting the relative accelerations between the corners (**Figure 3.26**) the northeast and the northwest corners of the model were moving in opposite directions before and after failure, although after failure the accelerations appeared more erratic. The northwest and southwest corners remained synchronized throughout the test, and reflected a difference close to zero. Elapsed time between the delamination and the end of the shaketable movement was about 7 seconds.

Figure 3.16: Test 2 Interior view of east wall with cracks above lintel and delamination



Figure 3.15: Test 2 east wall before test (initial crack above lintel outlined in red) *less compacted soil adjacent to edge of lintel*

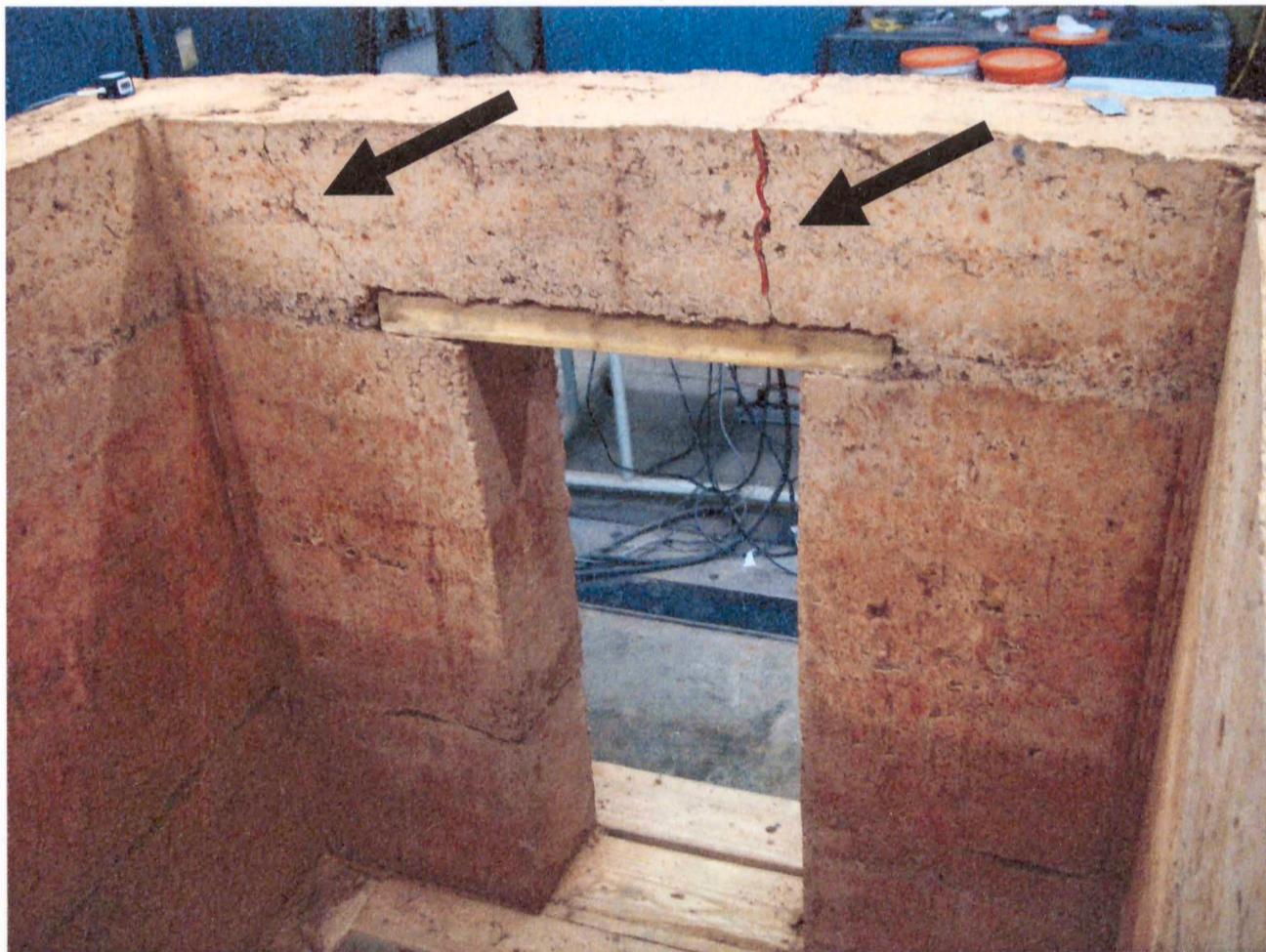


Figure 3.16: Test 2 Interior view of east wall with cracks above lintel and delamination



Figure 3.17: Test 2 close up view of crack in NE corner above lintel after test, note less compacted soil adjacent to edge of lintel

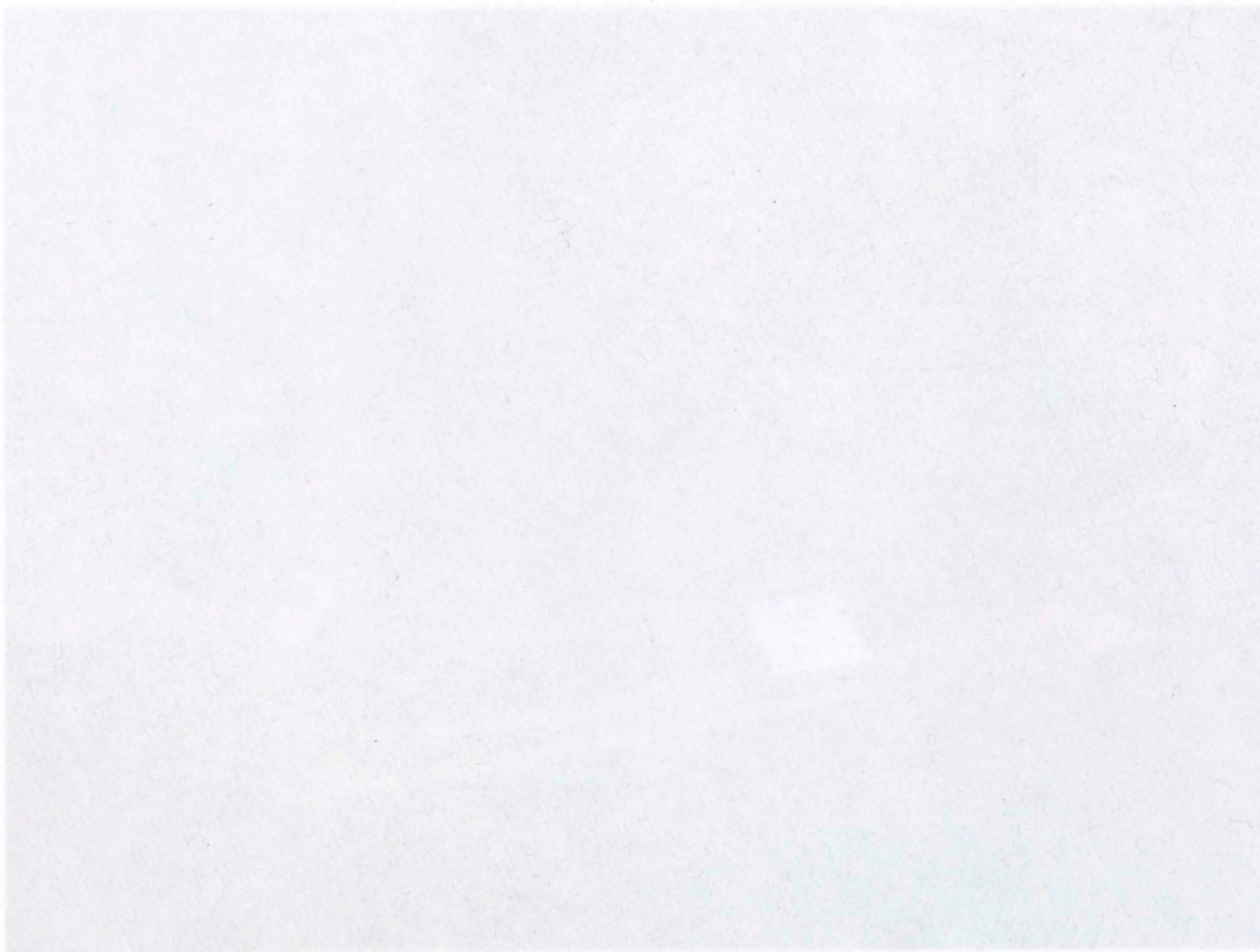


Figure 3.19: Test 2 delamination along north and west walls after test

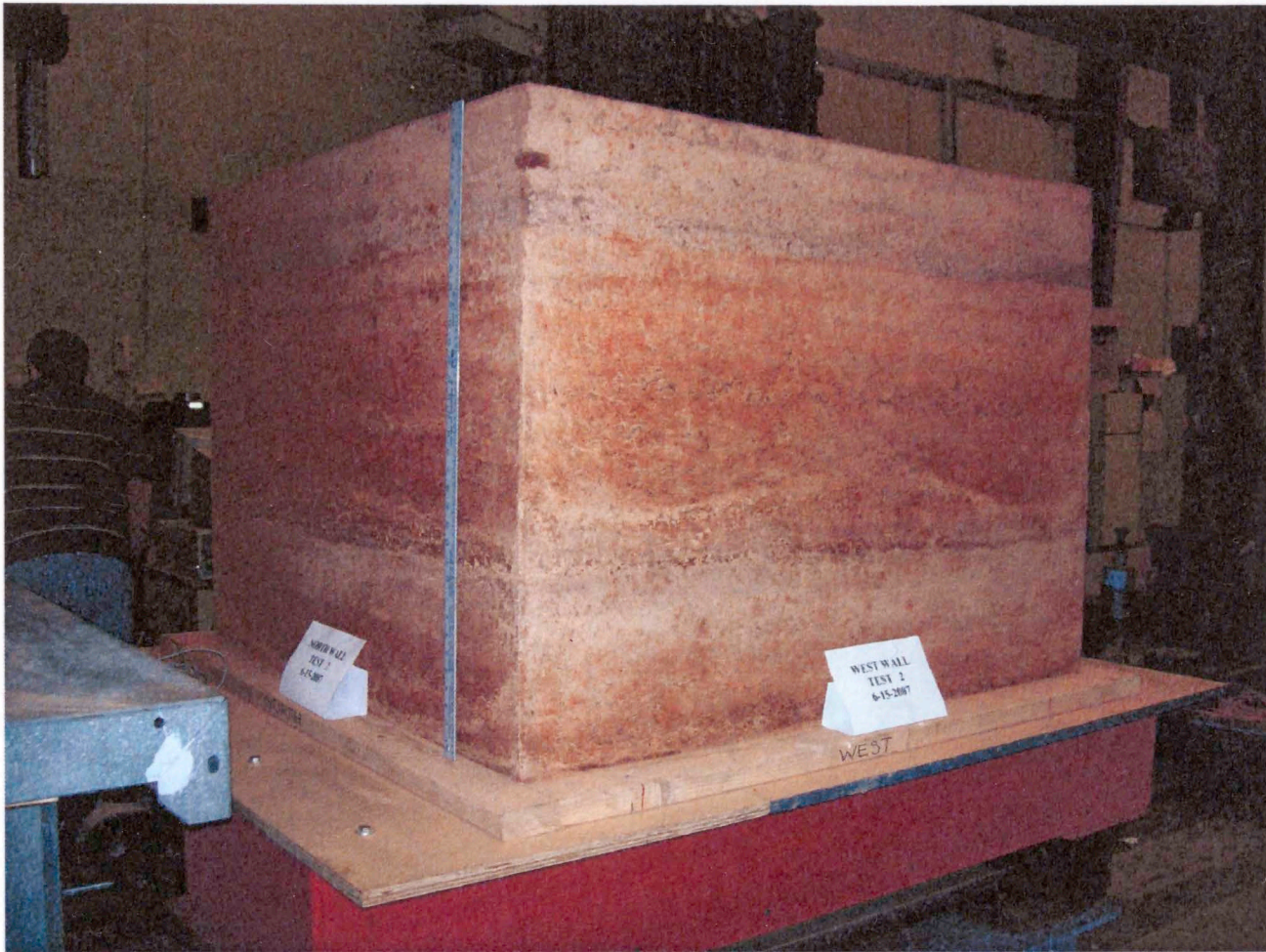


Figure 3.18: Test 2 view of north and west walls before test

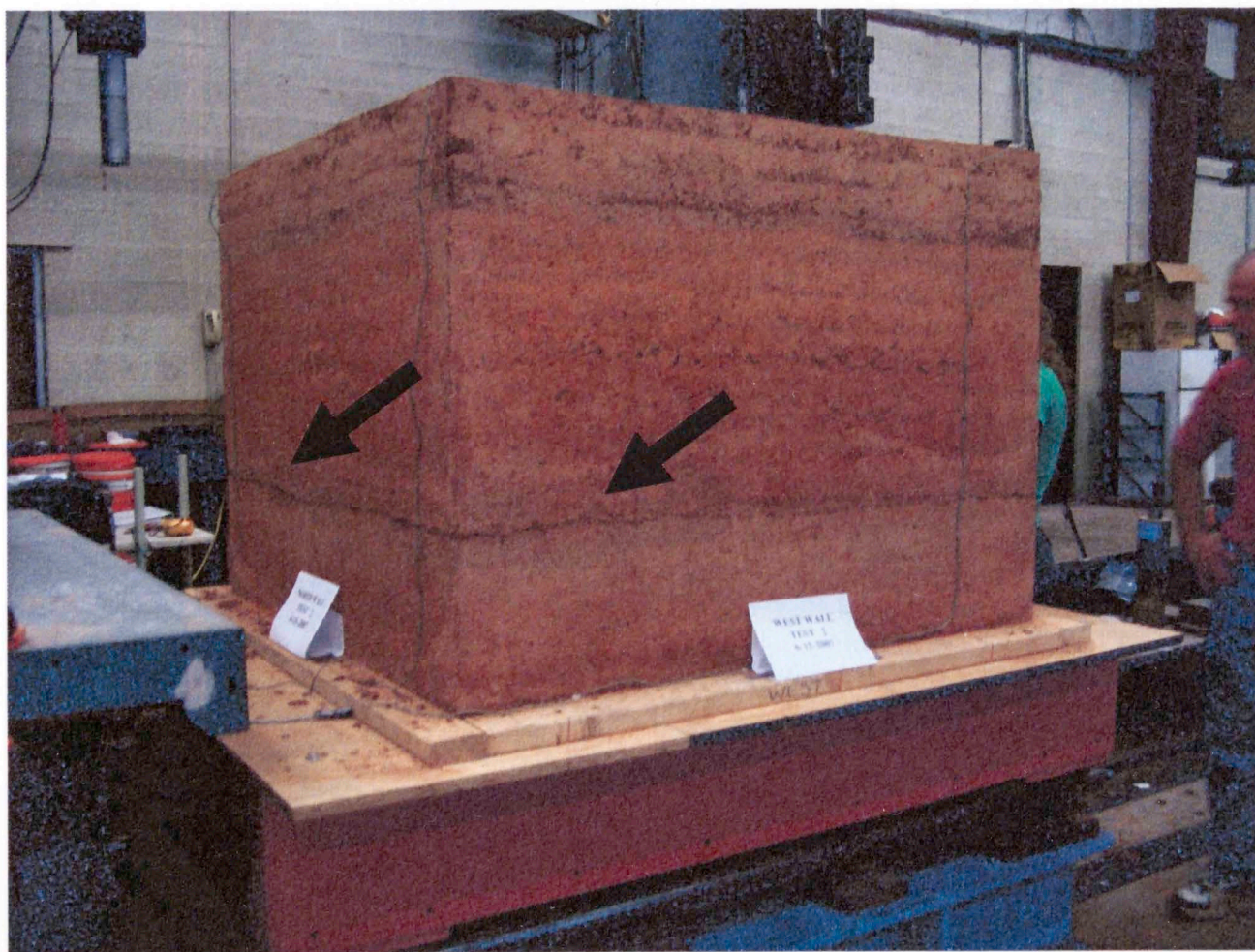


Figure 3.19: Test 2 delamination along north and west walls after test



Figure 3.20: Test 2 view of south and east walls before test

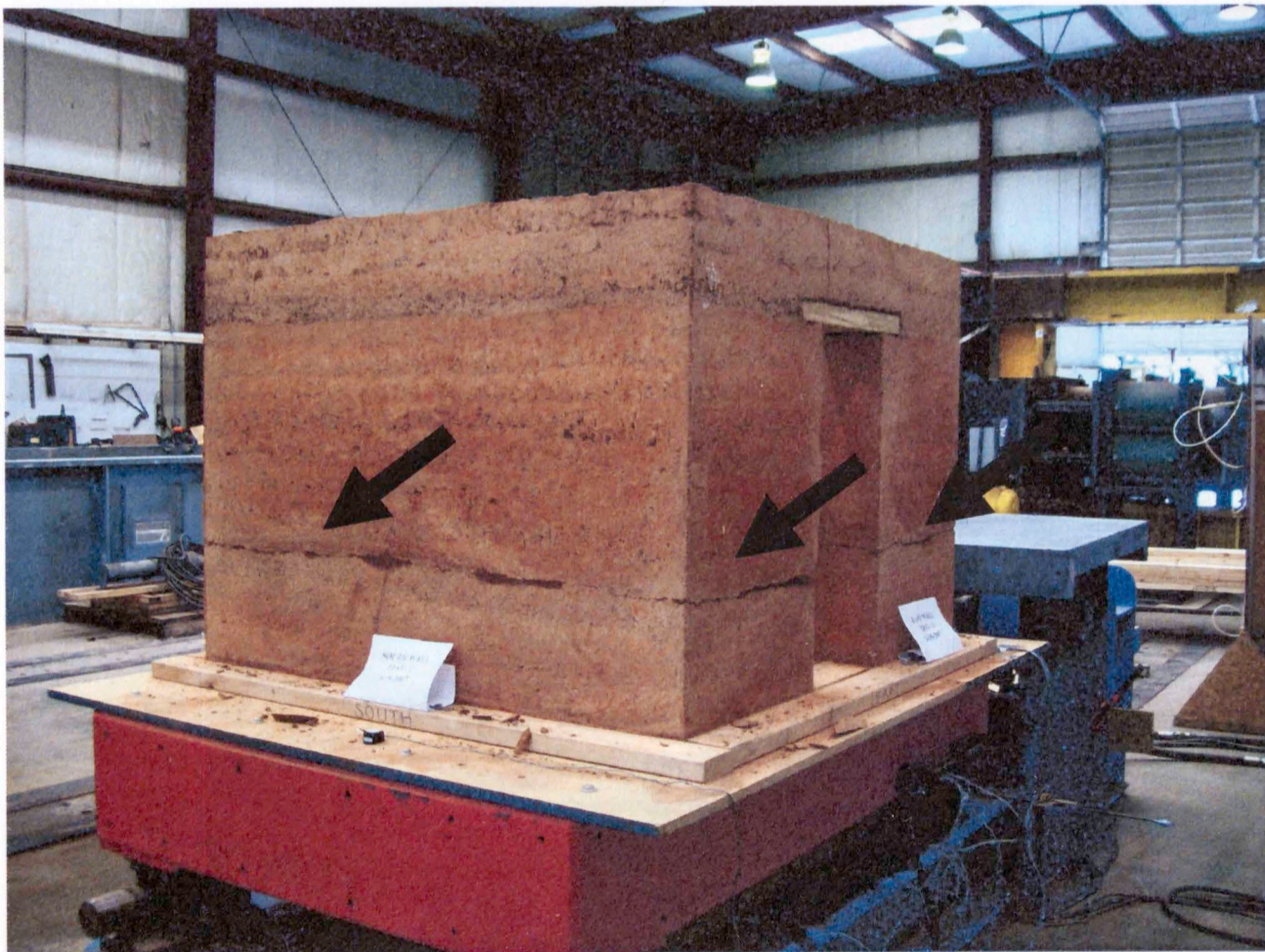


Figure 3.21: Test 2 delamination along south and east walls after test

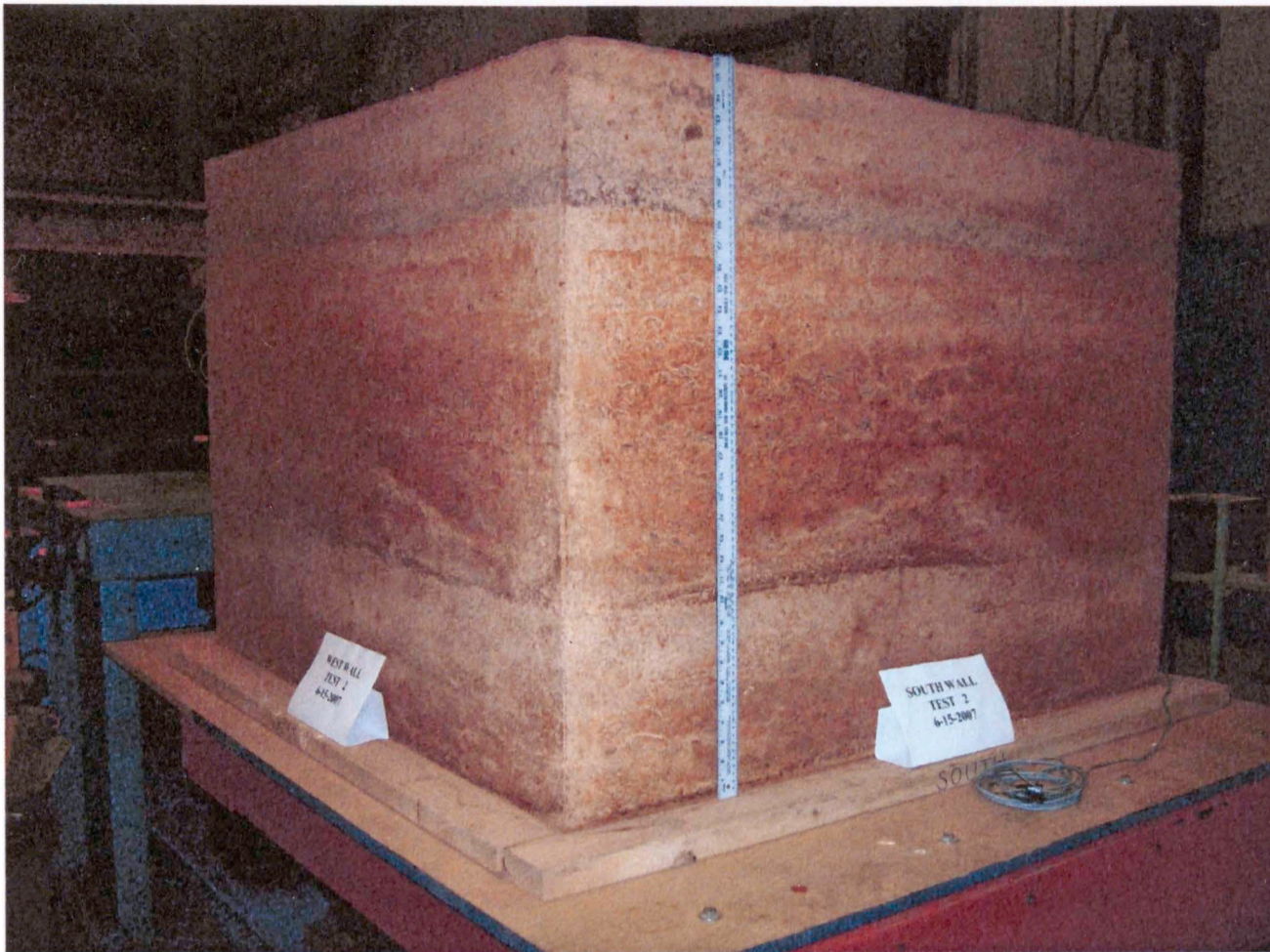


Figure 3.22: Test 2 view of west and south walls before test

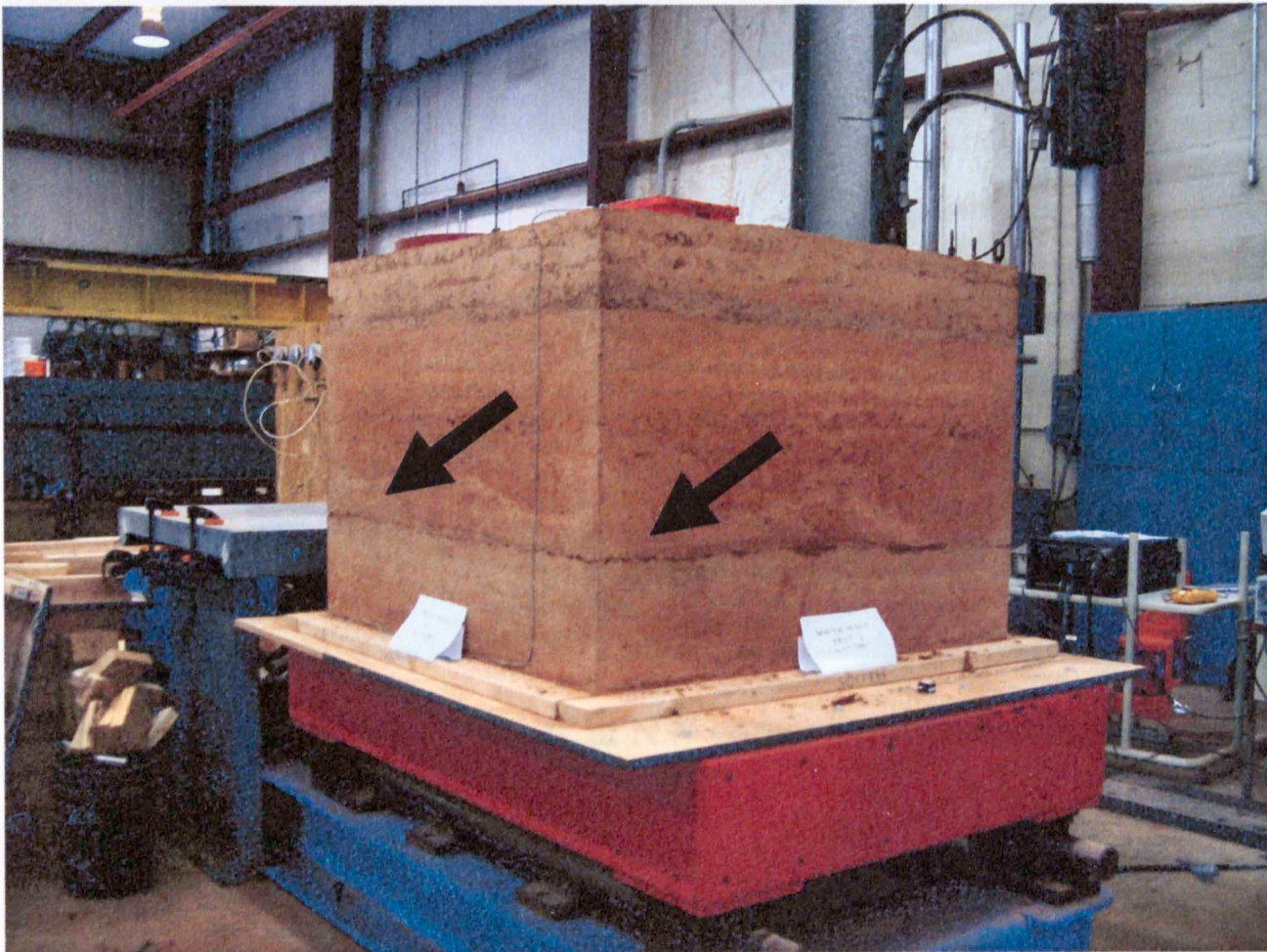


Figure 3.23: Test 2 delamination along west and south walls after test



Figure 3.24: Test 2 vertical crack at NW corner below delaminated layer

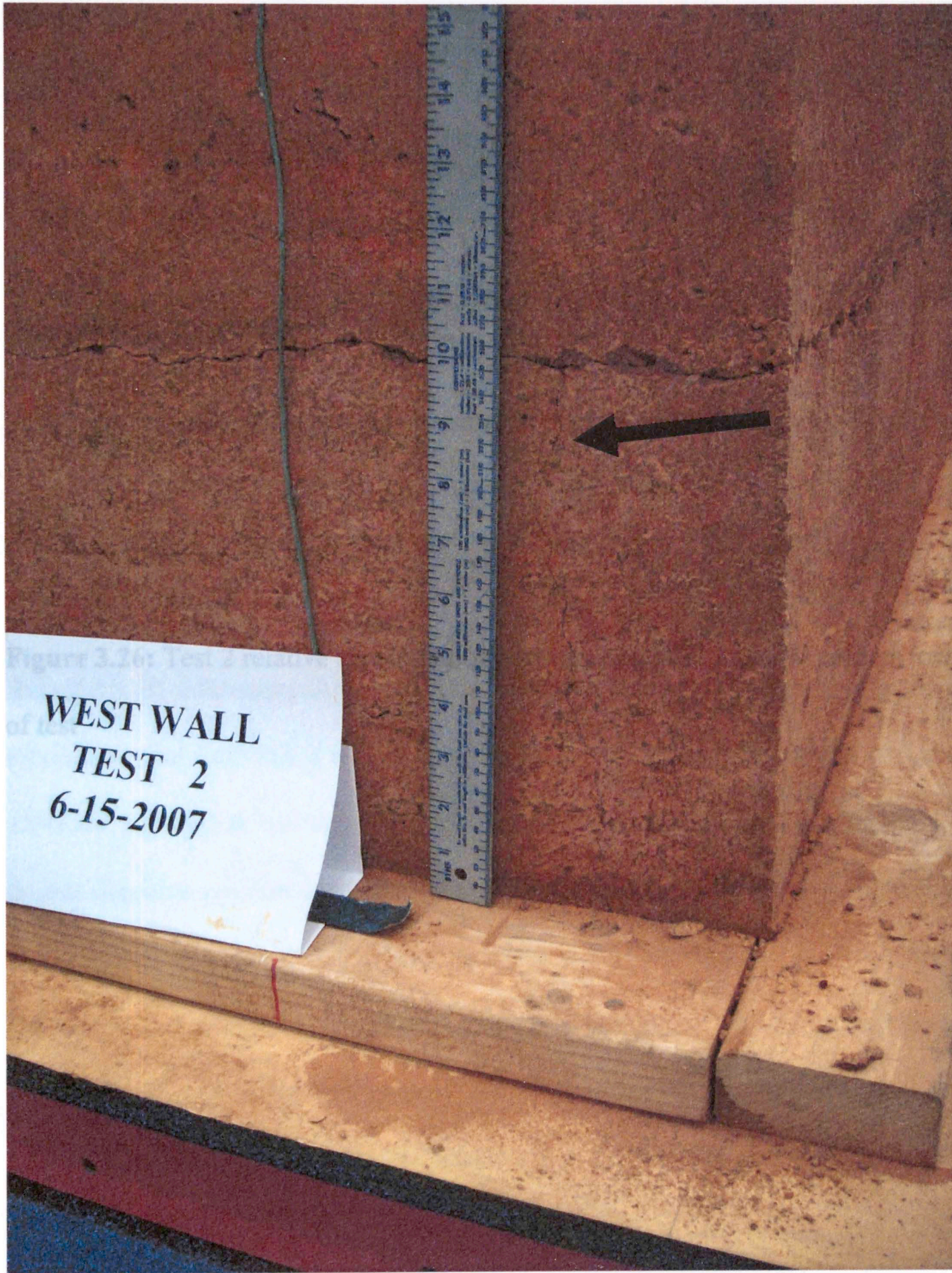


Figure 3.25: Test 2 vertical crack at SW corner below delaminated layer

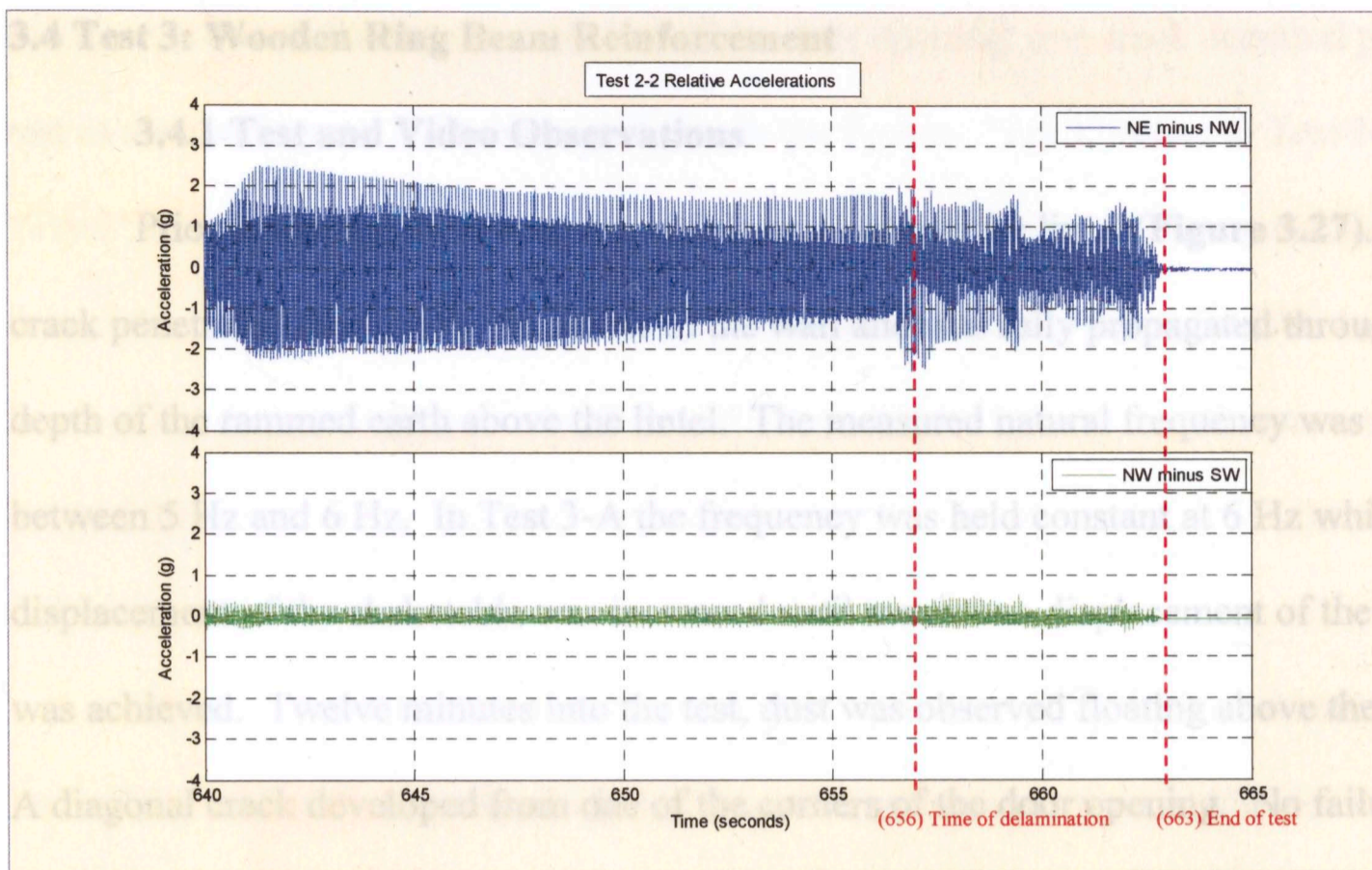


Figure 3.26: Test 2 relative accelerations between NE, NW, and SW corners towards end of test

of test
 model and dust was visible all around the model. At 12 Hz the overturning and the dust subsided, but a crack was developing at the west wall of the model. At 14 Hz the 45-degree diagonal crack at the south wall was visible, and more dust came from the model, but there was no collapse. At 16 Hz there was visible dust coming from the model, and a second crack developed at the south wall at a steeper angle. Testing was continued to further increase the frequency up to 18 Hz. Still no collapse occurred and the test was ended. Figure 27 through Figure 39 show the walls of the model before and after testing.

3.4.2 Picture and Demolition Observations

Three cracks total were located above the lintel at the east wall. The vertical crack near midspan of the lintel prior to testing had widened during testing, and the edges of the crack appeared eroded at the exterior wall (Figures 3.28 and 3.29). Two diagonal

3.4 Test 3: Wooden Ring Beam Reinforcement

3.4.1 Test and Video Observations

Prior to testing, there was one visible crack above the lintel (**Figure 3.27**). The crack penetrated through the thickness of the wall and was fully propagated through the depth of the rammed earth above the lintel. The measured natural frequency was between 5 Hz and 6 Hz. In Test 3-A the frequency was held constant at 6 Hz while the displacement of the shaketable was increased until maximum displacement of the table was achieved. Twelve minutes into the test, dust was observed floating above the model. A diagonal crack developed from one of the corners of the door opening. No failure occurred. In Test 3-B, at full shaketable displacement the frequency was increased at increments of 2 Hz every 30 seconds. At 10 Hz there was visible overturning of the model and dust was visible all around the model. At 12 Hz the overturning and the dust subsided, but a crack was developing at the west wall of the model. At 14 Hz the 45-degree diagonal crack at the south wall was visible, and more dust came from the model, but there was no collapse. At 16 Hz there was visible dust coming from the model, and a second crack developed at the south wall at a steeper angle. Testing was continued to further increase the frequency up to 18 Hz. Still no collapse occurred and the test was ended. **Figure 27** through **Figure 39** show the walls of the model before and after testing.

3.4.2 Picture and Demolition Observations

Three cracks total were located above the lintel at the east wall. The vertical crack near midspan of the lintel prior to testing had widened during testing, and the edges of the crack appeared eroded at the exterior wall (**Figures 3.28 and 3.29**). Two diagonal

cracks were located at the upper corners of the door opening: one crack occurred per sub-test as seen in **Figures 3.28 through 3.30**. In the figures, “Try 1” refers to Test 3-A and “Try 2” refers to Test 3-B. Spacing of the cracks above the lintel were approximately 9 in., 19 in., and 36 in. from the southeast corner of the model. The spikes for the ring beam along the east wall were also 9 in., 19 in., and 36 in. from the southeast corner. Two of the cracks above the lintel were at least within 1 in. of a spike, while the third crack was within 3 in. of a spike.

At the exterior southwest corner, the near vertical crack of the model started at the base of the west wall, approximately 3 in. from the exterior corner, and traveled upwards 21 in. before wrapping around the corner to the south wall (**Figure 3.31 through Figure 3.35**). Of the two diagonal cracks at the south wall, one was at a 45-degree angle to the top of the south wall at 16 in. from the corner, and the second almost vertical to the top of the south wall at 5 in. from the corner (**Figure 3.37 and 3.38**). Similar to the east wall, the 45-degree diagonal crack was within 3 in. of the nearest spike. Inside the model a vertical crack was observed at the reentrant corner between the south and west walls. At approximately two thirds of the height of the model, the crack at the reentrant corner branched into the 45-degree angle crack on the south wall (**Figure 3.39**). Beyond the diagonal crack, the vertical crack at the reentrant corner continued to the top of the wall.

During demolition, most of the cracks from the test were still visible (**Figure 3.40**). The cracked section of rammed earth at the upper south wall remained attached to the spike and suspended in the air (**Figure 3.41**). The model was more difficult to demolish than previous models. The ring beam had to be forced off the model first, before the walls could collapse.

3.4.3 Data Observations

In plotting the accelerometer data, there were no drastic changes in acceleration. Although the southwest corner cracked at 14 Hz, the accelerometers did not suddenly increase or decrease in acceleration as in previous tests. The greatest increase in acceleration reflected in the data was between the northeast and the northwest corners when the frequency was changed from 8 Hz to 10 Hz at approximately 270 seconds (**Figure 3.42**). Relative accelerations between the northwest and the southwest corners reflected a slight increase in acceleration at the same time, but the magnitude remained close to zero. By the end of the test all three corners were relatively uniform in their response and had similar accelerations (**Figure 3.43**).



Figure 3.27: Test 3 view of east wall before test, note crack above door opening

Figure 3.29: Test 3 cracks above lintel near NE corner of east wall



Figure 3.28: Test 3 cracks above lintel near SE corner of east wall



Figure 3.29: Test 3 cracks above lintel near NE corner of east wall

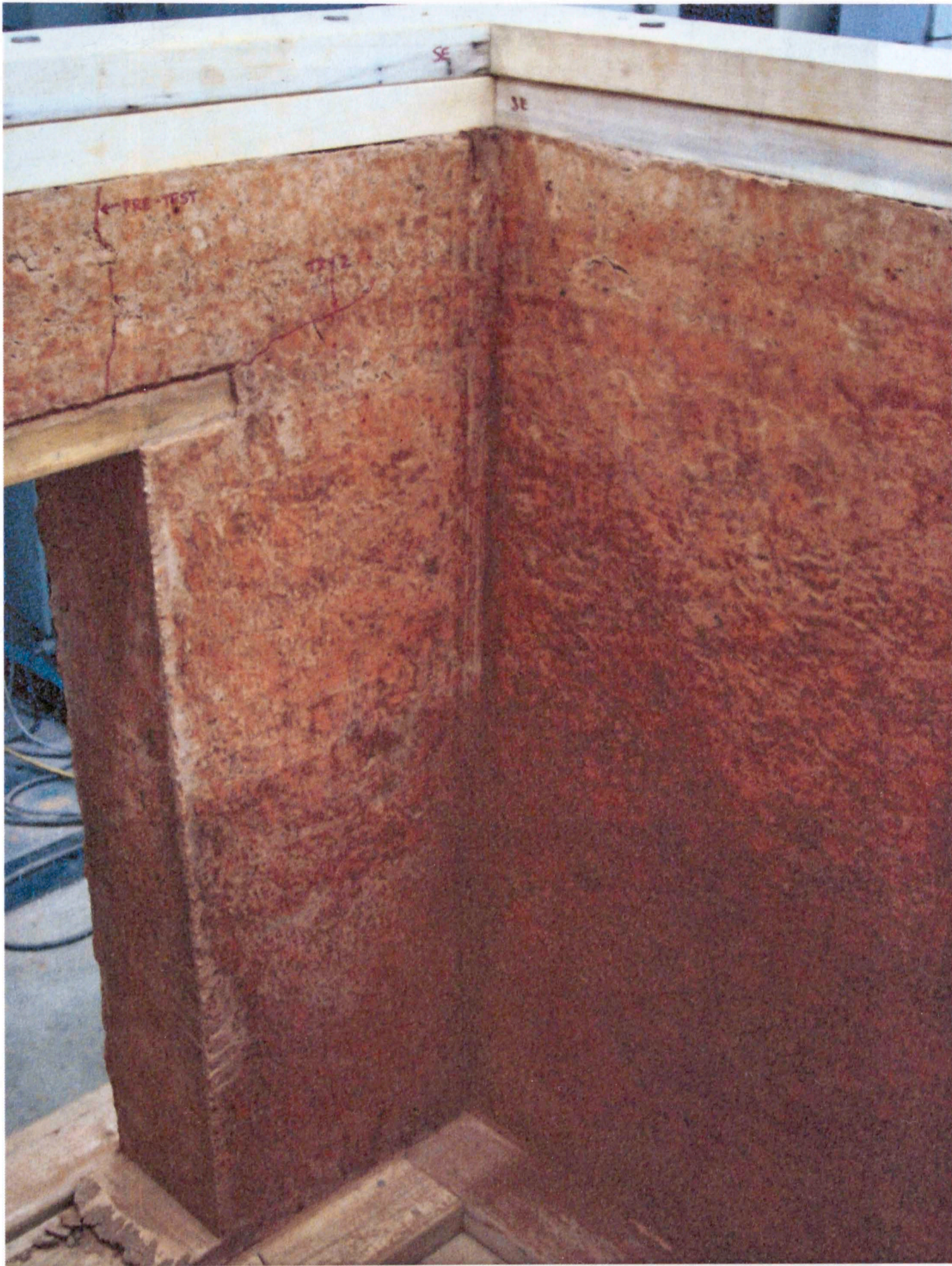


Figure 3.30: Test 3 view of interior southeast corner after test, note cracks outlined in red

Figure 3.32: Test 3 view of west wall after test



Figure 3.31: Test 3 view of west wall before test



Figure 3.32: Test 3 view of west wall after test



Figure 3.33: Test 3 view of crack near base of west wall at SW corner



Figure 3.34: Test 3 width of fractured section at SW corner along base of west wall

Figure 3.35: Test 3 view of cracks across SW corner

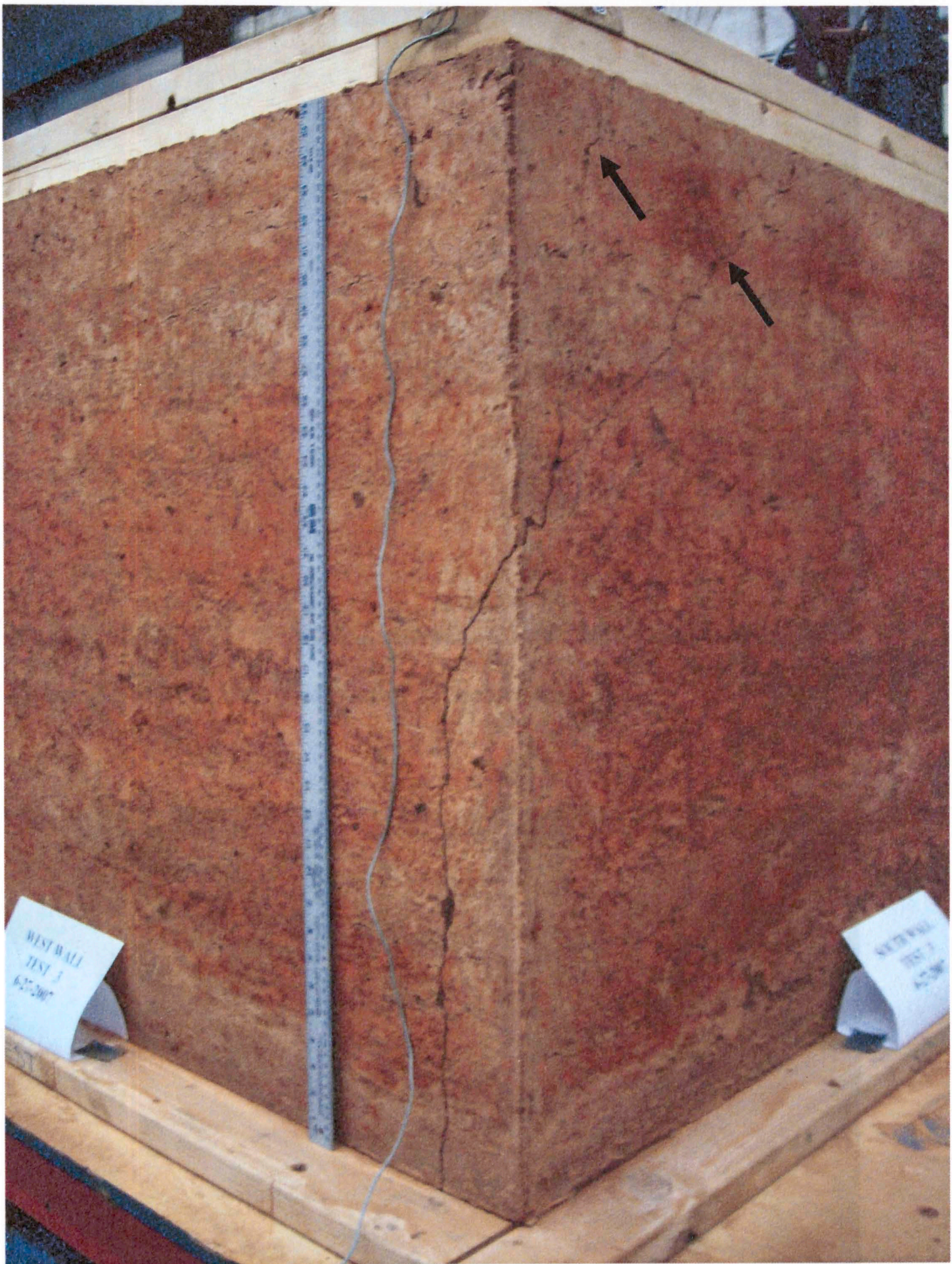


Figure 3.35: Test 3 view of cracks across SW corner

Figure 3.37: Test 3 view of south wall after test. Arrows point to fractures



Figure 3.36: Test 3 view of south wall before test



Figure 3.37: Test 3 view of south wall after test. Arrows point to fractures

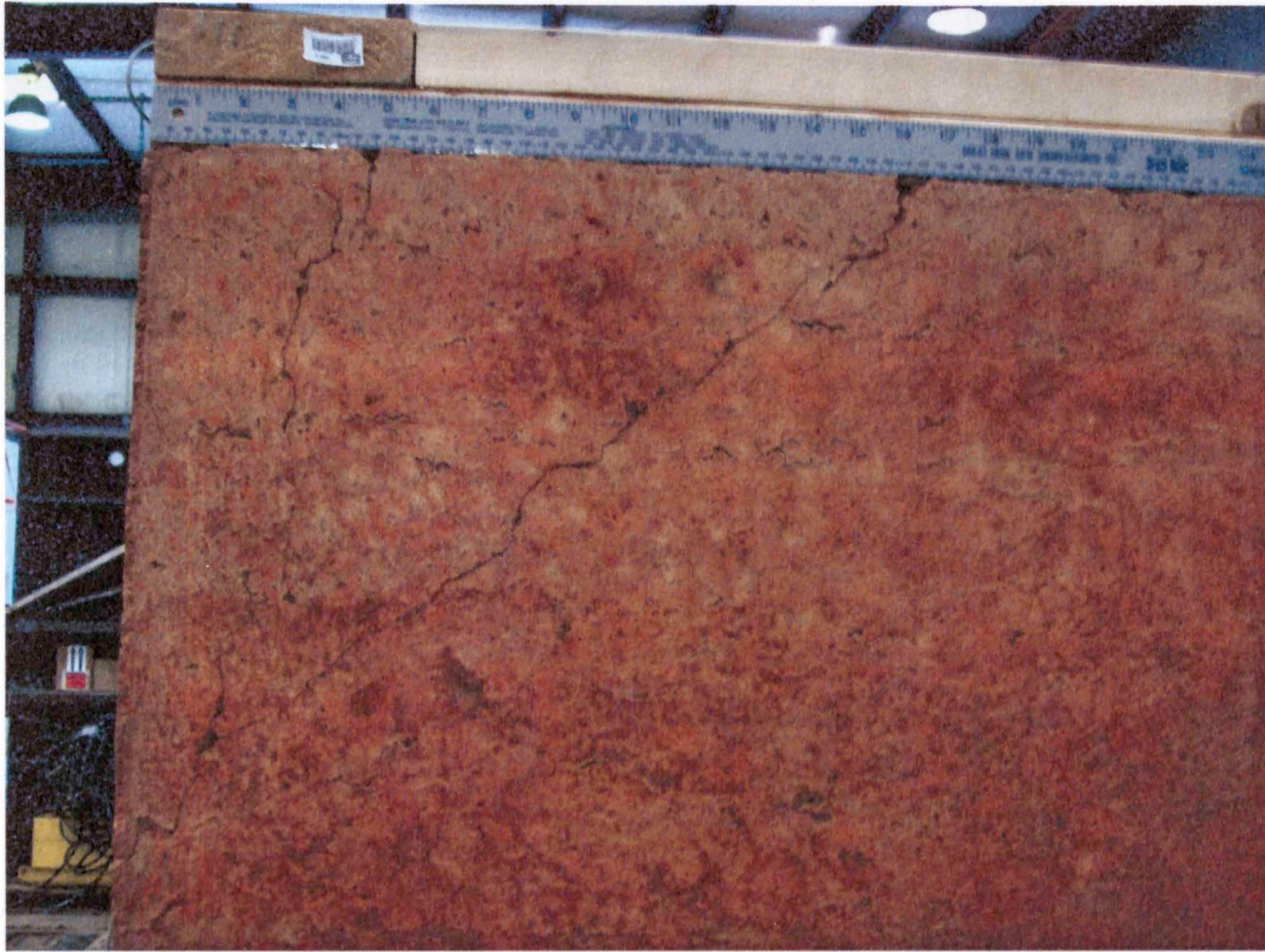


Figure 3.38: Test 3 close-up of previous photograph

Figure 3.39: Test 3 measurement of diagonal crack at interior of SW corner



Figure 3.39: Test 3 measurement of diagonal crack at interior of SW corner

Figure 3.41: Test 3 view of suspended rammed earth at ring beam



Figure 3.40: Test 3 model after demolition (arrows point to cracks from testing)

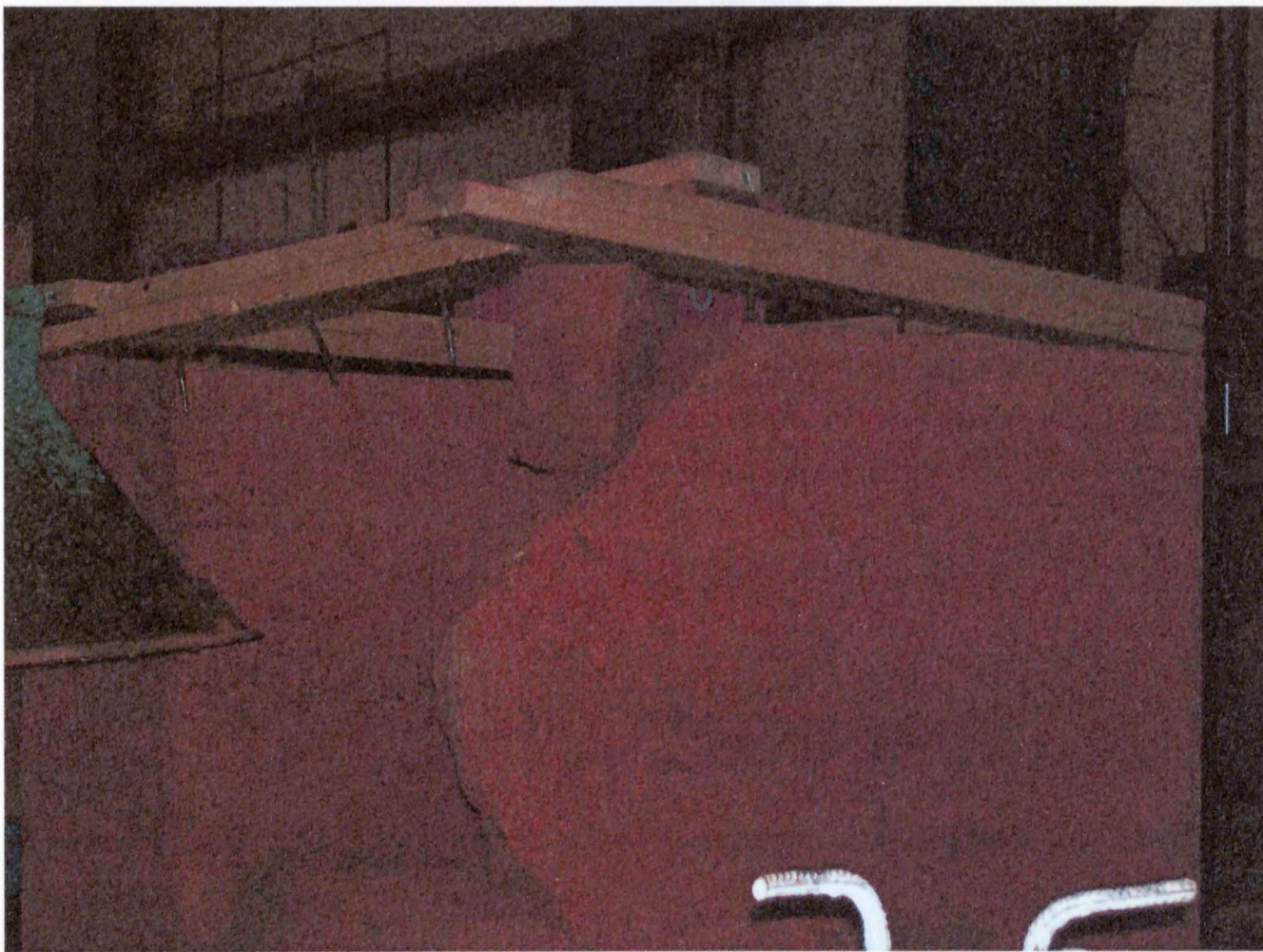


Figure 3.41: Test 3 view of suspended rammed earth at ring beam

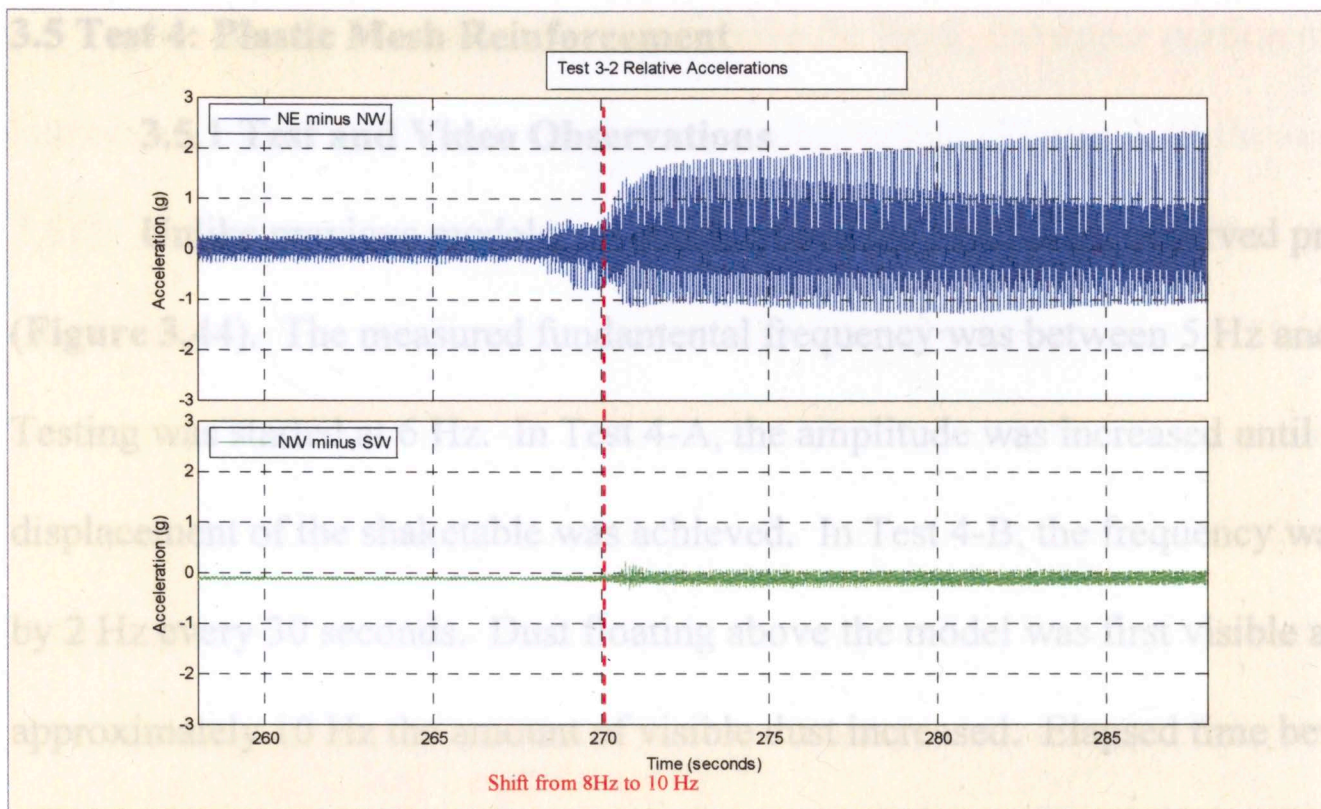


Figure 3.42: Test 3-B relative accelerations between corners from 8Hz to 10Hz, note increase in accelerations at approximately 270 seconds

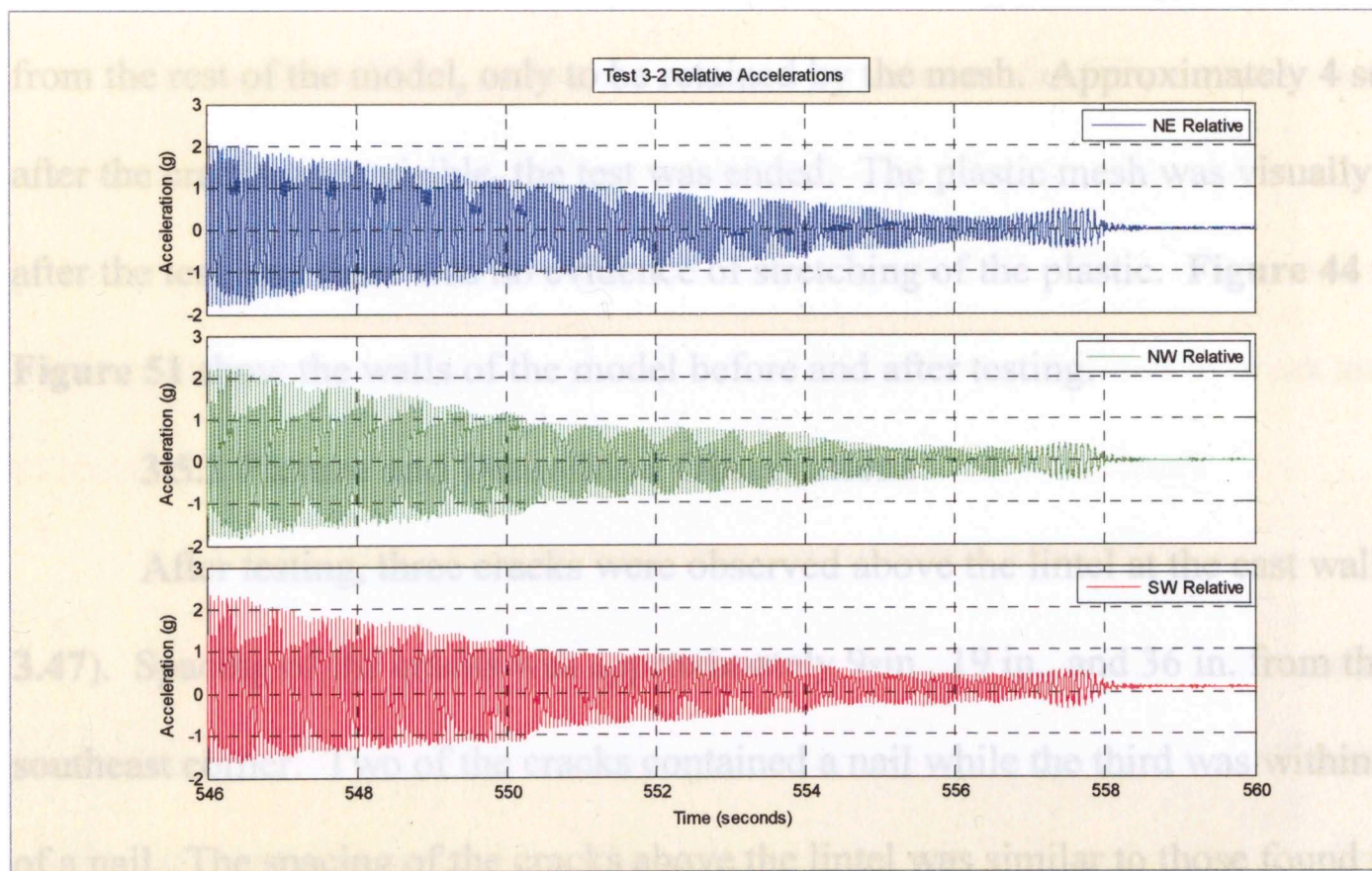


Figure 3.43: Test 3-B relative accelerations, note uniform accelerations between corners

3.5 Test 4: Plastic Mesh Reinforcement

3.5.1 Test and Video Observations

Unlike previous models, no cracks above the lintel were observed prior to testing (**Figure 3.44**). The measured fundamental frequency was between 5 Hz and 6 Hz. Testing was started at 6 Hz. In Test 4-A, the amplitude was increased until full displacement of the shaketable was achieved. In Test 4-B, the frequency was increased by 2 Hz every 30 seconds. Dust floating above the model was first visible at 8 Hz. At approximately 10 Hz the amount of visible dust increased. Elapsed time between 10 Hz and 12 Hz was approximately 36 seconds. At 12 Hz a crack above the door opening was visible at the east wall. Simultaneously, the northwest corner fully cracked along the north and west walls. There was visible separation between the fractured portion of the northwest corner and the remainder of the west wall. The corner appeared to fall away from the rest of the model, only to be retained by the mesh. Approximately 4 seconds after the cracks were visible, the test was ended. The plastic mesh was visually evaluated after the test, and there was no evidence of stretching of the plastic. **Figure 44** through **Figure 51** show the walls of the model before and after testing.

3.5.2 Picture and Demolition Observations

After testing, three cracks were observed above the lintel at the east wall (**Figure 3.47**). Spacing of the cracks was approximately 9 in., 19 in., and 36 in. from the southeast corner. Two of the cracks contained a nail while the third was within 3 inches of a nail. The spacing of the cracks above the lintel was similar to those found in the model for Test 3.

Along with the cracks observed above the lintel, the upper portion of the northwest corner was completely fractured after testing (**Figure 3.49 through Figure 3.51**). A crack approximately 45 degrees was located in the upper half of the north wall was of the model, extending from the exterior corner to approximately 24 inches on the north wall. The diagonal crack at the north wall intersected the diagonal cracks long the west wall at approximately 14 inches from the base. There was a vertical crack observed at the reentrant corner between the north and west walls. The vertical crack intersected the diagonal cracks at the north and west walls at approximately midheight of the model (18 inches from the base) (**Figure 3.50**). The cracked section along the upper half of the west wall extended approximately 18 inches from the exterior northwest corner. One nail was located within the crack at the base of the west wall. In total, only four of the 131 nails used in the model appeared within a crack.

During demolition, a clearer view was provided of the failure planes in the northwest corner of the model (**Figure 3.52**). One of the walls fractured into several pieces upon impact with the ground, as seen in **Figure 3.53**. This was unusual since portions of the rammed earth in previous models were very difficult to break and tended to remain in portions larger than 2 ft², even if they fell onto the floor.

3.5.3 Data Observations

The crack at the northwest corner occurred at approximately 353 seconds, and was reflected in the graph as an increase in accelerations between the northwest and the southwest corner (**Figure 3.54**). The end of the test was reflected in the accelerometer data as a sharp decline at approximately 357 seconds.

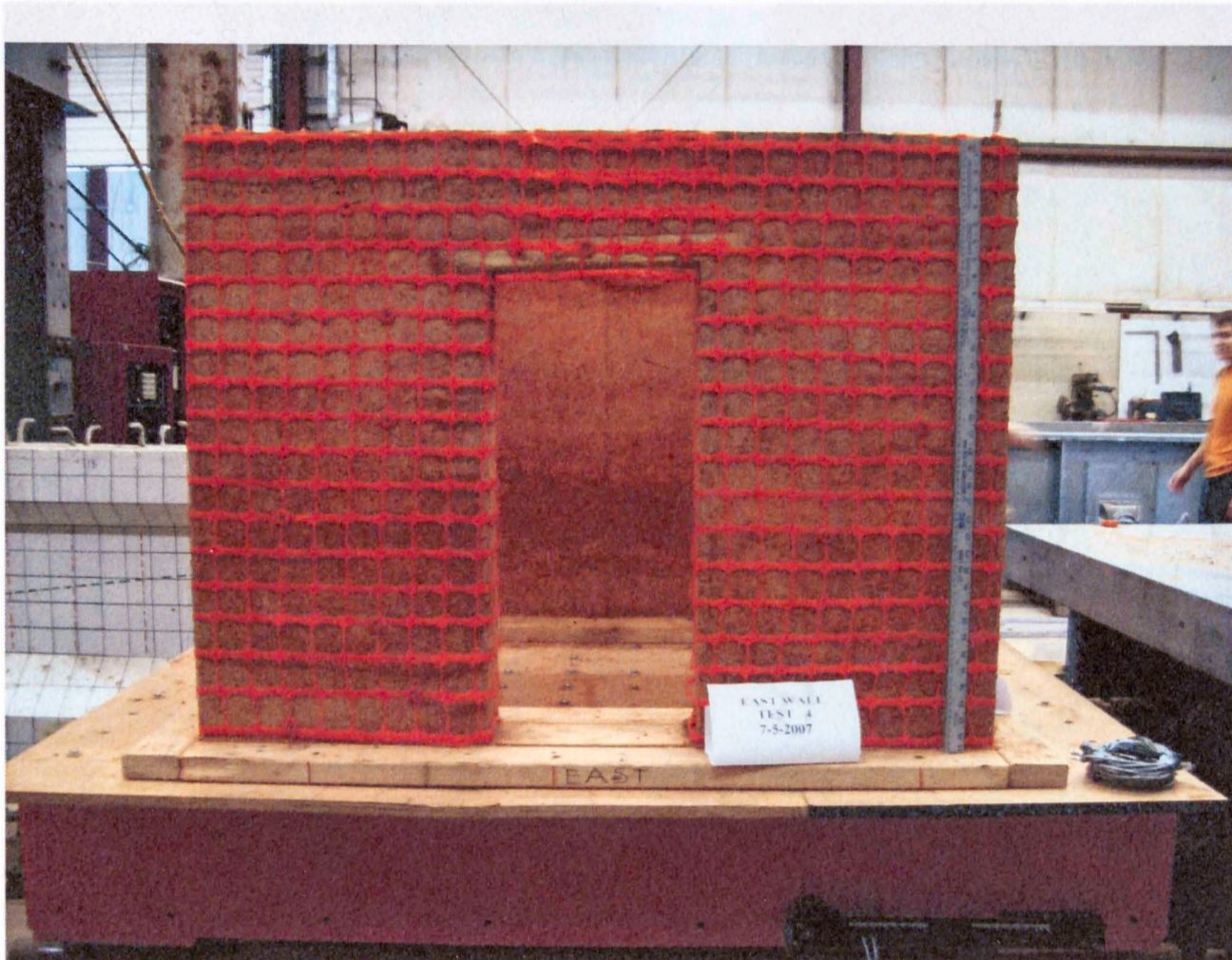


Figure 3.44: Test 4 view of east wall before testing

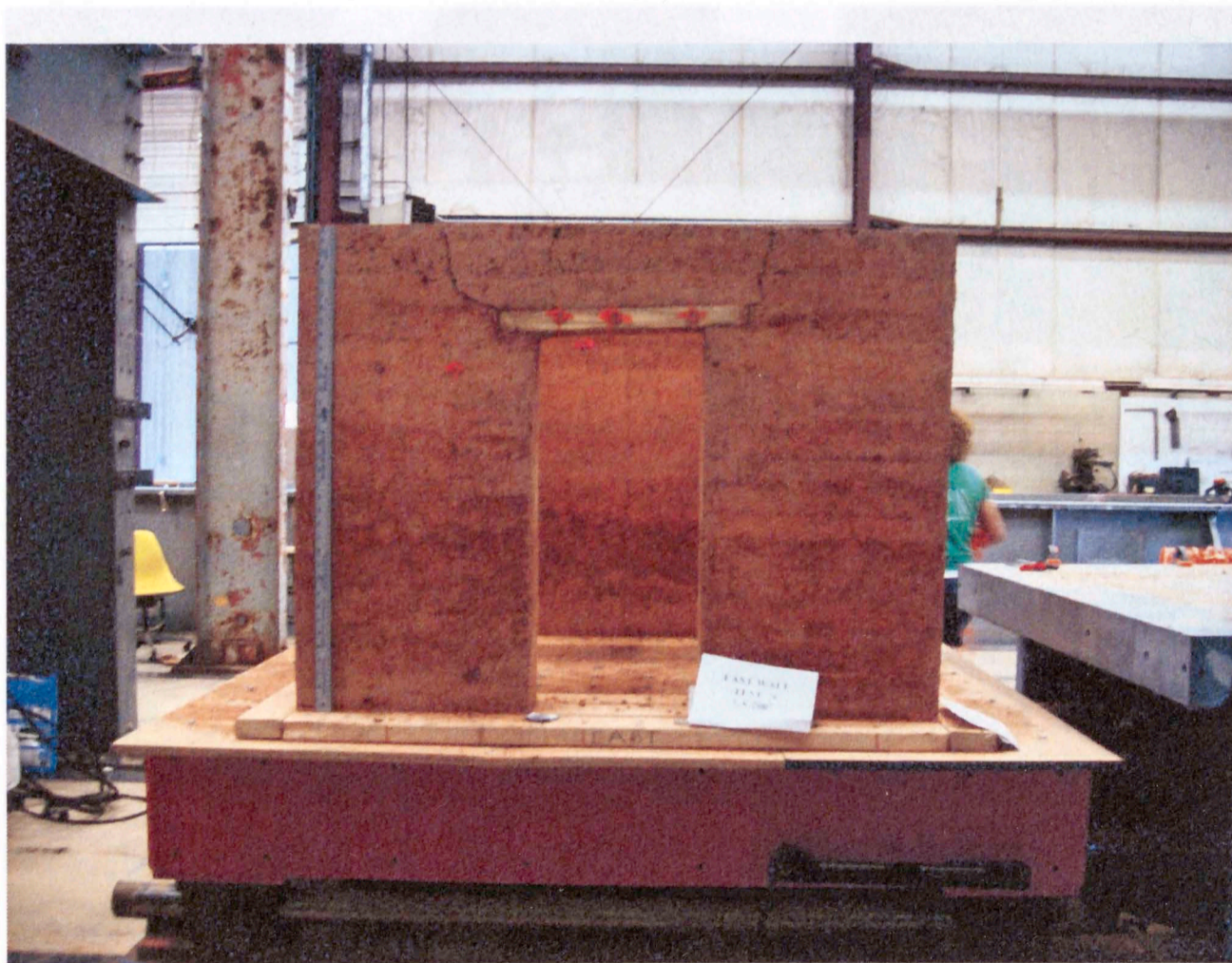


Figure 3.45: Test 4 view of east wall after test with the mesh removed

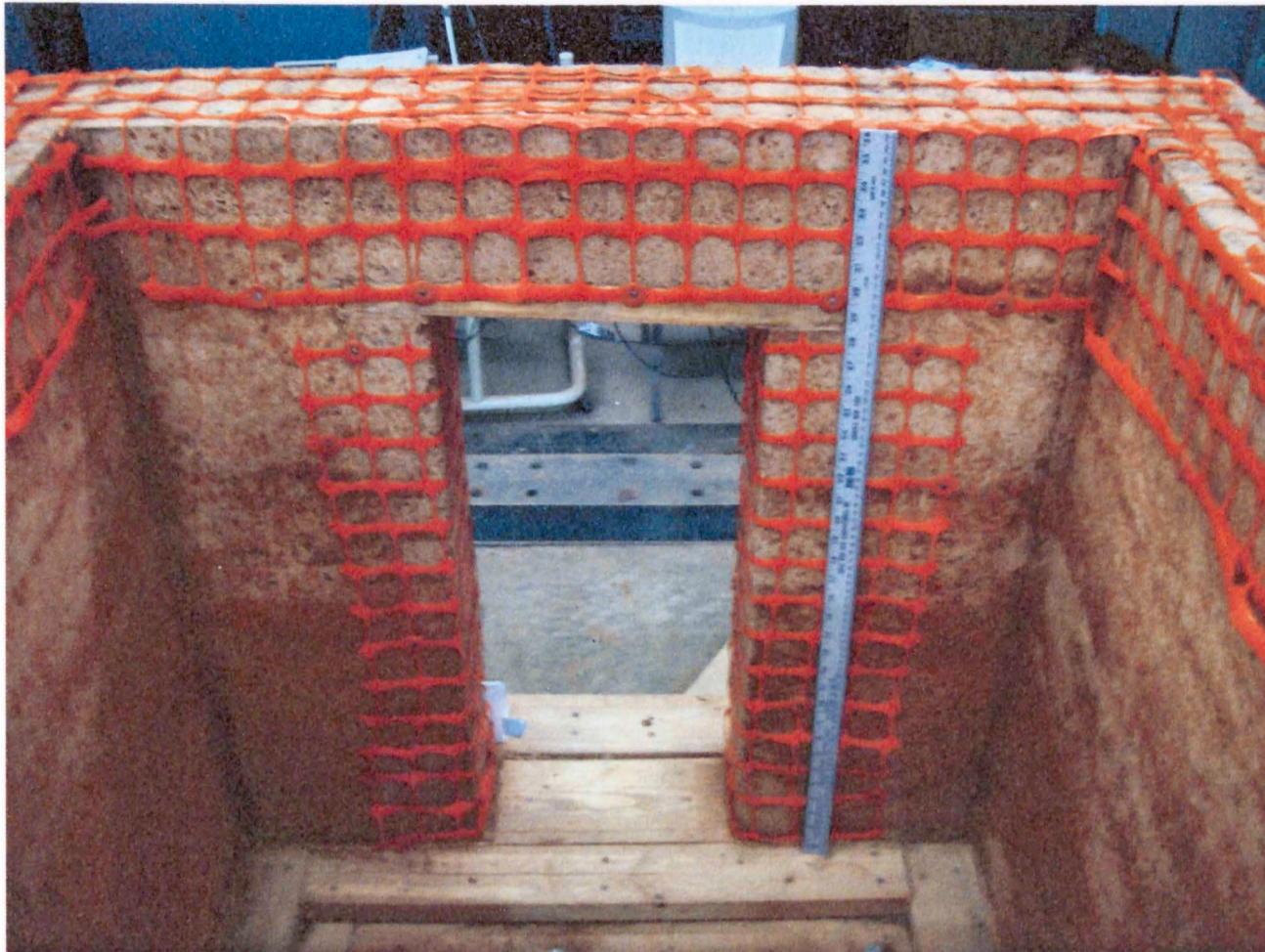


Figure 3.46: Test 4 interior of east wall before testing

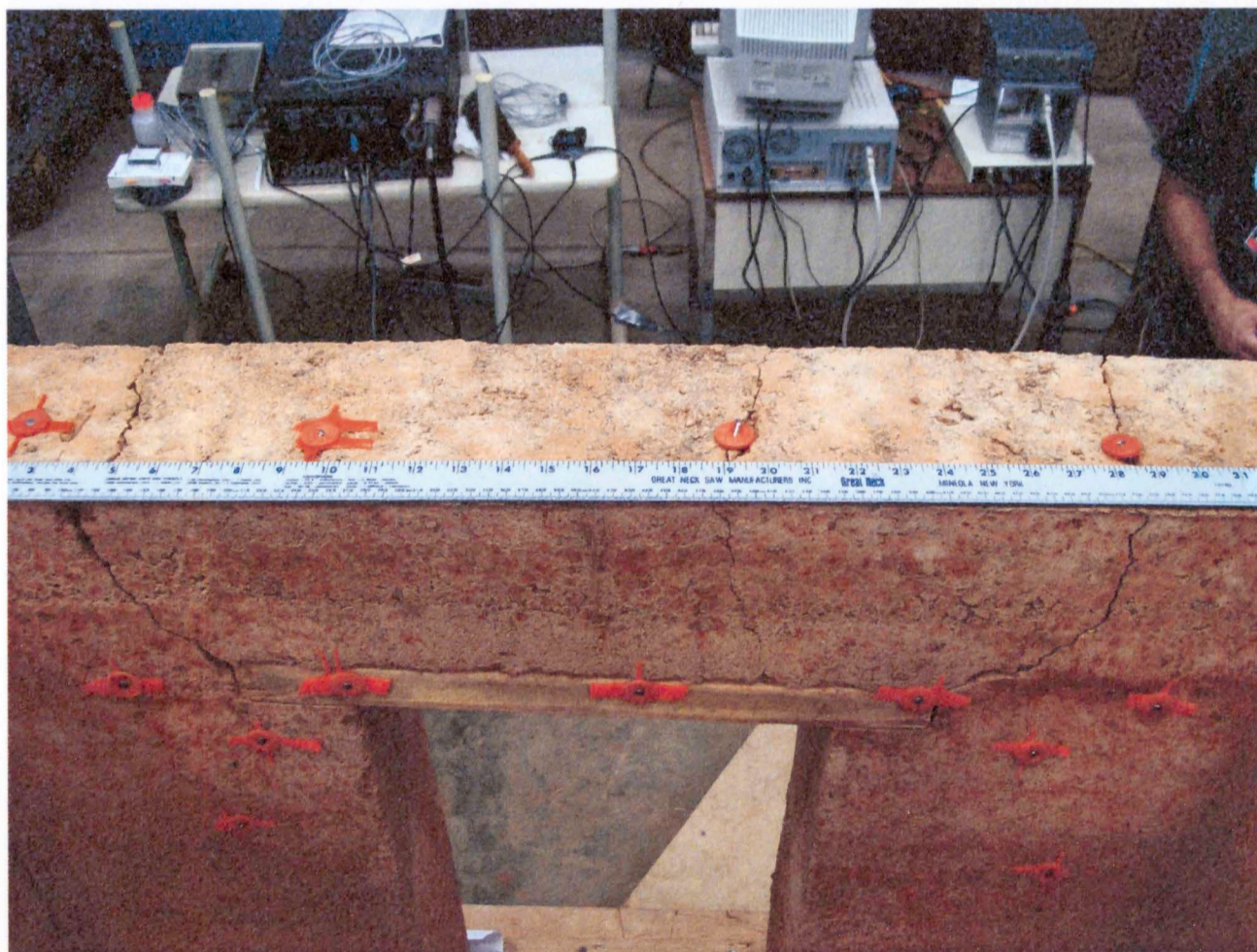


Figure 3.47: Test 4 view of cracks with nails above lintel in east wall after test

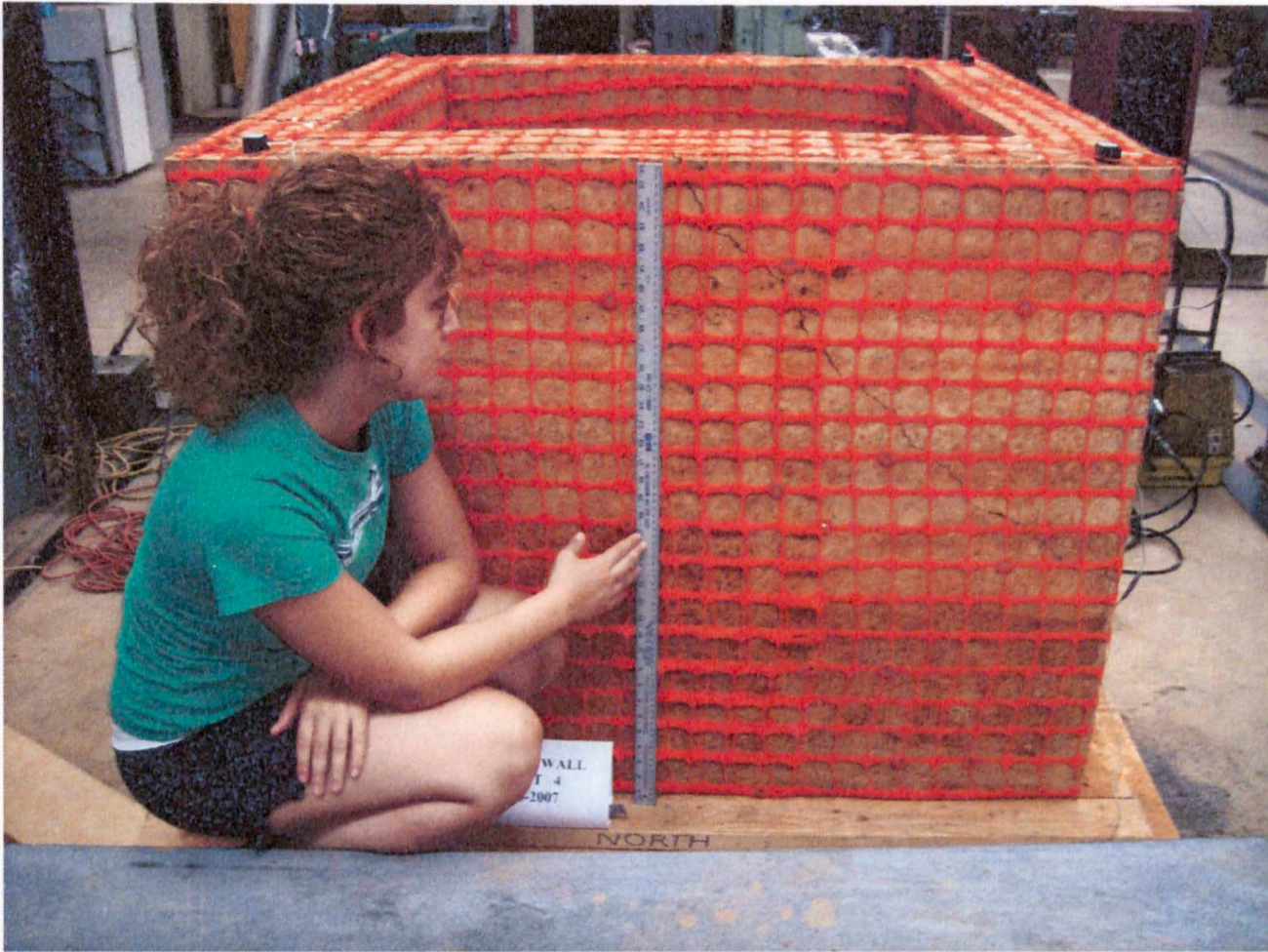


Figure 3.48: Test 4 view of diagonal crack along north wall with mesh after test



Figure 3.49: Test 4 view of diagonal crack along north wall after test



Figure 3.50: Test 4 interior view of NW corner after test

Figure 3.51: Test 4 view of diagonal crack at northwest corner of west wall after test

Figure 3.52: Test 4 view of diagonal crack at northwest corner of west wall after test



Figure 3.51: Test 4 view of diagonal crack at northwest corner of west wall after test

Figure 3.52: Test 4 view of exposed failure planes at north and west walls during demolition



Figure 3.52: Test 4 view of exposed failure planes at north and west walls during demolition



Figure 3.53: Test 4 view of wall that fractured upon impact with the floor

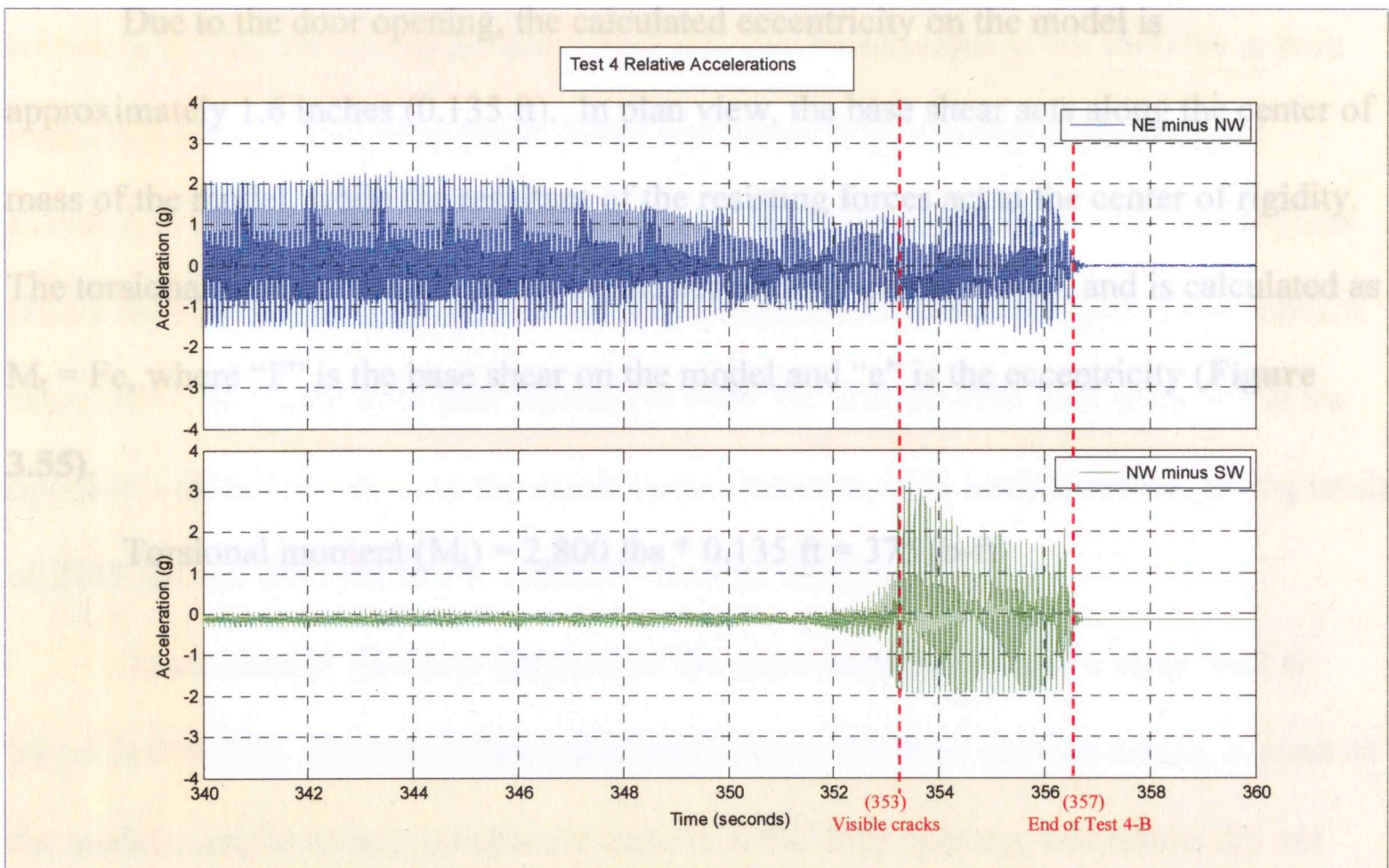


Figure 3.54: Test 4 relative accelerations between corners at failure

3.6 Discussion:

3.6.1 Calculation of Forces

The forces of interest in this study are in-plane shears and torsion. Because each model was designed with an opening at the east shear wall, an imbalance of stiffness was created in the model. Forces and strengths of the model are outlined below.

Using the equation $F = ma$, and an average density of 140 pcf, the amount of force delivered to the model at 1 g is the self-weight of the model, or approximately 2,800 lbs. Using an unconfined compressive strength of 663 psi, and formulas from DTi, the following estimated strengths of the rammed earth are:

$$\text{Compressive strength } (f_c) = \Phi * f_{uc} = 0.6 * 663 \text{ psi} = 400 \text{ psi}$$

$$\text{Shear strength } (f_v) = 0.07 * 400 \text{ psi} = 28 \text{ psi}$$

Due to the door opening, the calculated eccentricity on the model is approximately 1.6 inches (0.135 ft). In plan view, the base shear acts along the center of mass of the model, while the resultant of the resisting forces act at the center of rigidity. The torsional moment (M_t) depends on the eccentricity on the model, and is calculated as $M_t = Fe$, where “F” is the base shear on the model and “e” is the eccentricity (**Figure 3.55**).

$$\text{Torsional moment } (M_t) = 2,800 \text{ lbs} * 0.135 \text{ ft} = 375 \text{ lb-ft}$$

Theoretically, the shear capacity of the cross-sectional area of a shear wall at 28 psi is 8064 lbs. Because of the initial crack above the lintel prior to testing in most of the models, and/or loosely compacted corners at the door opening, test results did not reflect this capacity. Results of Test 1 showed that the pre-test crack above the lintel was

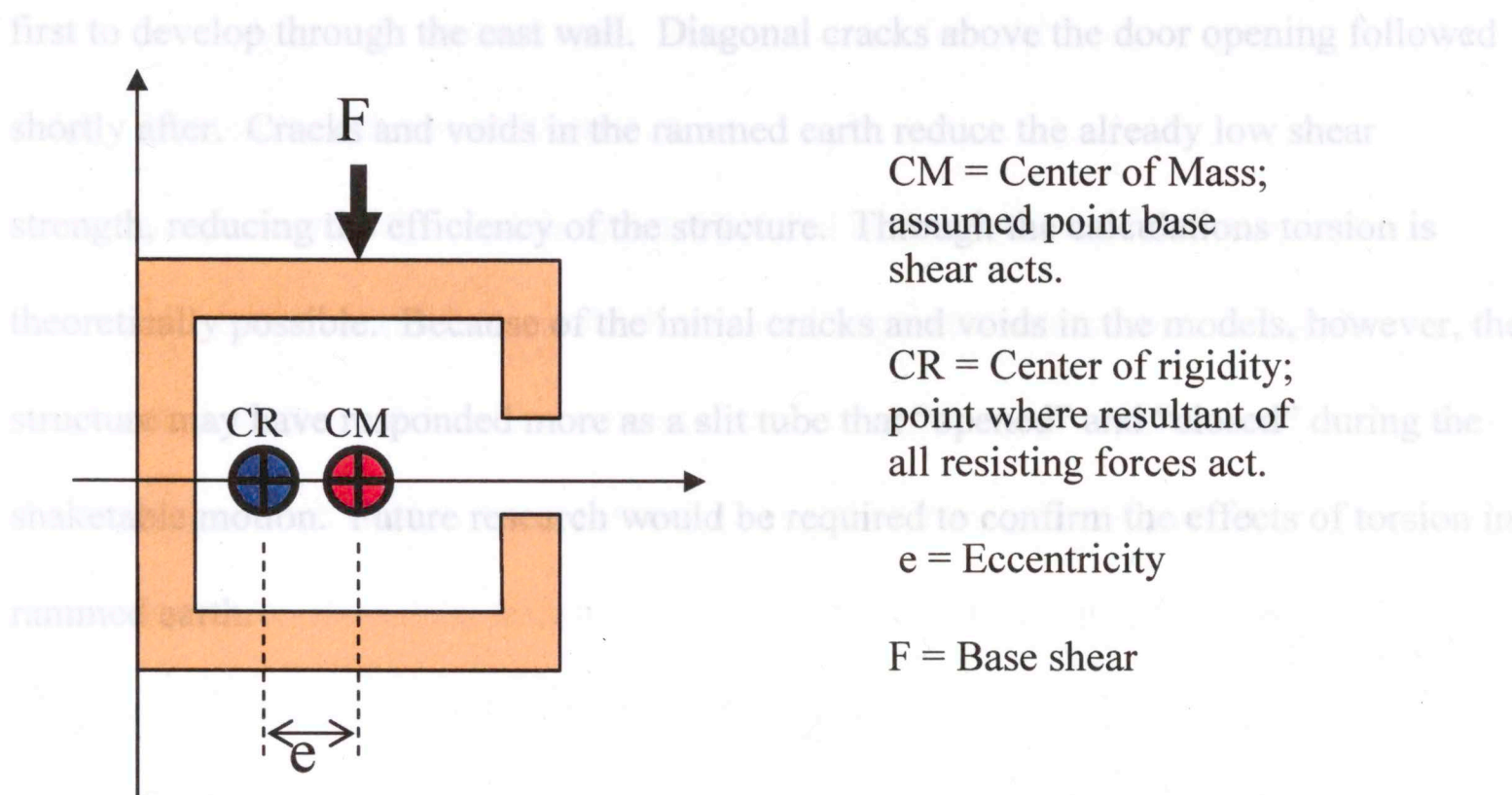


Figure 3.55: Sketch of location of base shear and eccentricity

Resolving the moment to an equivalent couple, the forces along each shear wall due to torsion is 94 lbs. Resolving the base shear into two components gives 1400 lbs at each wall. The combination of in-plane shears and forces from a torsional moment are sketched in **Figure 3.56**. As seen in the figure, the addition of torsion with the in-plane shears reduces the resultant load at one shear wall, and increases the load at the opposite shear wall. At 1 g the total load increase is 1494 lbs, and the total load reduction at the opposite wall is 1306 lbs. As the accelerations increase, both loads increase, giving totals of 2989 lbs and 2611 lbs at 2 g, and 4767 lbs and 3633 lbs at 3 g.

Theoretically, the shear capacity of the cross-sectional area of a shear wall at 28 psi is 8064 lbs. Because of the initial crack above the lintel prior to testing in most of the models, and/or loosely compacted corners at the door opening, test results did not reflect this capacity. Results of Test 1 showed that the pre-test crack above the lintel was

first to develop through the east wall. Diagonal cracks above the door opening followed shortly after. Cracks and voids in the rammed earth reduce the already low shear strength, reducing the efficiency of the structure. Through the calculations torsion is theoretically possible. Because of the initial cracks and voids in the models, however, the structure may have responded more as a slit tube that “opened” and “closed” during the shaketable motion. Future research would be required to confirm the effects of torsion in rammed earth.

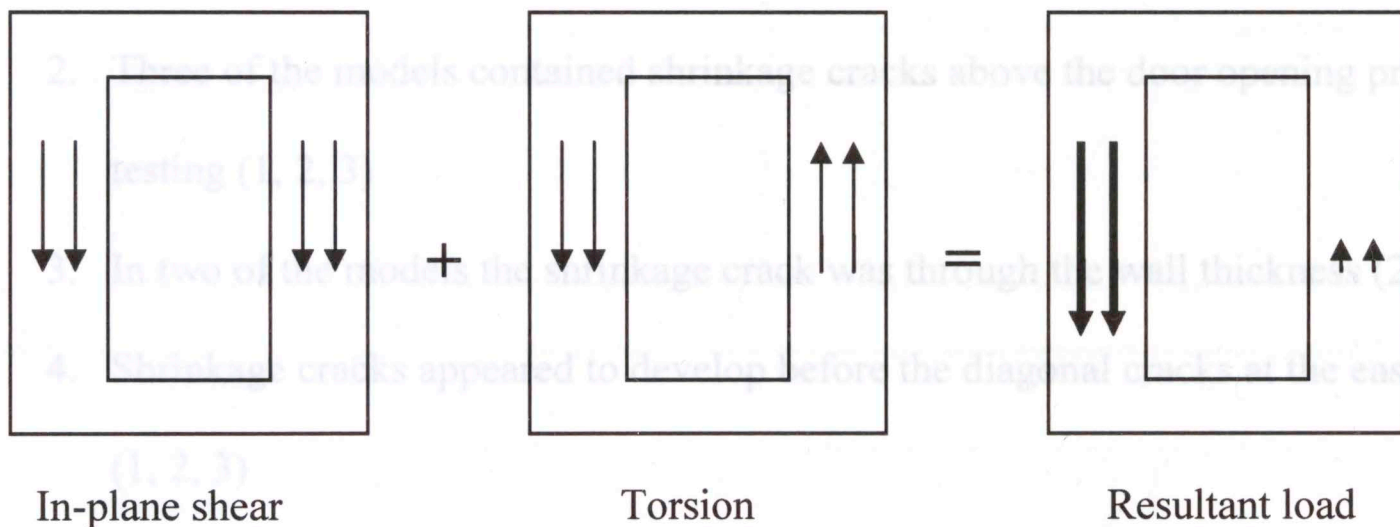


Figure 3.56: Sketch of resultant forces on model

A visual summary of the cracks observed at the exterior walls of each test is provided in

Figure 3.57.

3.6.2 Similarities Between Tests

Although none of the models appeared to fail at the measured fundamental frequency, each model had a unique failure which revealed important information including weaknesses of the model and locations of stress concentrations. When comparing all of the failures of each model, some patterns emerged in three general categories: crack locations, acceleration data, and dust. A summary of results is provided below (correlating tests are numbered in parenthesis):

1. All models contained diagonal cracks from the upper corners of the door opening.
2. Three of the models contained shrinkage cracks above the door opening prior to testing (1, 2, 3)
3. In two of the models the shrinkage crack was through the wall thickness (2, 3)
4. Shrinkage cracks appeared to develop before the diagonal cracks at the east wall (1, 2, 3)
5. In all models, the first reflected differences in accelerations were between northeast corner and the northwest corner.
6. In all models, dust clouds occurred prior to large fractures in the exterior walls.
7. All models contained vertical cracks at reentrant corners of the west wall.
8. Approximately 45-degree diagonal cracks were located in either the north or south wall (1, 3, 4)

The list and the figure show that in general, the door opening in the east wall and reentrant corners of the west wall were common locations of stress concentrations.

Figure 3.57.

Results of Test 1 and 2 showed that the cracks above the lintel develop first and cracks along the remaining walls originate from the base. Diagonal cracks at a door (or

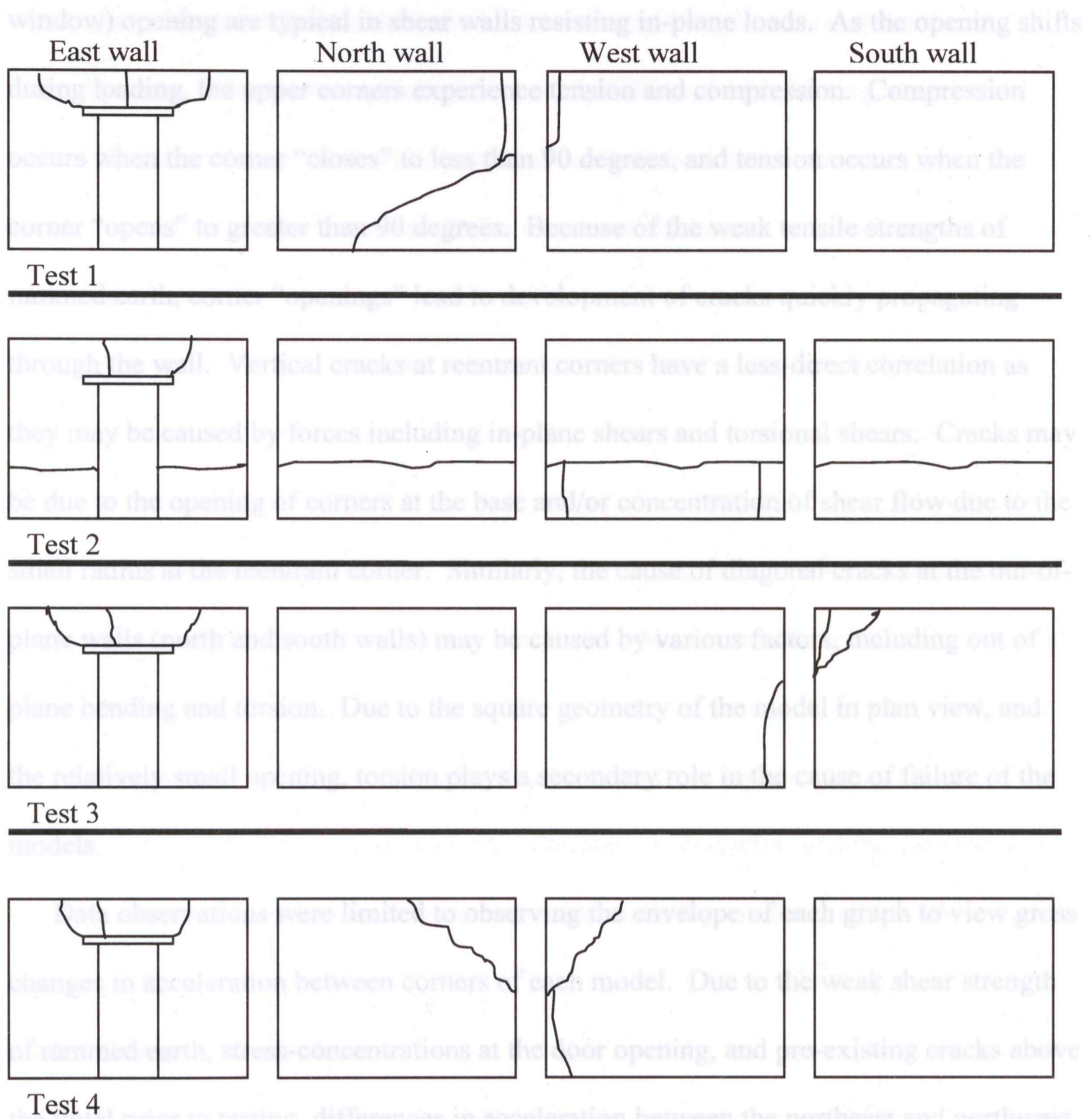


Figure 3.57: Summary of cracks on exterior walls of all models

The list and the figure show that in general, the door opening in the east wall and rammed earth can potentially open and close at cracks during cyclic loading. Towards reentrant corners of the west wall were common locations of stress concentrations. Results of Test 4 showed that at the end of Test 4, the relative difference between northwest and southwest corners. Results of Test 1 and 2 showed that the cracks above the lintel develop first and cracks increased approximately at the time the crack was observed at the northwest corner. Cracks along the remaining walls originate from the base. Diagonal cracks at a door (or

window) opening are typical in shear walls resisting in-plane loads. As the opening shifts during loading, the upper corners experience tension and compression. Compression occurs when the corner "closes" to less than 90 degrees, and tension occurs when the corner "opens" to greater than 90 degrees. Because of the weak tensile strengths of rammed earth, corner "openings" lead to development of cracks quickly propagating through the wall. Vertical cracks at reentrant corners have a less-direct correlation as they may be caused by forces including in-plane shears and torsional shears. Cracks may be due to the opening of corners at the base and/or concentration of shear flow due to the small radius at the reentrant corner. Similarly, the cause of diagonal cracks at the out-of-plane walls (north and south walls) may be caused by various factors, including out of plane bending and torsion. Due to the square geometry of the model in plan view, and the relatively small opening, torsion plays a secondary role in the cause of failure of the models. Because the presence of dust was consistent in Tests 2-4, and the amount of dust

Data observations were limited to observing the envelope of each graph to view gross changes in acceleration between corners of each model. Due to the weak shear strength of rammed earth, stress-concentrations at the door opening, and pre-existing cracks above the lintel prior to testing, differences in acceleration between the northeast and northwest corners are likely due to cracking in the east wall. Differences in accelerations between the northeast and the northwest corners were reflected prior to cracking of the other corners, which correlated with the visual observations. Results from Test 4 showed that rammed earth can potentially open and close at cracks during cyclic loading. Towards the end of Test 4, the relative difference between northwest and southwest corners increased approximately at the time the crack was observed at the northwest corner.

Cracks in the shear walls would allow for separations of the corners and increased displacements. With the exception of the model reinforced with the ring beam, which will be discussed further in the reinforcement section, the corners are essentially loose and free to displace. The increased displacement would then be reflected in the data as increased acceleration.

The presence of dust is somewhat enigmatic. Dust typically appeared prior to visible cracks in the exterior walls of the model. Without video cameras in the interior space of the model, it is difficult to determine the cause of the dust. At the very least, existence of dust indicates friction in the rammed earth model. The cause of friction could be between the model and the wooden base, or due to cracks developing within the model. Dust typically appeared around 10Hz or 12Hz for Tests 2-4. For the model in Test 2, the presence of dust was significant prior to failure, and the delaminated layer was eroded. Because the presence of dust was consistent in Tests 2-4, and the amount of dust would increase prior to failure, it is likely the dust indicates cracking within the model.

3.6.3 Effects of Reinforcement

Results of Test 3 showed the model initially responding as an unreinforced model and later as a model with added ductility. Cracks in the east wall still played a role in the displacement of the northeast corner, despite the ring beam. Location of the spikes appeared insignificant since the cracks did not occur at the spikes. The data reflected that the northeast and the northwest corners still had differences in acceleration similar to the other models. With the ring beam in place, the wood was not likely able to completely compensate for the lack of shear strength in the model. The approximate 3000 lb mass of

the model was no match for the small ring beam composed of two rows of studs with steel spikes. Once the cracks developed, however, the ring beam was able to maintain the model intact and better distributed the accelerations between the corners as reflected in the data towards the end of the test. Once the rammed earth cracked, the ring beam could provide some ductility and damping. With the ring beam in place, torsion was likely to play a larger role. However, because the accelerometers were uniaxial, this effect could not be confirmed by our testing.

Results of Test 4 showed that the plastic mesh added no structural strength, but simply prevented collapse of the northwest corner. Location of the nails also appeared to affect the location of the cracks at the west wall. At the east wall, two of the cracks contained nails. The location of the cracks were similar to previous models, however, indicating the cracks would have developed with or without the nails. During demolition the rammed earth walls did fracture into several smaller fragments. The ratio of nail depth to wall thickness is greater in the model than in a full-scale structure, and it is likely such fracture of the rammed earth would not occur in a full size structure.

3.6.5 In summary both forms of reinforcement prevented collapse of the model despite cracks fully propagated through the walls. The ring beam better distributed the acceleration between the corners, and provided some damping. The plastic mesh simply held the fragments in place and prevented collapse. The efficiency of each method of reinforcement would depend on the types of soil in the region and accessible materials.

initial expectations, crack locations such as at the door opening were within expectations since rammed earth is weak in shear and tension. In addition, when compared back to Figure 1.1, model failures at the corners resembled failures in the field. If confirmed by

3.6.4 Effects of Workmanship

Results from all tests provided insight on the importance of proper workmanship. In the first model, the north wall uncharacteristically cracked approximately midspan at the base. The lower layers were less compacted than the upper layers and provided less shear resistance. In the second model all walls delaminated at the cold joint, where there was less of a bond between the layers. Also noticed were the less-compacted upper corners of the door opening. Because the lintel was a loosely placed member, compaction around the lintel was more difficult as the lintel shifted inside the formwork. In the third model much care was taken in eliminating cold joints and constructing the ring beam. Results of test 4 showed that there is some forgiveness in placement of the plastic mesh onto the model. Random nail pattern appeared insignificant to location of cracks. Care was taken however to eliminate the cold joint at the midheight of the model. Based on the results the bond between layers and proper compaction is crucial to the performance of the structure.

3.6.5 Loading Protocol

The rammed earth models were expected to fail at the fundamental frequency. Instead, results from Tests 2-4 showed that models failed at approximately 10-12 Hz, or two times the measured fundamental frequency. Further research would be required to confirm and/or explain this phenomenon. Although failure frequencies did not meet initial expectations, crack locations such as at the door opening were within expectations since rammed earth is weak in shear and tension. In addition, when compared back to **Figure 1.1**, model failures at the corners resembled failures in the field. If confirmed by

future research, this loading protocol may serve as an alternative to loading models with complicated earthquake data when programming resources are limited.

4.1 Summary

This study investigated the dynamic response of a one-third scaled rammed earth house. Models were built using standard, traditional techniques. Proportions by total weight of the rammed earth mix consisted of 50% sand, 25% #10, 9% cement, 8% clay, and 8% water. Cylindrical tests of the mix showed that mid-range compressive strengths were possible. Four models were constructed: two without any reinforcement, one reinforced with a steel beam, and the last reinforced with a plastic mesh. In Tests 1-4 each model was loaded by a sine wave base motion which started at the fundamental frequency. During the test the frequency and amplitude of the sine wave was increased until failure. In Test 1, the model was loaded at three times the fundamental frequency. Gross failure of each model was recorded through video, pictures and accelerometer data. Effectiveness of the two types of reinforcement was assessed.

4.2 Conclusions

Results of Tests 2-4 showed that the models did not fail at the measured fundamental frequency as expected, but at two times the fundamental frequency. Failures at the corners and door opening, however, were similar to failure in the field. More research would be required to verify this phenomenon. If confirmed, loading a scaled model at the fundamental or superharmonic of the frequency may be a viable alternative to dynamic loading when programming resources are limited.

CHAPTER 4: CONCLUSIONS AND RECOMMENDATIONS

4.1 Summary

This study investigated the dynamic response of a one-third scaled rammed earth house. Models were built using manual, traditional techniques. Proportions by total weight of the rammed earth mix consisted of 50% sand, 25% silt, 9% cement, 8% clay, and 8% water. Cylinder tests of the mix showed that mid-range compressive strengths were possible. Four models were constructed: two without any reinforcement, one reinforced with a ring beam, and the last reinforced with a plastic mesh. In Tests 2-4 each model was loaded by a sine wave base motion which started at the fundamental frequency. During the test the frequency and amplitude of the sine wave was increased until failure. In Test 1, the model was loaded at three times the fundamental frequency. Gross failure of each model was recorded through video, pictures and accelerometer data. Effectiveness of the two types of reinforcement was assessed.

4.2 Conclusions

Results of Tests 2-4 showed that the models did not fail at the measured fundamental frequency as expected, but at two times the fundamental frequency. Failures at the corners and door opening, however, were similar to failure in the field. More research would be required to verify this phenomenon. If confirmed, loading a scaled model at the fundamental or superharmonic of the frequency may be a viable alternative to dynamic loading when programming resources are limited.

Results of all tests showed stress concentrations at the door opening and reentrant corners of the west wall were typical failures. In addition, the presence of dust prior to visible cracks may indicate the development of those cracks during loading. Causes of stress-concentrations are mostly attributed to in-plane shear forces. Torsional forces are possible in the model reinforced with the ring beam, however the torsion could not be confirmed because the accelerometers measured in only one direction. In the remaining models, the recorded increases in acceleration of the northeast corner and the differences in accelerations between corners indicate cracking at the shear walls and separation of the corners from the rest of the model.

Results of Tests 3 and 4 showed that both types of reinforcement were effective in preventing collapse. Acceleration data showed the ring beam provided some damping of the model once the cracks had developed. Results of Test 4 showed the rammed earth was mostly forgiving of a random nail-pattern on its walls. Four of 131 nails were located within cracks. The east wall contained two nails in cracks, although the location of the cracks were similar to previous tests. The west wall cracked unlike previous tests, however, and contained 2 nails within its cracks. It is likely the nail penetration would not be an issue in a full-scaled rammed earth structure since the walls would be thicker than six inches.

In general, workmanship proved to be affect strength of rammed earth. Although the main material—earth—is easily accessible, proper compaction at corners and bond between layers at the lower third of the model is essential. Results from Test 2 showed that a horizontal cold joint near the base is not desirable, and could result in catastrophic failure.

4.3 Recommendations

To broaden understanding of rammed earth structures, it is recommended that future research include:

- High-speed cameras to better record crack development and locations
- At least one additional camera viewing the interior model to verify source of dust.
- Reparability of cracks after testing
- Beveled reentrant corners and arched openings.
- Alternative reinforcement materials specific to certain regions depending on availability
- Full-scale testing to verify results of scaled testing, and whether possible to test at fundamental frequency or superharmonic.

This study was intended to be one of several stepping stones towards better understanding rammed earth as an earthquake-resistant structure. Rammed earth has been used for centuries and in various parts of the world. This study focused on methods and materials useful to a homeowner in a developing nation where resources are limited. Reinforcement of rammed earth is necessary to resist lateral loads. A wooden ring beam installed with steel spikes provided some damping to the structure and prevented collapse. Where wood is scarce, reinforcement such as the plastic mesh could be considered to prevent collapse. As research progresses, more options of reinforcement and structural designs will be developed that will not only be affordable in a developing nation, but save lives.

REFERENCES

- [1] Blondet M., Vargas J., Velasquez J., and Tarque N., "Seismic Reinforcement of Adobe Houses Using External Polymer Mesh," *Proceedings, Fourth International Adobe Conference of the Adobe Association of the Southwest*, El Rito, NM, pp.184 - 193, 2007.
- [2] Hamilton III H.R., McBride J., and Grill J., "Cyclic Testing of Rammed-Earth Walls Containing Post-tensioned Reinforcement," *Earthquake Spectra*, Vol. 22, No. 4, Nov. 2006, pp. 937-959.
- [3] International Association for Earthquake Engineering, "Guidelines for Earthquake-Resistant Non-Engineered Construction," 2004, Tokyo, Japan. (http://www.nicee.org/IAEE_English.php).
- [4] Jaquin, P.A., Augarde, C.E. and Gerrard, C.M., "Analysis of Historic Rammed Earth Construction," *Structural Analysis of Historical Constructions*, New Delhi, 2006. ISBN 972-8692-27-7
- [5] Kuehn J.L., *Semi-Active Structural Control Systems with Nonlinear Actuator Dynamics: Design, Stability Analysis, and Experimental Verification*, Doctoral Dissertation, University of Oklahoma, School of Aerospace and Mechanical Engineering, 2000.

- [6] Maniatidis V., Walker P., "A Review of Rammed Earth Construction," DTi Partners in Innovation Project, University of Bath, May 2003, Bath, England, 109 pages.
[\(\[http://files.starship-enterprises.net/Rammed_Earth_Review.pdf\]\(http://files.starship-enterprises.net/Rammed_Earth_Review.pdf\)\)](http://files.starship-enterprises.net/Rammed_Earth_Review.pdf).
- [7] McHenry P. G., *Adobe and Rammed Earth Buildings: design and construction*, The University of Arizona Press, AZ, 1984.
- [8] Tolles E.L., Kimbro E.E., Webster F.A., and Ginell W.S., "Seismic Stabilization of Historic Adobe Structures—Final Report of the Getty Seismic Adobe Project," GCI Scientific Program Reports, The Getty Conservation Institute, 2000, Los Angeles, CA.
[\(<http://www.getty.edu/conservation/resources/seismicstabilization.pdf>\)](http://www.getty.edu/conservation/resources/seismicstabilization.pdf).
- [9] Vargas J., "Earthquake Resistant Rammed-Earth (Tapial) Buildings," Memoria Proceedings, International Symposium on Earthquake Disaster Prevention, Vol. III, 1992, pp. 140-151.
[\(<http://www.crid.or.cr/digitalizacion/pdf/eng/doc3295-contenido.pdf>\)](http://www.crid.or.cr/digitalizacion/pdf/eng/doc3295-contenido.pdf).

- [10] Vargas J., Blondet M., and Tarque N., "Building Codes for Earthen Buildings in Seismic Areas: The Peruvian Experience," Catholic University of Peru, 2004, Lima, Peru.
http://www.pucp.edu.pe/secc/civil/publicaciones/Building_codes_for_earthen_buildings_in_seismic_areas.pdf.
- [11] www.lamasperu.com

This volume is the property of the University of Oklahoma, but the literary rights of the author are a separate property and must be respected. Passages must not be copied or closely paraphrased without the previous written consent of the author. If the reader obtains any assistance from this volume, he must give proper credit in his own work.

I grant the University of Oklahoma Libraries permission to make a copy of my thesis upon the request of individuals or libraries. This permission is granted with the understanding that a copy will be provided for research purposes only, and that requestors will be informed of these restrictions.

NAME _____

DATE _____

A library which borrows this thesis for use by its patrons is expected to secure the signature of each user.

This thesis by CARMEN MARLENE DIAZ has been used by the following persons, whose signatures attest their acceptance of the above restrictions.

NAME AND ADDRESS

DATE